# Molecular and Functional Characterization of Ion Transporters in Rice and Barley: Roles in Salinity Stress Tolerance

**March, 2026**

**SHAHIN IMRAN**

**Graduate School of**

**Environmental, Life,**

**Natural Science and Technology**

**(Doctor's Course)**

**OKAYAMA UNIVERSITY**

# DECLARATION

I hereby declare that my dissertation, entitled:

**“Molecular and Functional Characterization of Ion Transporters in Rice and Barley: Roles in Salinity Stress Tolerance”**

has been composed by me, and that the work presented herein is entirely my own, except where due acknowledgment is made in the text. I further declare that this dissertation has not been submitted, either wholly or in part, for any other degree or professional qualification at Okayama University or at any other institution, except as explicitly stated.

Parts of this work have been published in the *International Journal of Molecular Sciences* and *Phyton: International Journal of Experimental Botany*.

Date: March 2026

Signature:

Shahin Imran

# TABLE OF CONTENTS

# CHAPTER 1

## General Introduction

Soil salinity is a globally alarming environmental issue that severely limits agricultural productivity and threatens food security, particularly in arid and semi-arid regions where irrigation often leads to the accumulation of soluble salts in the soil (Munns and Tester, 2008; Shrivastava and Kumar, 2015). Excessive concentrations of sodium ($Na^+$) and chloride ($Cl^-$) ions disrupt plant physiological and metabolic processes by inducing osmotic stress, ion toxicity, and nutrient imbalance, ultimately resulting in reduced germination, stunted growth, and decreased crop yields (Gupta and Huang, 2014). Among major cereal crops, rice (*Oryza sativa*) is one of the most salt-sensitive species, while barley (*Hordeum vulgare*) exhibits comparatively higher salt tolerance (Munns and Tester, 2008; Gupta et al., 2014). Therefore, understanding the molecular and physiological mechanisms underlying plant responses to salinity is essential for developing salt-tolerant crop varieties.

Plants have evolved sophisticated strategies to cope with saline environments, including ion exclusion, compartmentation, and osmotic adjustment. Proper regulation of $Na^+$ and $K^+$ transport across cellular membranes is crucial for maintaining cytosolic ion homeostasis and ensuring plant survival under salt stress. Ion transporters and channels located in the plasma membrane (Figure 1.1) and tonoplast play pivotal roles in these adaptive mechanisms.

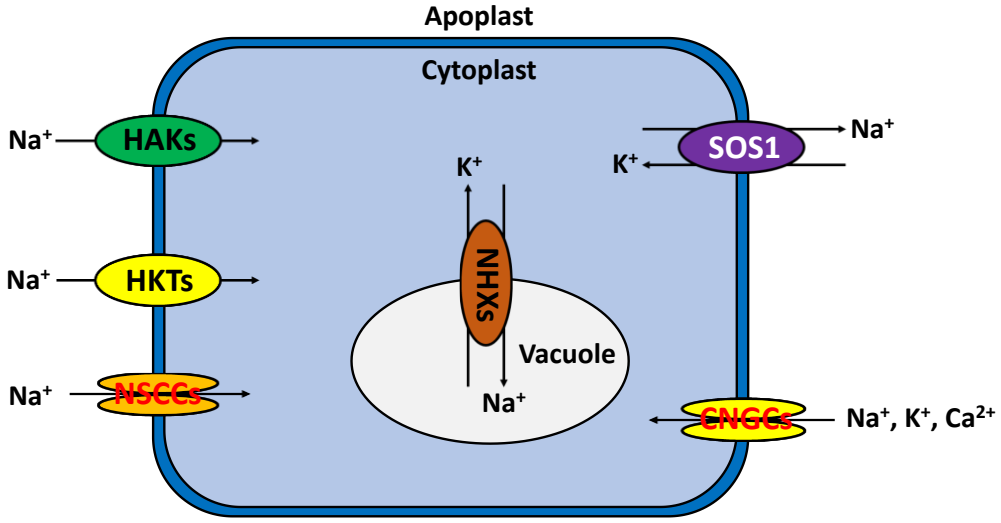


**Figure 1.1.** Channels and transporters involved in $Na^+$ transport in plants. CNGC: cyclic nucleotide-gated channel; HKT: high-affinity potassium transporter; HAK: High-Affinity

Potassium transporter; NHX: $Na^+/H^+$ antiporter; NSCC: non-selective cation channel; SOS: salt overly sensitive. Modified from Kaisham et al. 2018.

Among these, High-affinity potassium transporters (HKTs) have been identified as key determinants in controlling $Na^+$ and $K^+$ partitioning between roots and shoots, thereby maintaining an optimal $Na^+/K^+$ ratio under salinity stress (Rus et al., 2001; Mäser et al., 2002; Horie et al., 2009). HKTs are classified into two major subfamilies based on their ion selectivity: class 1 HKTs (HKT1-type), which are primarily $Na^+$-selective and occur in both monocotyledonous and dicotyledonous plants, and class 2 HKTs (HKT2-type), specific to monocots, which are capable of transporting both $Na^+$ and $K^+$ (Figure 1.2; Platten et al., 2006; Hauser and Horie, 2010). The first plant *HKT* gene *TaHKT2;1* from bread wheat (*Triticum aestivum*), was characterized as a $Na^+$-$K^+$ co-transporter (Rubio et al., 1995). In rice, nine functional *OsHKT* genes have been identified in the japonica cultivar, of which four (*OsHKT1;1*, *OsHKT1;3*, *OsHKT1;4*, and *OsHKT1;5*) belong to class 1 and showing $Na^+$ selectivity, as demonstrated in *Xenopus laevis* oocytes using two-electrode voltage clamp assays (Garciadeblás et al., 2003; Ren et al., 2005; Jabnoune et al., 2009; Rosas-Santiago et al., 2015; Suzuki et al., 2016). Within class 2, *OsHKT2;1* primarily transports $Na^+$, while *OsHKT2;2* mediates both $Na^+$-dependent $K^+$ and $K^+$-dependent $Na^+$ transport (Horie et al., 2001, 2007; Jabnoune et al., 2009). Furthermore, *OsHKT2;4* exhibits higher permeability to $K^+$ compared to $Na^+$ and can also conduct $Mg^{2+}$ and $Ca^{2+}$ in the absence of $K^+$ (Lan et al., 2010; Horie et al., 2011; Sassi et al., 2012). Interestingly, the chimeric transporter *OsHKT2;2/1* from the salt-tolerant indica landrace Nona Bokra demonstrates high permeability to both $Na^+$ and $K^+$, even at high $Na^+$ levels (Yao et al., 2010; Oomen et al., 2012; Suzuki et al., 2016).

HKTs have been shown to play a crucial role in $Na^+$ tolerance by restricting $Na^+$ influx into plant cells and facilitating $Na^+$ recirculation (Apse and Blumwald, 2007). Quantitative trait locus (QTL) analysis between the salt-tolerant indica landrace Nona Bokra and the japonica cultivar Koshihikari identified the *Shoot $K^+$ Content 1 (SKC1)* locus, which maintains higher $K^+$ and lower $Na^+$ levels in shoots under salt stress (Ren et al., 2005). The *OsHKT1;5* gene, which encodes a plasma membrane-localized $Na^+$ transporter, was identified as the causal gene for the *SKC1* QTL and shown to mediate $Na^+$ unloading from xylem vessels, thus reducing shoot $Na^+$ accumulation and improving salt tolerance (Ren et al., 2005; Kobayashi et al., 2017). Similarly,

*OsHKT1;1* plays a vital role in $Na^+$ exclusion from the xylem and in reducing shoot $Na^+$ accumulation, as shown by *Tos17*-insertion mutants (Wang et al., 2015). The *OsHKT1;1* mutation causes increased $Na^+$ in the xylem sap but decreased $Na^+$ in the phloem, similar to what is observed in the *athkt1;1* mutant of *Arabidopsis* (Sunarpi et al., 2005; Møller et al., 2009; Wang et al., 2015). Genetic studies have further demonstrated that *OsHKT1;1* is a key determinant of rice salt tolerance (Takagi et al., 2015; Campbell et al., 2017). Notably, the *OsHKT1;1* isoform from the salt-tolerant indica cultivar Pokkali exhibits stronger inward $Na^+$ currents than that from the japonica cultivar Nipponbare, possibly due to a less negative voltage threshold for inward current activation (Campbell et al., 2017).

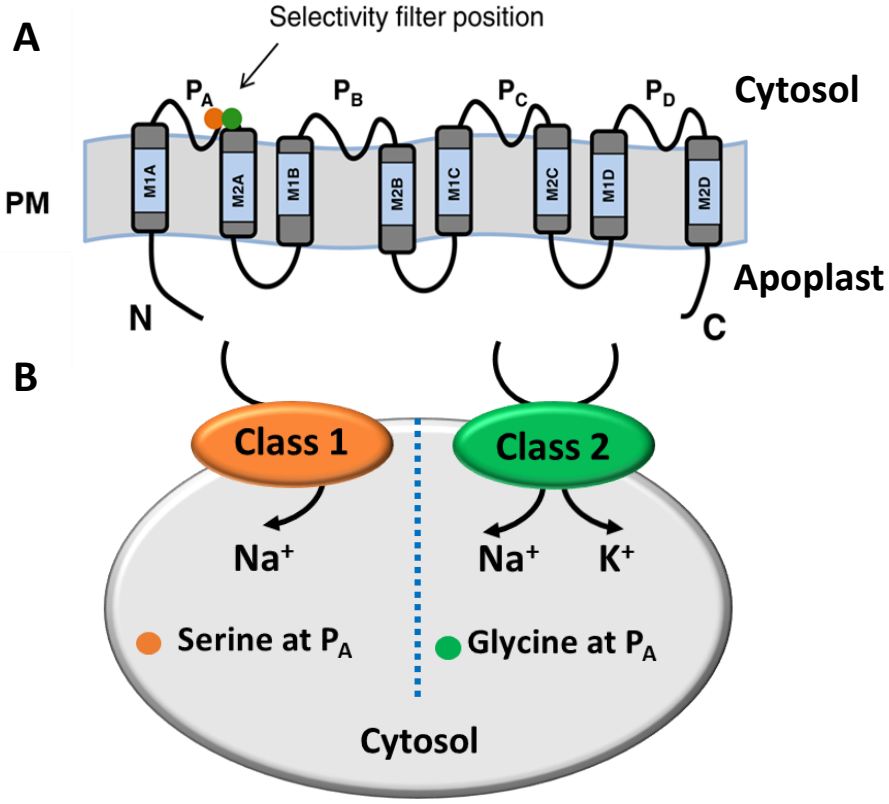


**Figure 1.2.** Structure and classification of HKT proteins. (**A**) Basic structure of the HKT proteins. HKTs have eight transmembrane domains ($M1_A$–$M2_D$) and four pore-loop domains ($P_A$–$P_D$). Serine (orange) and glycine (green) residues responsible for $Na^+/K^+$ selection are indicated by an arrow in the first pore-loop region, which is known as the selectivity filter position. N and C indicate N- and C-terminus of HKT proteins. (**B**) HKT proteins are divided into two classes, classes 1 and 2. Most members of class 1 possess a serine residue in the selectivity filter position, whereas most class 2 transporters contain a glycine residue at the same position (Ali et al., 2020).

While previous studies have mainly focused on the full-length OsHKT1;1 transcript, recent findings have revealed the presence of alternative splicing variants of OsHKT1;1 that may contribute to functional diversity and differential salinity responses among rice cultivars (Ren et al., 2015; Imran et al., 2020, 2021). These variants may influence the transport properties and expression patterns of HKT proteins, thereby modulating $Na^+$ and $K^+$ homeostasis under saline conditions. In barley, a homologous gene, HvHKT1;1, has been characterized as a $Na^+$-selective transporter involved in $Na^+$ exclusion and salt tolerance (Han et al., 2018). However, whether HvHKT1;1 also produces multiple mRNA variants remains unknown. Elucidating the diversity and function of HKT variants across cereal species can thus provide new insights into the molecular basis of salt tolerance and guide breeding strategies for improved stress resilience.

Beyond HKTs, other classes of ion channels also play critical roles in regulating ionic and signaling processes in plants. Among these, Cyclic Nucleotide-Gated Channels (CNGCs) are an important family of non-selective cation channels that mediate the transport of $Ca^{2+}$, $K^+$, and $Na^+$ across membranes, contributing to ion homeostasis, stress signaling, and developmental regulation (Figure 1.1; Jha et al., 2016; Duszyn et al., 2019). Originally discovered in animal sensory systems (Fesenko et al., 1985; Nakamura and Gold, 1987), plant CNGCs are now recognized for their roles in transducing environmental and hormonal signals. They are typically activated by cyclic nucleotides such as cAMP and cGMP and regulated through $Ca^{2+}$/calmodulin-dependent feedback mechanisms (Kaplan et al., 2007; Ungerer et al., 2011).

Genome-wide analyses have identified approximately 20 CNGC genes in *Arabidopsis thaliana*, 16 in *Oryza sativa*, and 9 in *Hordeum vulgare* (Mäser et al., 2001; Nawaz et al., 2014; Mori et al., 2018). Functional studies in *Arabidopsis* have revealed diverse physiological roles for CNGCs, including pathogen defense (AtCNGC2, AtCNGC4), $Ca^{2+}$ signaling (AtCNGC5, AtCNGC6), $K^+$ transport (AtCNGC10), and salt stress responses (AtCNGC19, AtCNGC20) (Clough et al., 2000; Borsics et al., 2007; Oranab et al., 2021). In rice, several OsCNGCs are transcriptionally responsive to abiotic stresses such as salinity and drought (Nawaz et al., 2014), but their electrophysiological properties and exact physiological functions remain largely unknown.

Taken together, ion transporters and channels such as HKTs and CNGCs form an integrated network that governs $Na^+$, $K^+$, and $Ca^{2+}$ transport, contributing to ion

homeostasis, signaling, and stress adaptation in plants. However, despite significant advances, many questions remain regarding their functional diversity, regulatory mechanisms, and physiological significance in monocot crops like rice and barley.

In this study, I focus on (1) the molecular characterization and functional analysis of OsHKT1;1 variants in rice cultivars with differing salt tolerance, (2) the identification and functional evaluation of HvHKT1;1 variants in barley, and (3) the electrophysiological characterization of OsCNGC2 in rice. Through gene expression analyses, heterologous expression in *Xenopus laevis* oocytes, and subcellular localization studies, this work aims to provide a comprehensive understanding of ion transport mechanisms that underpin salt tolerance in cereals. Insights gained from these investigations will contribute to the broader goal of improving crop resilience and productivity under salinity stress.

**References**


Ali A, Raddatz N, Pardo JM, Yun DJ. HKT sodium and potassium transporters in *Arabidopsis thaliana* and related halophyte species. Physiologia Plantarum. **2021**;171(4):546-58. https://doi.org/10.1111/ppl.13166

Apse MP, Blumwald E. $Na^+$ transport in plants. FEBS Letters. 2007;581(12):2247-54. https://doi.org/10.1016/j.febslet.2007.04.014

Borsics T, Webb D, Andeme-Ondzighi C, Staehelin LA, Christopher DA. The cyclic nucleotide-gated calmodulin-binding channel AtCNGC10 localizes to the plasma membrane and influences numerous growth responses and starch accumulation in *Arabidopsis thaliana*. Planta. **2007**;225(3):563-73. https://doi.org/10.1007/s00425-006-0372-3

Campbell MT, Bandillo N, Al Shiblawi FR, Sharma S, Liu K, Du Q, Schmitz AJ, Zhang C, Véry AA, Lorenz AJ, Walia H. Allelic variants of OsHKT1;1 underlie the divergence between indica and japonica subspecies of rice (*Oryza sativa*) for root sodium content. PLoS Genetics. **2017**;13(6):e1006823. https://doi.org/10.1371/journal.pgen.1006823

Clough SJ, Fengler KA, Yu IC, Lippok B, Smith Jr RK, Bent AF. The *Arabidopsis dnd1* "defense, no death" gene encodes a mutated cyclic nucleotide-gated ion channel. Proceedings of the National Academy of Sciences. **2000**;97(16):9323-8. https://doi.org/10.1073/pnas.150005697

Duszyn M, Świeżawska B, Szmidt-Jaworska A, Jaworski K. Cyclic nucleotide gated channels (CNGCs) in plant signalling—Current knowledge and perspectives. Journal of Plant Physiology. **2019**;241:153035. https://doi.org/10.1016/j.jplph.2019.153035

Fesenko EE, Kolesnikov SS, Lyubarsky AL. Induction by cyclic GMP of cationic conductance in plasma membrane of retinal rod outer segment. Nature. **1985**;313(6000):310-313. https://doi.org/10.1038/313310a0

Garciadeblás B, Senn ME, Bañuelos MA, Rodríguez-Navarro A. Sodium transport and HKT transporters: the rice model. The Plant Journal. **2003**;34(6):788-801. https://doi.org/10.1046/j.1365-313X.2003.01764.x

Gupta B, Huang B. Mechanism of salinity tolerance in plants: physiological, biochemical, and molecular characterization. International Journal of Genomics. **2014**;2014(1):701596. https://doi.org/10.1155/2014/701596

Han Y, Yin S, Huang L, Wu X, Zeng J, Liu X, Qiu L, Munns R, Chen ZH, Zhang G. A sodium transporter HvHKT1;1 confers salt tolerance in barley via regulating tissue and cell ion homeostasis. Plant and Cell Physiology. **2018**;59(10):1976-1689. https://doi.org/10.1093/pcp/pcy116

Hauser F, Horie T. A conserved primary salt tolerance mechanism mediated by HKT transporters: a mechanism for sodium exclusion and maintenance of high $K^+/Na^+$ ratio in leaves during salinity stress. Plant, Cell & Environment. **2010**;33(4):552-565. https://doi.org/10.1111/j.1365-3040.2009.02056.x

Horie T, Hauser F, Schroeder JI. HKT transporter-mediated salinity resistance mechanisms in Arabidopsis and monocot crop plants. Trends in Plant Science. **2009**;14(12):660-668. https://doi.org/10.1016/j.tplants.2009.08.009

Horie T, Brodsky DE, Costa A, Kaneko T, Lo Schiavo F, Katsuhara M, Schroeder JI. $K^+$ transport by the OsHKT2;4 transporter from rice with atypical $Na^+$ transport properties and competition in permeation of $K^+$ over $Mg^{2+}$ and $Ca^{2+}$ ions. Plant Physiology. **2011**;156(3):1493-1507. https://doi.org/10.1104/pp.110.168047

Horie T, Costa A, Kim TH, Han MJ, Horie R, Leung HY, Miyao A, Hirochika H, An G, Schroeder JI. Rice OsHKT2;1 transporter mediates large $Na^+$ influx component into $K^+$-starved roots for growth. The EMBO Journal. **2007**;26(12):3003-3014. https://doi.org/10.1038/sj.emboj.7601732

Horie T, Yoshida K, Nakayama H, Yamada K, Oiki S, Shinmyo A. Two types of HKT transporters with different properties of $Na^+$ and $K^+$ transport in *Oryza sativa*.

The Plant Journal. **2001**;27(2):129-138. https://doi.org/10.1046/j.1365-313x.2001.01077.x

Huang S, Spielmeyer W, Lagudah ES, Munns R. Comparative mapping of HKT genes in wheat, barley, and rice, key determinants of $Na^+$ transport, and salt tolerance. Journal of Experimental Botany. **2008**;59(4):927-937. https://doi.org/10.1093/jxb/ern033

Imran S, Horie T, Katsuhara M. Expression and ion transport activity of rice OsHKT1;1 variants. Plants. **2020**;9(1):16. https://doi.org/10.3390/plants9010016

Imran S, Tsuchiya Y, Tran ST, Katsuhara M. Identification and characterization of rice OsHKT1;3 variants. Plants. **2021**;10(10):2006. https://doi.org/10.3390/plants10102006

Jabnoune M, Espeout S, Mieulet D, Fizames C, Verdeil JL, Conéjéro G, Rodríguez-Navarro A, Sentenac H, Guiderdoni E, Abdelly C, Véry AA. Diversity in expression patterns and functional properties in the rice HKT transporter family. Plant Physiology. **2009**;150(4):1955-1971. https://doi.org/10.1104/pp.109.138008

Jha SK, Sharma M, Pandey GK. Role of cyclic nucleotide gated channels in stress management in plants. Current Genomics. **2016**;17(4):315-329. https://doi.org/10.2174/1389202917666160331202125

Kaplan B, Sherman T, Fromm H. Cyclic nucleotide-gated channels in plants. FEBS Letters. **2007**;581(12):2237-2246. https://doi.org/10.1016/j.febslet.2007.02.017

Keisham M, Mukherjee S, Bhatla SC. Mechanisms of sodium transport in plants—progresses and challenges. International Journal of Molecular Sciences. **2018**;19(3):647. https://doi.org/10.3390/ijms19030647

Kobayashi NI, Yamaji N, Yamamoto H, Okubo K, Ueno H, Costa A, Tanoi K, Matsumura H, Fujii-Kashino M, Horiuchi T, Nayef MA. OsHKT1;5 mediates $Na^+$ exclusion in the vasculature to protect leaf blades and reproductive tissues from salt toxicity in rice. The Plant Journal. **2017**;91(4):657-670. https://doi.org/10.1111/tpj.13595

Lan WZ, Wang W, Wang SM, Li LG, Buchanan BB, Lin HX, Gao JP, Luan S. A rice high-affinity potassium transporter (HKT) conceals a calcium-permeable cation channel. Proceedings of the National Academy of Sciences. **2010**;107(15):7089-7094. https://doi.org/10.1073/pnas.1000698107

Mäser P, Thomine S, Schroeder JI, Ward JM, Hirschi K, Sze H, Talke IN, Amtmann A, Maathuis FJ, Sanders D, Harper JF. Phylogenetic relationships within cation transporter families of Arabidopsis. Plant Physiology. **2001**;126(4):1646-1667. https://doi.org/10.1104/pp.126.4.1646

Mäser P, Eckelman B, Vaidyanathan R, Horie T, Fairbairn DJ, Kubo M, Yamagami M, Yamaguchi K, Nishimura M, Uozumi N, Robertson W. Altered shoot/root $Na^+$ distribution and bifurcating salt sensitivity in Arabidopsis by genetic disruption of the $Na^+$ transporter *AtHKT1*. FEBS Letters. **2002**;531(2):157-1561. https://doi.org/10.1016/S0014-5793(02)03488-9

Møller IS, Gilliham M, Jha D, Mayo GM, Roy SJ, Coates JC, Haseloff J, Tester M. Shoot $Na^+$ exclusion and increased salinity tolerance engineered by cell type–specific alteration of $Na^+$ transport in *Arabidopsis*. The Plant Cell. **2009**;21(7):2163-78. https://doi.org/10.1105/tpc.108.064568

Mori IC, Nobukiyo Y, Nakahara Y, Shibasaka M, Furuichi T, Katsuhara M. A cyclic nucleotide-gated channel, HvCNGC2-3, is activated by the co-presence of $Na^+$ and $K^+$ and permeable to $Na^+$ and $K^+$ non-selectively. Plants. **2018**;7(3):61. https://doi.org/10.3390/plants7030061

Munns R, Tester M. Mechanisms of salinity tolerance. Annual Review of Plant Biology. **2008**;59(1):651-681. https://doi.org/10.1146/annurev.arplant.59.032607.092911

Nakamura T, Gold GH. A cyclic nucleotide-gated conductance in olfactory receptor cilia. Nature. **1987**;325(6103):442-444. https://doi.org/10.1038/325442a0

Nawaz Z, Kakar KU, Saand MA, Shu QY. Cyclic nucleotide-gated ion channel gene family in rice, identification, characterization and experimental analysis of expression response to plant hormones, biotic and abiotic stresses. BMC Genomics. **2014**;15(1):853. https://doi.org/10.1186/1471-2164-15-853

Oomen RJ, Benito B, Sentenac H, Rodríguez-Navarro A, Talón M, Véry AA, Domingo C. HKT2;2/1, a $K^+$-permeable transporter identified in a salt-tolerant rice cultivar through surveys of natural genetic polymorphism. The Plant Journal. **2012**;71(5):750-762. https://doi.org/10.1111/j.1365-313X.2012.05031.x

Oranab S, Ghaffar A, Kiran S, Yameen M, Munir B, Zulfiqar S, Abbas S, Batool F, Farooq MU, Ahmad B, Ilyas H. Molecular characterization and expression of cyclic nucleotide gated ion channels 19 and 20 in *Arabidopsis thaliana* for their

potential role in salt stress. Saudi Journal of Biological Sciences. **2021**;28(10):5800-5807. https://doi.org/10.1016/j.sjbs.2021.06.027

Platten JD, Cotsaftis O, Berthomieu P, Bohnert H, Davenport RJ, Fairbairn DJ, Horie T, Leigh RA, Lin HX, Luan S, Mäser P. Nomenclature for HKT transporters, key determinants of plant salinity tolerance. Trends in Plant Science. **2006**;11(8):372-374. https://doi.org/10.1016/j.tplants.2006.06.001

Ren Z, Liu Y, Kang D, Fan K, Wang C, Wang G, Liu Y. Two alternative splicing variants of maize HKT1;1 confer salt tolerance in transgenic tobacco plants. Plant Cell, Tissue and Organ Culture. **2015**;123(3):569-578. https://doi.org/10.1007/s11240-015-0861-9

Ren ZH, Gao JP, Li LG, Cai XL, Huang W, Chao DY, Zhu MZ, Wang ZY, Luan S, Lin HX. A rice quantitative trait locus for salt tolerance encodes a sodium transporter. Nature Genetics. **2005**;37(10):1141-1146. https://doi.org/10.1038/ng1643

Rosas-Santiago P, Lagunas-Gómez D, Barkla BJ, Vera-Estrella R, Lalonde S, Jones A, Frommer WB, Zimmermannova O, Sychrová H, Pantoja O. Identification of rice cornichon as a possible cargo receptor for the Golgi-localized sodium transporter OsHKT1;3. Journal of Experimental Botany. **2015**;66(9):2733-2748. https://doi.org/10.1093/jxb/erv069

Rubio F, Gassmann W, Schroeder JI. Sodium-driven potassium uptake by the plant potassium transporter HKT1 and mutations conferring salt tolerance. Science. **1995**;270(5242):1660-1663. https://doi.org/10.1126/science.270.5242.1660

Rus A, Yokoi S, Sharkhuu A, Reddy M, Lee BH, Matsumoto TK, Koiwa H, Zhu JK, Bressan RA, Hasegawa PM. AtHKT1 is a salt tolerance determinant that controls $Na^+$ entry into plant roots. Proceedings of the National Academy of Sciences. **2001**;98(24):14150-14155. https://doi.org/10.1073/pnas.241501798

Sassi A, Mieulet D, Khan I, Moreau B, Gaillard I, Sentenac H, Véry AA. The rice monovalent cation transporter OsHKT2;4: revisited ionic selectivity. Plant Physiology. **2012**;160(1):498-510. https://doi.org/10.1104/pp.112.194936

Schachtman DP, Schroeder JI. Structure and transport mechanism of a high-affinity potassium uptake transporter from higher plants. Nature. **1994**;370(6491):655-658. https://doi.org/10.1038/370655a0

Shrivastava P, Kumar R. Soil salinity: A serious environmental issue and plant growth promoting bacteria as one of the tools for its alleviation. Saudi Journal of

Biological Sciences. **2015**;22(2):123-131. https://doi.org/10.1016/j.sjbs.2014.12.001

Sunarpi X, Horie T, Motoda J, Kubo M, Yang H, Yoda K, Horie R, Chan WY, Leung HY, Hattori K, Konomi M. Enhanced salt tolerance mediated by AtHKT1 transporter-induced $Na^+$ unloading from xylem vessels to xylem parenchyma cells. The Plant Journal. **2005**;44(6):928-938. https://doi.org/10.1111/j.1365-313X.2005.02595.x

Suzuki K, Costa A, Nakayama H, Katsuhara M, Shinmyo A, Horie T. OsHKT2;2/1-mediated $Na^+$ influx over $K^+$ uptake in roots potentially increases toxic $Na^+$ accumulation in a salt-tolerant landrace of rice Nona Bokra upon salinity stress. Journal of Plant Research. **2016**;129(1):67-77. https://doi.org/10.1007/s10265-015-0764-1

Takagi H, Tamiru M, Abe A, Yoshida K, Uemura A, Yaegashi H, Obara T, Oikawa K, Utsushi H, Kanzaki E, Mitsuoka C. MutMap accelerates breeding of a salt-tolerant rice cultivar. Nature Biotechnology. **2015**;33(5):445-449. https://doi.org/10.1038/nbt.3188

Ungerer N, Mücke N, Broecker J, Keller S, Frings S, Möhrlen F. Distinct binding properties distinguish LQ-type calmodulin-binding domains in cyclic nucleotide-gated channels. Biochemistry. **2011**;50(15):3221-3228. https://doi.org/10.1021/bi200115m

Wang R, Jing W, Xiao L, Jin Y, Shen L, Zhang W. The rice high-affinity potassium transporter1;1 is involved in salt tolerance and regulated by an MYB-type transcription factor. Plant Physiology. **2015**;168(3):1076-1090. https://doi.org/10.1104/pp.15.00298

Xue S, Yao X, Luo W, Jha D, Tester M, Horie T, Schroeder JI. AtHKT1;1 mediates nernstian sodium channel transport properties in *Arabidopsis* root stelar cells. PloS One. **2011**;6(9):e24725. https://doi.org/10.1371/journal.pone.0024725

Yao X, Horie T, Xue S, Leung HY, Katsuhara M, Brodsky DE, Wu Y, Schroeder JI. Differential sodium and potassium transport selectivities of the rice OsHKT2;1 and OsHKT2;2 transporters in plant cells. Plant Physiology. **2010**;152(1):341-355. https://doi.org/10.1104/pp.109.145722

# CHAPTER 2

# SECTION 1

# Chloride-Transporting OsHKT1;1 Splice Variants and Their Expression Profiles Under Salinity Stress in Rice

## Introduction

High concentrations of soluble or exchangeable salts (in most cases, the cation is $Na^+$) inhibit plant growth under salinity stress, which is a globally alarming issue that significantly lowers the yield and development of major crops. Rice (*Oryza sativa*) is the most susceptible to salt stress among cereal crops (Munns and Tester, 2008; Singh et al., 2009). When toxic Na ions are adequately excluded, redistributed, and compartmentalized in the plant body, the plants are likely to exhibit tolerance to salinity stress.

High-affinity $K^+$ transporters (HKTs) are known to be involved in the transport of $Na^+$ and $K^+$ in plants, and some of them are crucial for maintaining $Na^+/K^+$ balance under salinity stress (Rus et al., 2001; Mäser et al., 2002). Therefore, HKTs have been widely examined since the first report of the *TaHKT2;1* gene in bread wheat (*Triticum aestivum*) (Rubio et al., 1995). HKTs are classified into two subfamilies, and transporters belonging to subfamily 1 (HKT1s) have generally been shown to be selective for $Na^+$ (Hauser and Horie, 2010; Xue et al., 2012; Imran et al., 2020, 2021). The ability of plants to withstand salt has been demonstrated for both HKT1s and HKT2s.

In monocotyledon rice, the *japonica* cultivar was reported to maintain seven functional *HKT* genes, among which four genes (*OsHKT1;1*, *OsHKT1;3*, *OsHKT1;4*, and *OsHKT1;5*) were grouped in subfamily 1 (Garciadeblás et al., 2003; Horie et al., 2009). Heterologous expression studies of OsHKT1;1 from rice using *Xenopus laevis* (*X. laevis*) oocytes showed $Na^+$-selective transport in an inward-rectifying manner (Jabnoune et al., 2009; Imran et al., 2020). HKT1;1 transporters identified in various plant species exhibit robust $Na^+$ selectivity when expressed in *X. laevis* oocytes: AtHKT1;1 from *Arabidopsis* (Xue et al., 2011), HvHKT1;1 from barley (Han et al., 20118), CmHKT1;1 from pumpkin Wei et al., 2023a), SvHKT1;1 from halophytic turf

grass (*Sporobolus virginicus*) (Kawakami et al., 2020), VviHKT1;1 from grapevine (Henderson et al., 2018), and VcHKT1;1 from blueberry (Song et al., 2024). Some HKT1 transporters interact with other ion homeostasis systems, such as the SOS pathway and $K^+$ transporters (Shi et al., 2000; Zhu et al., 2002), forming a coordinated regulatory network that maintains ionic balance and cellular stability under salinity stress (Shabala and Cuin, 2008; Hasegawa et al., 2013). OsHKT1;1 has been shown to be involved in limiting $Na^+$ accumulation in leaves and contributing to salt tolerance based on the analysis of an insertional mutation in the *OsHKT1;1* gene (Wang et al., 2015a). Recent studies have further demonstrated that natural allelic variations in *OsHKT1;1* contribute significantly to genotypic differences in $Na^+$ distribution within rice. Genome-wide association analysis using a global diversity panel identified *OsHKT1;1* as the gene underlying a major QTL (RNC4) that regulates root $Na^+$ content, with indica accessions generally carrying alleles that promote higher root $Na^+$ accumulation than japonica accessions (Campbell et al., 2017). Functional assays revealed that three indica-predominant non-synonymous substitutions increased the inward $Na^+$ transport activity of OsHKT1;1, and introduction of the indica allele into a japonica background reproduced the high-root-$Na^+$ phenotype. These results support earlier findings that *OsHKT1;1* limits $Na^+$ accumulation in shoots and improves salt tolerance (Wang et al., 2015a). Furthermore, a combination of screening of salt-tolerant rice mutant lines and the MutMap method identified a key transcription factor gene that encodes a B-type response regulator OsRR22, suggesting the involvement of *OsHKT1;1* in rice salt tolerance (Takagi et al., 2015).

In my previous study, an interesting phenomenon was found in the *OsHKT1;1* gene in a salt-tolerant landrace, Pokkali, in which potential alternative splicing variants encoding transporters that show distinct ion selectivity were identified in addition to the full-length *OsHKT1;1* transcript (Imran et al., 2020). Alternative splicing (AS) is a post-transcriptional process that fine-tunes gene function. In rice, AS is broadly reprogrammed by salinity and other abiotic stresses, generating isoforms that adjust protein abundance and activity as conditions change (Ganie and Reddy, 2021). This regulatory flexibility is evident in genes such as *OsDREB2B*, *OsHSFA2d*, and *OsMYB7*, where stress-dependent switching to functional splice variants enhances stress tolerance (Magaraggia et al., 1997; Matsukura et al., 2010; Cheng et al., 2015; Ganie and Reddy, 2021). Similar patterns in other species reinforce the central role of AS in stress adaptation. In foxtail millet, for example, salt stress induces two *SiCYP19* splice

variants, and *SiCYP19-b* more effectively improves tolerance by increasing proline and reducing ROS (Zhang et al., 2024). In *Populus euphratica*, AS of *PeuHKT1;3* generates the isoform *PeuHKT1;3a*, which alters pore-loop structure, enhances $K^+$ transport, and improves $K^+/Na^+$ homeostasis (Lv et al., 2024). In *Arabidopsis*, *At-SRAS1* produces two splice variants with opposite functions: *At-SRAS1.1* (full-length, active E3 ligase) enhances salt tolerance, while *At-SRAS1.2* (truncated) reduces it (Zhou et al., 2021). In the halophyte *Thellungiella salsuginea*, salt stress induces multiple splice variants of *TsHKT1;2*, among which the functional isoforms (TsHKT1;2a/2b) interact with other HKT1 proteins to reduce $Na^+$ uptake and enhance salt tolerance (Lv et al., 2025). In rice, *OsHKT1;4* also shows tissue-dependent splice variation that affects $Na^+$ retrieval and supports ionic balance under salinity (Cotsaftis et al., 2012). Despite these findings, AS regulation of HKT transporters in rice remains largely uncharacterized, and only a few other studies have reported splicing variants of HKTs (Ren et al., 2015; Imran et al., 2021). Although alternative splicing of *OsHKT1;1* has been reported, the functional analyses of these variants, particularly whether they exhibit different transport characteristics from the full-length protein, remain unclear. Therefore, in the present study, I focused on one of the eight variants of the *OsHKT1;1* gene from Pokkali, *OsHKT1;1-V2*, to characterize its expression profile and transport properties. I present the results of heterologous expression analyses, which exhibit $Cl^-$ transport features with far less selectivity for $Na^+$ of OsHKT1;1-V2 than those of full-length OsHKT1;1. Furthermore, I showed evidence that identical potential splicing variants exist in a salt-sensitive *japonica* cultivar, Nipponbare, and that OsHKT1;1-V2 from Nipponbare also exhibits similar $Cl^-$ transport properties, although the expression levels of the full-length and OsHKT1;1-V2 variant seemed to be differentially regulated between the two varieties. I provide new insights into the mechanisms of ion homeostasis in rice, mediated by the potential alternative splicing of an important salt tolerance gene, *OsHKT1;1*, and discuss questions to be elucidated for pursuing the physiological impacts.

## Materials and Methods

### Plant Material and Growth Conditions

Seeds of Pokkali (*Oryza sativa* L. ssp. *indica*), a salt-tolerant rice cultivar, and Nipponbare (*Oryza sativa* L. ssp. *japonica*), a salt-sensitive rice cultivar, were used. Seeds were sterilized twice by using 50% bleach for 10 minutes and then washed five

times with sterilized water. For germination, ten seeds were placed on a mesh in a sterilized pot with 20 mL of 1 mM $CaSO_4$. Plants were grown in a controlled environment growth chamber. The temperature was maintained at 28˚C and 25˚C in a 12-h day (250 μmol $m^{-2}$ $s^{-1}$ illumination) and 12-h night, respectively. 5-day-old seedlings were transferred to 3.5-liter pots and grown hydroponically with the solutions containing 4 mM $KNO_3$, 1 mM $NH_4H_2PO_4.2H_2O$, 1 mM $CaCl_2.2H_2O$, 1 mM $MgSO_4.7H_2O$, and micronutrients (1 ppm Fe, 0,5 ppm B, 0.5 ppm Mn, 0.05 ppm Zn, 0.02 ppm Cu, and 0.01 ppm Mo). The pH of the nutrient solution was adjusted to 5.5 with NaOH. 9-day old plants were used for cDNA isolation. For the gene expression study, 14-day-old plants were subjected to 100 mM NaCl stress for 0 hr (control), 6 hr, 12 hr, 24 hr, and 48 hr. Roots and shoots were then collected separately at different time points.

**Extraction of RNA, and cDNA Synthesis**

Total RNA was extracted from root or shoot samples using a RNeasy Plant Mini Kit (Qiagen) and then treated with RNase-free DNase I (Ambion, Austin, TX, USA). The quality and integrity of RNA samples were determined by a NanoDrop ND-1000 Spectrophotometer (Nanodrop, Wilmington, DE, USA). The first strand coding DNA (cDNA) was synthesized from total RNA using ReverTra Ace qPCR RT Master Mix (TOYOBO), according to the manufacturer's instructions. *OsHKT1;1* cDNAs was amplified by using *OsHKT1;1* cloning primers (Table 1.1) and confirmed by analyzing the sequence after cloning into the pCR4 topo vector (Invitrogen).

**Table 1.1.** Gene-specific primer pairs were used for the cloning and in the real-time PCR experiments.

| | 5' → 3' | For full-length cloning | For RT-PCR and real-time RT-PCR |
|---|---|---|---|
| OsHKT1;1-FL | Fw | GTTGAAGAATGCATCCACCAAG | |
| | Rv | CTCATTTCAGGATGAACTCCTTG | |
| OsHKT1;1-FL | Fw | | CCCTTTGGTAGTTCAGCTCGTTT |
| | Rv | | GATGACAGAACTGGAAATGACAG |
| OsHKT1;1-V2 | Fw | | CGCAAAACCAGATGCAAGAAATG |
| | Rv | | CCTCACATGCAAATGTTTGTAGCC |

**Preparation of cRNA for *X. laevis* Oocytes Heterologous Expression**

The full-length of OsHKT1:1 (OsHKT1;1-FL; accession number: LC533375) and a variant (OsHKT1;1-V2; accession number: LC533377) cRNAs from Pokkali

(*Oryza sativa* L. ssp. *indica*) were already prepared (Imran et al., 2020). *OsHKT1;1* cDNAs from Nipponbare were subcloned into the pXβG vector between the 5′ and 3′ untranslated regions of the *Xenopus* β-globin gene. cRNAs were synthesized *in vitro* from the linearized vector using the mMESSAGE mMACHINE T3 kit (Ambion). Oocytes were collected and injected with 50 nL of cRNA at a concentration of 50 ng or 2.5 ng, or with 50 nL of nuclease-free water for the negative control group. The oocytes were then incubated at 18 °C in a modified Barth's solution (MBS; 88 mM NaCl, 1 mM KCl, 2.4 mM $NaHCO_3$, 15 mM Tris-HCl (pH 7.6), 0.3 mM $Ca(NO_3)_2.4H_2O$, 0.41 mM $CaCl_2.4H_2O$, 0.82 mM $MgSO_4.7H_2O$, 10 μg $ml^{-1}$ sodium penicillin, and 10 μg $ml^{-1}$ streptomycin sulfate) until electrophysiological recordings as described previously (Katsuhara et al., 2002).

**Electrophysiology**

Oocyte currents were measured using the two-electrode voltage-clamp (TEVC) technique (Figure 2.1), conducted 1 d after cRNA injection unless otherwise mentioned. The two-electrode voltage-clamp recordings and data analysis were performed using an Axoclamp 900A amplifier and an Axon Instruments Digidata 1440A and pCLAMP 10 (Molecular Devices, USA). Both membrane potential and currents were recorded. A correction was made for voltage drop through the series resistance of the bath and the reference electrode using a voltage recording microelectrode in the bath close to the oocyte surface (potential difference between the local electrode and the reference subtracted from the potential of intracellular electrodes in the amplifier for real-time series resistance correction). All electrodes were filled with 3M KCl. The oocyte was continuously perfused during the voltage-clamp experiment. The bath solutions were prepared with a baseline concentration of 1.8 mM MgCl2, 1.8 mM CaCl2, and 10 mM HEPES at pH 7.5 with Tris, and chloride salts of monovalent cations were used. Gluconic acid magnesium (II) salt or D-mannitol was added as needed to keep the osmolality of external solutions between 200 and 220 mOsm in all measurements. To get current-voltage relationships, voltage steps (2 sec) were applied from +30 to −120 mV in 15 mV decrements unless otherwise mentioned. All experiments were performed at room temperature (20-22 ˚C).

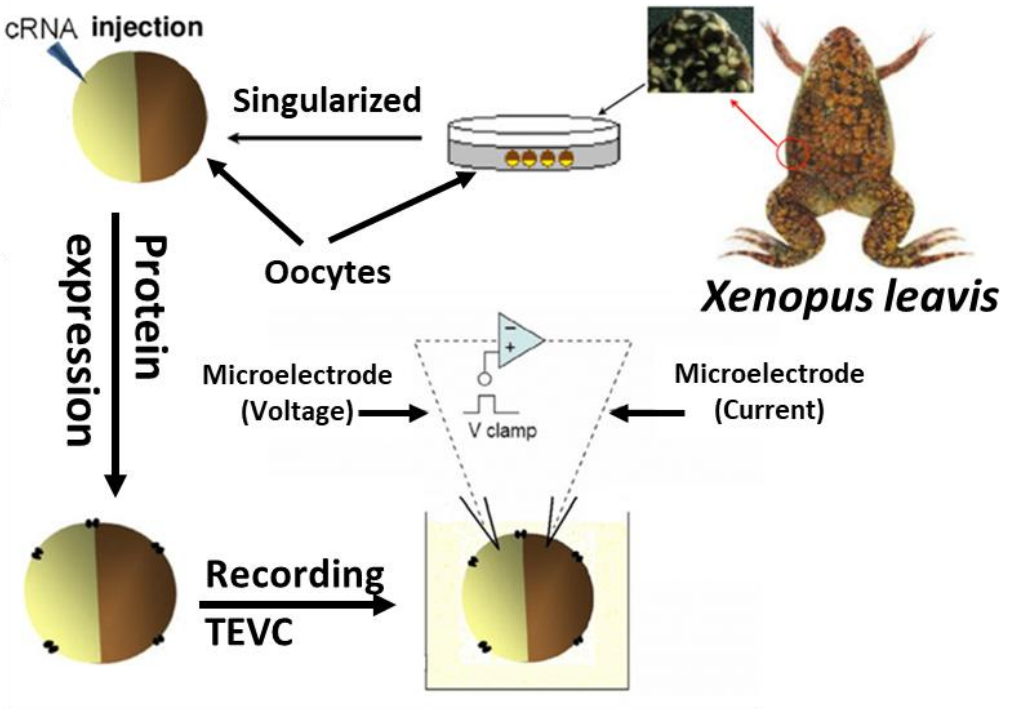


**Figure 2.1.** An overview of oocyte preparation, cRNA injection, protein expression in oocytes, and TEVC measurement. Frog was operated and oocytes were taken from ovarian sacs, treated with collagenase to be singularized. After that treatment, oocytes were washed, sorted, injected, and then incubated for protein expression in MBS storage solution at 18ºC. Oocytes were pierced with two microelectrodes, one to maintain a constant voltage, the other to register changes in current, and then were recorded. Modified from Sopjani, 2010.

**Determination of $Cl^-$ Content in *X. laevis* Oocytes**

Oocytes were injected with 50 nl of water or cRNA of *OsHKT1;1-FL* (2.5 ng and 25 ng) and *OsHKT1;1-V2* (2.5 ng and 25 ng), then incubated in 1× MBS medium for 24 hours (*OsHKT1;1-FL*) or 4 hours (*OsHKT1;1-V2*) at 18°C. For the measurement of $Cl^-$ accumulation, the oocytes were transferred to 1 mL of Na-gluconate or choline-Cl solutions. The Na-gluconate solution contained 96 mM Na gluconate, 1.8 mM Ca gluconate, 1.8 mM Mg gluconate, 1.8 mM mannitol, and 10 mM HEPES (pH 7.5 with Tris). The choline-Cl solution contained 96 mM choline Cl, 1.8 mM Ca gluconate, 1.8 mM Mg gluconate, 1.8 mM mannitol, and 10 mM HEPES (pH 7.5 with Tris). After a 6-hour incubation at room temperature, the oocytes were washed three times with isotonic Ca-gluconate solution and then placed in a 1.5 mL tube to homogenize in Milli-Q water. Cell debris was removed by centrifugation. The supernatant was collected, diluted, and used for ion analysis using an anion chromatography system with the cooperation of Dr. Horie at Shinshu University.

**Subcellular Localization Analysis in Plant Cells Using *Arabidopsis* Protoplasts**

Subcellular localization analysis of OsHKT1;1-FL and OsHKT1;1-V2 proteins was conducted in Arabidopsis leaf protoplasts (Wu et al., 2009), which were transfected with the modified pTH2 vector (Chiu et al., 1999) containing OsHKT1;1-FL or OsHKT1;1-V2 fused with GFP at the N-terminus under the control of the CaMV 35S promoter. Transfection was performed using the polyethylene glycol (PEG 4000) method, as described by Yoo et al. (2007) and Sasaki et al. (2016). Protoplasts suspended in the re-suspension solution (0.5 M mannitol, 20 mM KCl, and 4 mM MES, pH 5.7) were incubated in the dark at 24 °C for 16 hr (Zhang et al., 2011). The plasma membrane was visualized using FM4-64 (16 μM, 5 min). Images of the protoplasts were captured using an Olympus FluoView 1000 Confocal Microscope (Olympus Corporation, Hachioji, Tokyo, Japan). GFP was detected using 473 nm excitation with a 490–525 nm bandpass filter, whereas FM4-64 and chlorophyll were observed with 543 nm excitation and a 560–620 nm bandpass filter.

**Subcellular Localization in Oocytes by Immunocytochemistry**

Subcellular localization in oocytes was analyzed using OsHKT1;1-FL and OsHKT1;1-V2 with a FLAG tag (DYKDDDDK) at their N-termini. cRNAs were synthesized using an oocyte expression vector, pXβG vector, including O*sHKT1;1-FL* or *OsHKT1;1-V2* with the sequence of FLAG tag, according to the procedure outlined by Imran et al. (2020). Immunohistochemical analysis was performed as described by Shibasaka et al. (2021). A volume of 50 nL for OsHKT1;1-FL or OsHKT1;1-V2 cRNA (50 ng or 2.5 ng), or RNase-free water as a negative control was injected into the oocyte and incubated at 18 °C for 24 hr (OsHKT1;1-FL) or 4 hr (OsHKT1;1-V2). Subsequently, the samples were fixed for 3 hr in 4% (w/v) formaldehyde solution (pH 7.4) and embedded in 5% agarose. Sections of 100 μm thickness were prepared using a micro slicer (Doshin EM, Osaka, Japan) and subjected to blocking in a buffer containing 50 mM Tris (pH 8.0), 150 mM NaCl, 0.1% Tween 20, and 3% BSA for 1 hr at 25°C. Immunolabeling was performed using primary antibodies, including rabbit anti-FLAG (raised against the synthetic peptide CDYKDDDDK, Invitrogen, Carlsbad, CA, USA), applied overnight at 4°C. After three washes, the samples were incubated for another hour with a secondary antibody (Alexa Fluor 488-conjugated goat anti-rabbit IgG, Invitrogen, Carlsbad, CA, USA). After two washes with TBS-T (50 mM Tris, pH 8.0, 150 mM NaCl, 0.1% Tween 20) and a final wash with TBS (50 mM Tris,

pH 8.0, 150 mM NaCl), fluorescent signals were observed using a fluorescence microscope (BZ-X700, Keyence, Osaka, Japan).

**Functional Characterization of OsHKT1;1-FL and OsHKT1;1-V2 in Yeast**

The CDSs of OsHKT1;1-FL, and OsHKT1;1-V2 were cloned into pYES2 vectors and then transformed into the well-known $Na^+$-sensitive yeast strain G19 that lacks $Na^+$ efflux transporters ENA1-4 (Quintero et al., 1996; Haxim et al., 2023) and $Cl^-$sensitive mutant yeast strain *gef1* that lacks $Cl^-$ efflux transporter GEF1 (Nakamura et al., 2006; Wei et al., 2016c). Positive transformants were selected on Ura-selective medium plates [0.67% (w/v) yeast nitrogen base without amino acids, 0.077% (w/v) drop out mix-Ura, 2% (w/v) glucose, and 2% (w/v) agar]. For growth assays, overnight cultures of each transformant were grown at 30 °C in SC-Ura medium and adjusted to an $OD_{600}$ of 1.0. Tenfold serial dilutions ($10^0$–$10^{-4}$) were prepared and spotted onto Ura-induction plates containing 0.67% (w/v) yeast nitrogen base without amino acids, 0.077% (w/v) dropout mix-Ura, 2% (w/v) galactose, 1% (w/v) raffinose, and 2% (w/v) agar. For the G19 strain (Figure 2.13), plates contained either 0 mM or 50 mM NaCl and were incubated at 30 °C for 4 days. For the *gef1* strain (Figures 2.14, 2.15), transformants were spotted on plates supplemented with 0 mM, 0.8 M, 1.2 M, or 1.5 M NaCl, or with 1.5 M NMDG-Cl. These plates were incubated at 30 °C for 6–11 days, depending on the salt concentration. After incubation, yeast growth patterns were documented.

**Determination of $Na^+$ Contents in Yeast Cells**

To quantify intracellular $Na^+$, each transgenic G19 line was grown in liquid synthetic complete (SC) medium supplemented with or without 50 mM NaCl and galactose at 30 °C. Prior to the main culture, each transformant was cultured in a glass test tube filled with 5 ml SC-Ura glucose medium for overnight at 30 °C. 0.1 ml of each full growth-culture solution was inoculated in a 300 ml Erlenmeyer flask filled with 100 ml SC-Ura galactose medium. After incubation for 18 hr (control) and 21 hr (NaCl) at 30 °C at 130 rpm, each line was collected by swing-bucket centrifugation using 50 ml centrifuge tubes and then washed by 100 ml of sterilized ultrapure water. After 3-time washes, 10 ml of the washed culture solution was divided in a 15 mL centrifuge tube, and then samples were collected by swing-bucket centrifugation. All harvested samples were dried at 60 °C for 2 days. The dried samples were weighed and digested by 1 ml

of ultrapure nitric acid for 24 hr. Digests were subsequently heated at 95 °C for 15 min, which was repeated two times. Sodium ($Na^+$) concentrations were quantified by inductively coupled plasma–mass spectrometry (ICP-MS).

**Expression Analysis**

Total RNA extraction, first-strand cDNA synthesis, and absolute quantification of gene expression with specific cDNAs standards. The total RNA was treated with Dnase to remove any contaminating genomic DNA (gDNA). The *OsHKT1;1* variants were amplified using specific primers (Table 1). Absolute quantification was performed in the quantitative real-time PCR analysis (qPCR) using the 7300 real-time PCR machine (Applied Biosystem) as described in (Mahdieh et al., 2008) to analyze the expression level of each *OsHKT1;1* variant.

**Statistical Analyses**

Statistical analyses were performed using IBM SPSS Statistics (version 25). Significant differences were identified using a *t*-test (***$p < 0.001$) and a one-way ANOVA, and Tukey's HSD test ($p < 0.05$).

**Results**

**Identification of a Functional Frame in the OsHKT1;1-V2 Variant**

In my previous study, two start codons were identified in the *OsHKT1;1-V2* variant (Figure 2.2A) (Imran et al., 2020). I artificially truncated and produced two fragments of *OsHKT1;1-V2* named *OsHKT1;1-V2(1)* and *OsHKT1;1-V2(2)*. *OsHKT1;1-V2(1)* is composed of 519 nucleotides, encoding 172 putative amino acid residues. In contrast, *OsHKT1;1-V2(2)* is composed of 957 nucleotides encoding 318 putative amino acid residues (Figures 2.2A, 2.3). *X. laevis* oocytes were injected with cRNAs of *OsHKT1;1-V2*, *OsHKT1;1-V2(1)*, and *OsHKT1;1-V2(2)*, and TEVC experiments were performed to identify which fragment induces bidirectional ionic currents like OsHKT1;1-V2 (Imran et al., 2020). OsHKT1;1-V2(1) but not OsHKT1;1-V2(2) showed ionic currents in both NaCl and KCl bath solutions as OsHKT1;1-V2 (Figure 2.2B, C). These results suggest that the start codon of OsHKT1;1-V2 is the 1$^{st}$ methionine. Furthermore, histochemical analysis indicated that fluorescence derived from FLAG tag-fused with OsHKT1;1-FL and OsHKT1;1-V2 proteins were localized

in the plasma membrane (PM) of oocytes (Figure 2.2D, E). In contrast, control oocytes injected with water showed no robust green fluorescence in the PM (Figure 2.2F).

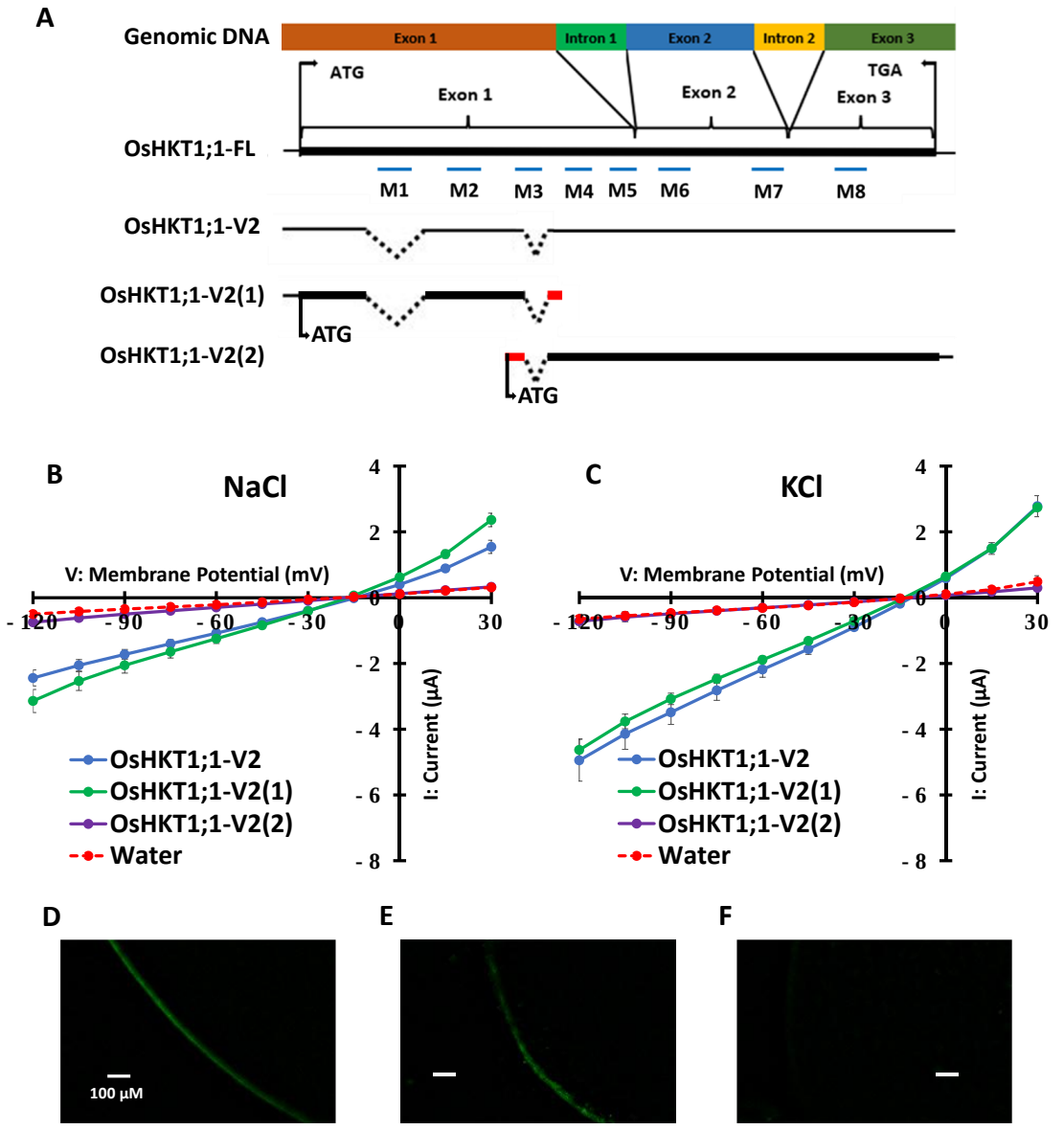


**Figure 2.2.** The first methionine functions as a start codon in the *OsHKT1;1-V2* variant. (**A**) Schematic representation of *OsHKT1;1-V2* mRNA, presumably produced by alternative splicing, and its artificially truncated fragments, OsHKT1;1-V2(1) and OsHKT1;1-V2(2), each of which contains only one first methionine that could function as a start codon. Boxes indicate amino acid regions that are the same as those in OsHKT1;1-FL (black) or different from those in OsHKT1;1-FL (red) because of the frameshift. Dotted lines indicate missing nucleotide regions (gaps compared to the OsHKT1;1-FL sequence) due to alternative splicing events. The predicted transmembrane domains (M1–M8) were annotated based on previously curated information in the UniProt database. (**B**, **C**) Transport properties of OsHKT1;1-V2 and its artificial variants, characterized by two-electrode voltage-clamp experiments using *X. laevis* oocytes immersed in external solutions containing 96 mM NaCl or 96 mM KCl. Data represent

means ± SE, *n* = 15–18, from three independent experiments performed using different batches of oocytes. (**D**-**F**) Detection of fluorescence derived from the FLAG-tag in oocytes expressing FLAG-OsHKT1;1-FL (**D**) or FLAG-OsHKT1;1-V2 I or in oocytes injected with water (**F**). All external solutions contained 1.8 mM $CaCl_2$, 1.8 mM $MgCl_2$, 1.8 mM mannitol, and 10 mM HEPES (pH 7.5 with Tris) as background elements. Oocytes were isolated and injected with 50 ng cRNAs/50 nL or 50 nL of nuclease-free water as a negative control, and then incubated for approximately 4 hr at 18 °C.

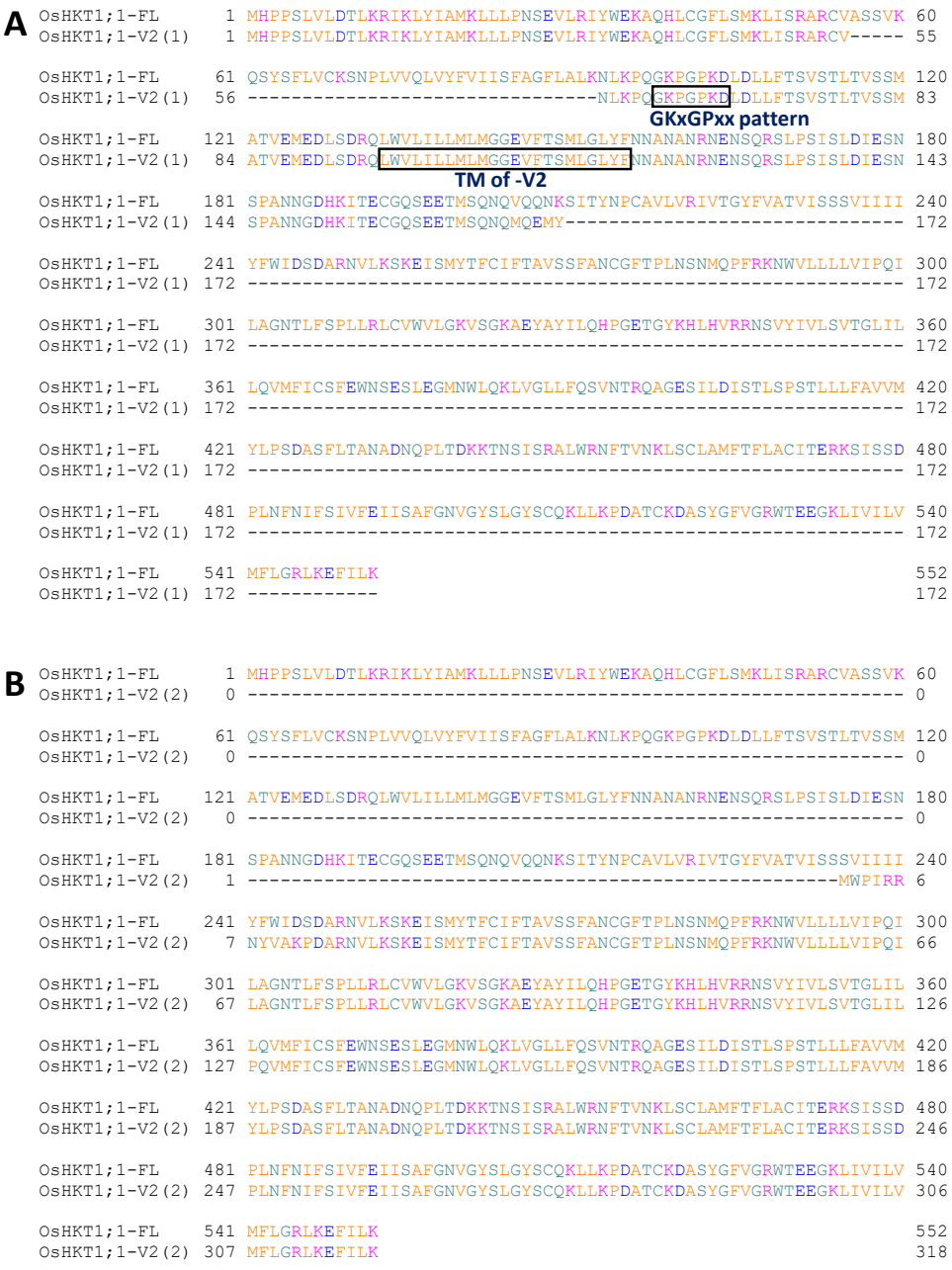


**Figure 2.3.** Amino acid sequence alignment of OsHKT1;1-FL and OsHKT1;1-V2. (**A**) OsHKT1;1-FL vs. OsHKT1;1-V2(1). (**B**) OsHKT1;1-FL vs. OsHKT1;1-V2(2). GENETYX ver. 16 was used for comparisons.

**Subcellular Localization of GFP-fused OsHKT1;1-FL and OsHKT1;1-V2 in Plant Cells**

To study the subcellular localization in plant cells, green fluorescence protein (GFP) was fused with OsHKT1;1-FL and OsHKT1;1-V2 at the N-terminus. DNA constructs to express either GFP, GFP-OsHKT1;1-FL, or GFP-OsHKT1;1-V2 were introduced into *Arabidopsis* leaf protoplasts (Wu et al., 2009). Cells expressing GFP showed strong fluorescence in the cytosol, which did not overlap with the plasma membrane marker FM4-64 (Figure 2.4A–D). GFP fluorescence from cells expressing GFP-OsHKT1;1-FL was observed at the cell periphery, overlapping with FM4-64 fluorescence (Figure 2.4F–I). A similar overlap of GFP and FM4-64 fluorescence was observed in cells expressing GFP-OsHKT1;1-V2 (Figure 2.4K–N). Plot-profile fluorescence intensity analysis of the merged fluorescence images supported the above-mentioned observation (Figure 2.4E, J, O). Together with the negative control experiments shown in Figure 2.4P-S, these results suggest the plasma membrane localization of OsHKT1;1-V2 as OsHKT1;1-FL.

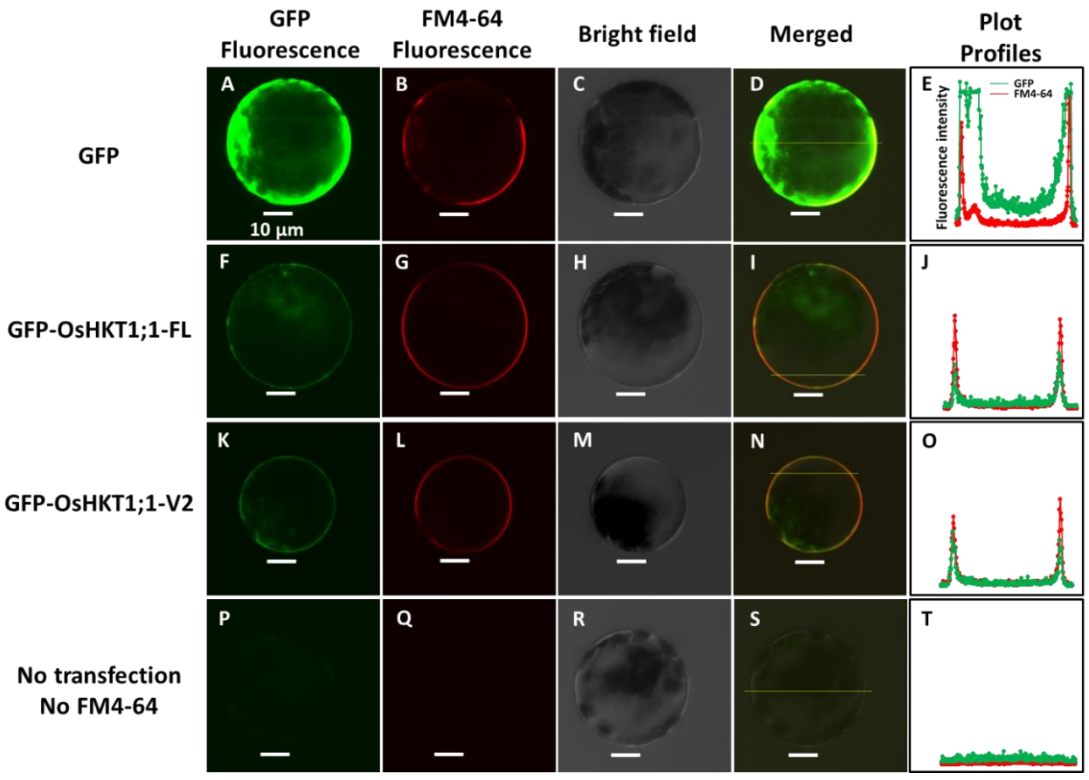


**Figure 2.4.** Subcellular localization of GFP-fused OsHKT1;1 transporters in Arabidopsis protoplasts. GFP (**A**–**D**), GFP-OsHKT1;1-FL (**F**–**I**), or GFP-OsHKT1;1-V2 (**K**–**N**) was transiently overexpressed in Arabidopsis leaf protoplasts. The cells were incubated with FM4-64, which was used as a PM marker. Protoplasts that were not transfected or treated with FM4-

64 (**P**–**S**) were used as negative controls. Plot-profile fluorescence intensity analysis of protoplasts expressing different constructs (red and green colors represent fluorescence from FM4-64 and GFP, respectively): GFP I, GFP-OsHKT1;1-FL (**J**), GFP-OsHKT1;1-V2 (**O**), and untransfected and no FM4-64-treated protoplast (**T**).

**Substrate Selectivity of OsHKT1;1-FL and OsHKT1;1-V2**

Current-voltage relationships were obtained in the presence of 96 mM NaCl (96 mM $Na^+$ and 96 mM $Cl^-$), 9.6 mM NaCl + 84.6 mM Na gluconate (total 96 mM $Na^+$ and 9.6 mM $Cl^-$), and 9.6 mM NaCl + 84.6 mM Choline Cl (9.6 mM $Na^+$ and total 96 mM $Cl^-$) by conducting electrophysiological TEVC experiments using *X. laevis* oocytes. As described previously (Jabnoune et al., 2009), a decrease in $Na^+$ concentration from 96 mM to 9.6 mM largely reduced the inward currents in OsHKT1;1-FL and showed no tendency to produce robust outward currents (Figure 2.5).

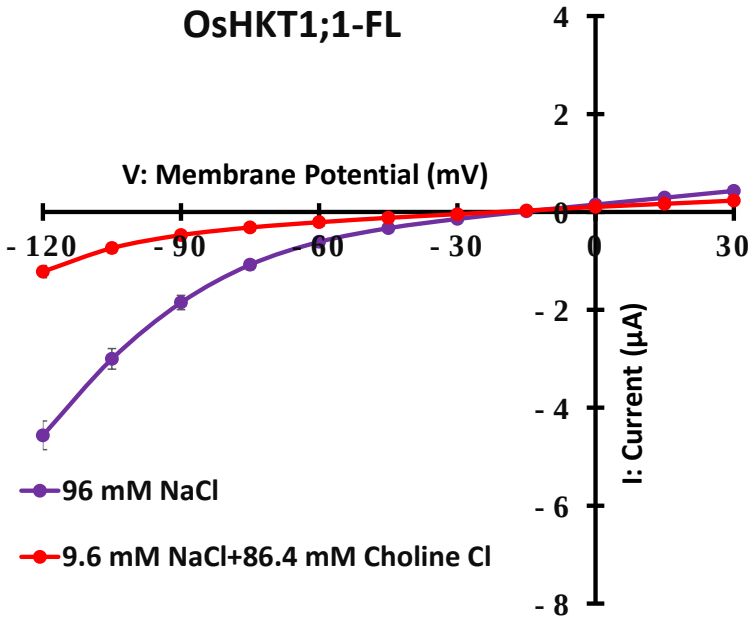


**Figure 2.5.** Current-voltage relationships in *X. laevis* oocytes expressing OsHKT1;1-FL (Pokkali-derived). The external solutions used were 96 mM NaCl or 9.6 mM NaCl + 86.4 mM choline chloride. All external solutions contain, as background elements, 1.8 mM $CaCl_2$, 1.8 mM $MgCl_2$, 1.8 mM mannitol, and 10 mM HEPES (pH 7.5 with Tris). Oocytes were injected with 50 ng cRNAs/50 nL and incubated for 18 hr at 18 °C before TEVC measurements. Data are presented as mean ± SE, $n$ = 8, from two independent experiments performed with different batches of oocytes.

In contrast, the same change in solution did not affect OsHKT1;1-V2-mediated currents (Figure 2.6A). Next, I changed the $Cl^-$ concentration of the bath solution while keeping the $Na^+$ concentration at 96 mM during TEVC measurements. The 10 times reduction in the $Cl^-$ concentration led to an increase in OsHKT1;1-V2-mediated currents with a positive shift in the reversal potential of 13 mV (Figure 2.6A, purple and green lines). Note that similar large currents were never observed in water-injected oocytes under any bath condition (Figure 2.6B).

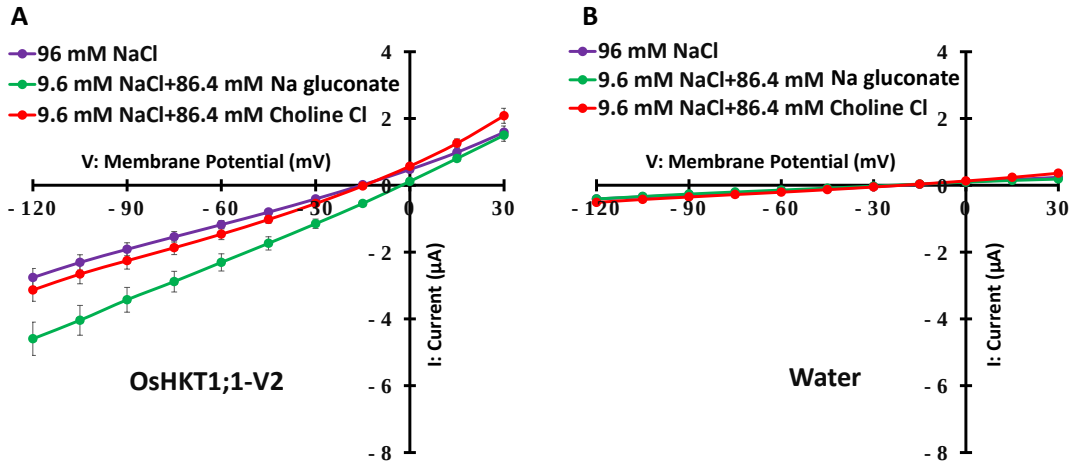


**Figure 2.6.** Current-voltage relationships of OsHKT1;1-V2 (**A**) expressed in *X.* laevis oocytes and the oocytes injected with water (**B**). The external solutions used were 96 mM NaCl, 9.6 mM NaCl + 86.4 mM Na gluconate, or 9.6 mM NaCl + 86.4 mM Choline Cl. All external solutions contain, as background elements, 1.8 mM $CaCl_2$, 1.8 mM $MgCl_2$, 1.8 mM mannitol, and 10 mM HEPES (pH 7.5 with Tris). Oocytes were injected with 50 ng cRNAs/50 nL and then incubated for approximately 4 hr (OsHKT1;1-V2) or 18 hr (water-injected oocytes) at 18 °C before TEVC measurements (note that incubation of V2-expressing oocytes for more than 4 hr made it difficult to use them for TEVC experiments due to apparent damage). Data are presented as means ± SE, $n$ = 10–15, from two independent experiments performed with different batches of oocytes.

Next, oocytes expressing OsHKT1;1-V2 were analyzed in 96 mM NaCl (96 mM $Na^+$ and 96 mM $Cl^-$), 96 mM Na gluconate (total 96 mM $Na^+$ and 0 mM $Cl^-$), and 96 mM Choline Cl (0 mM $Na^+$ and total 96 mM $Cl^-$) solutions with voltage steps from +90 to −120 mV in 15 mV decrements to examine outward currents. OsHKT1;1-V2 expressed in oocytes exhibited large outward currents with no reversal potential shift when the solution was changed from 96 mM NaCl to 96 mM Choline Cl, by which $Na^+$ concentration was decreased from 96 mM to 0 mM (Figure 2.7A, purple and red lines).

In contrast, reversal potential shifts occurred according to a change in extracellular $Cl^-$ concentration from 96 mM to 0 mM in OsHKT1;1-V2 (Figure 2.7A, purple and red lines vs. green line). Note that endogenous outward currents were also observed in water-injected oocytes, but they were never the same extent as OsHKT1;1-V2-expressing oocytes in every bath condition (Figure 2.7B). These results suggest that the currents induced by OsHKT1;1-V2 largely depend on $Cl^-$ influx.

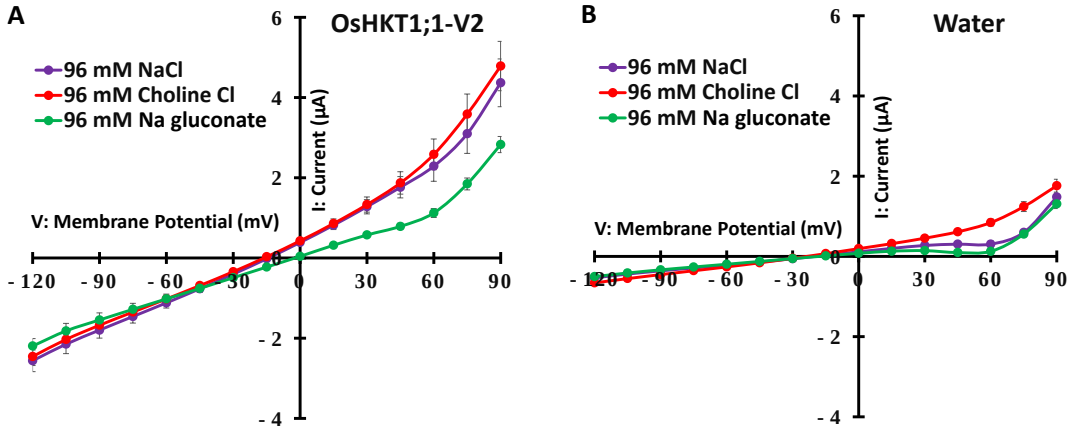


**Figure 2.7.** Current-voltage relationships of oocytes expressing OsHKT1;1-V2 (**A**) or oocytes injected with water (**B**) as a negative control. The external solutions included 96 mM NaCl, 96 mM Na gluconate, or 96 mM Choline Cl. The 96 mM NaCl solution contained background elements such as 1.8 mM $CaCl_2$, 1.8 mM $MgCl_2$, 1.8 mM mannitol, and 10 mM HEPES (pH 7.5 with Tris). The 96 mM Na gluconate and 96 mM choline chloride solutions contained background elements such as 1.8 mM Ca gluconate, 1.8 mM Mg gluconate, 1.8 mM mannitol, and 10 mM HEPES (pH 7.5 with Tris). Data are presented as mean ± SE, *n* = 10–16, from two independent experiments using different batches of oocytes.

### Substrate Concentration Dependency of OsHKT1;1-FL and OsHKT1;1-V2

Further TEVC measurements were performed using oocytes expressing OsHKT1;1-FL or OsHKT1;1-V2 in a series of bath solutions that contained $Cl^-$ as the sole permeable monovalent anion (96, 48, 12, and 6 mM as choline chloride) or $Na^+$ as the sole permeable monovalent cation (96, 48, 12, and 6 mM as Na gluconate). OsHKT1;1-FL-expressing oocytes showed currents comparable to those of water-injected control oocytes, with no reversal potential shift in a series of changes in $Cl^-$ concentration (Figures 2.8A, B, 2.9B). However, OsHKT1;1-FL showed large and various currents with reversal potential shifts in a series of changes in the $Na^+$ concentration (Figures 2.10A, B, 2.11). These data suggest that OsHKT1;1-FL mediates the transport of $Na^+$. In contrast, oocytes expressing OsHKT1;1-V2 exhibited

robust inward and outward currents with reversal potential shifts in a series of changes in the $Cl^-$ concentration (Figure 2.8C, D). OsHKT1;1-V2-expressing oocytes showed larger currents than water-injected control oocytes in accordance with a series change in the $Na^+$ concentration; however, the reversal potential did not alter as in oocytes expressing OsHKT1;1-FL (Figures 2.10B, C, D, 2.9A). These data suggest that, unlike OsHKT1;1-FL, OsHKT1;1-V2 is selective for $Cl^-$ and mediates its influx and efflux.

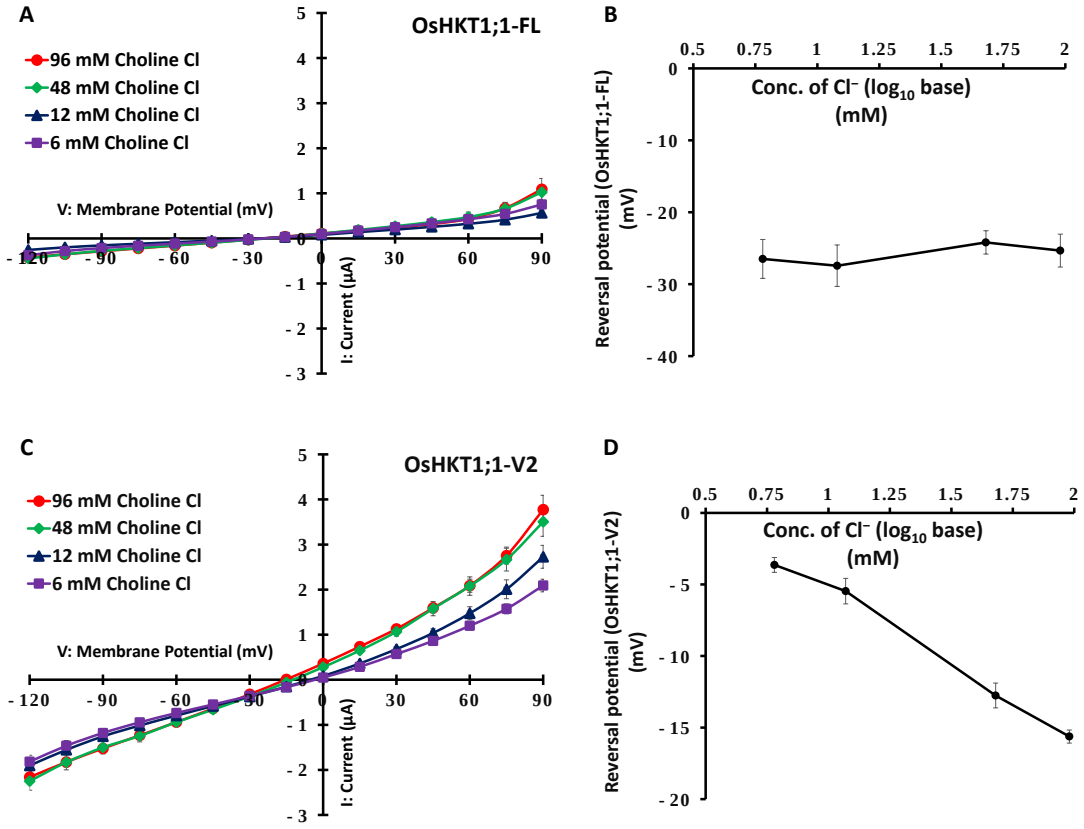


**Figure 2.8.** Chloride concentration dependency of OsHKT1;1-FL and OsHKT1;1-V2 expressed in X. laevis oocytes. (**A**, **C**) Current-voltage relationships of oocytes expressing OsHKT1;1-FL and OsHKT1;1-V2. (**B**, **D**) Log10 base reversal potential analysis of OsHKT1;1-FL and OsHKT1;1-V2, respectively. A series of choline chloride solutions with concentrations ranging from 96 mM to 6 mM was used as the external bath solution. The basic components of the solutions were 1.8 mM $CaCl_2$, 1.8 mM $MgCl_2$, 1.8 mM mannitol, and 10 mM HEPES, and the pH was adjusted to 7.5 using Tris. The 48-, 12-, and 6-mM choline chloride solutions contained 38-, 63-, and 68-mM Mg gluconate, respectively. Oocytes were isolated and injected with 2.5 ng cRNAs/50 nL and then incubated for approximately 18 hr for OsHKT1;1-FL or 4 hr for OsHKT1;1-V2 at 18 °C. To obtain current-voltage relationships, voltage steps (2 sec) were applied from +90 to −120 mV in 15 mV decrements. Data are presented as mean ± SE, $n$ = 16–18, from two independent experiments using different batches of oocytes.

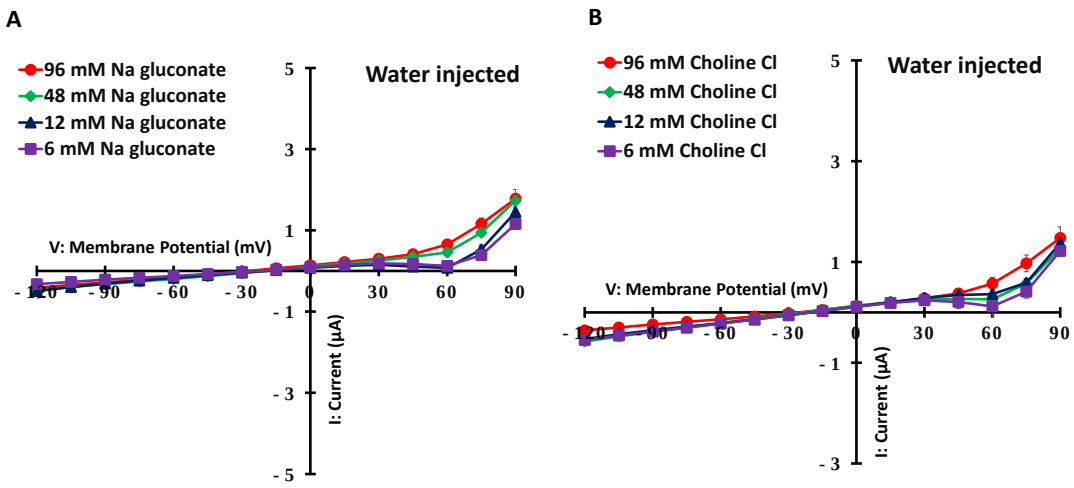


**Figure 2.9.** Current-voltage relationships of oocytes injected with water, obtained under various concentrations of Na gluconate (**A**) or Choline Cl (**B**). Na gluconate solutions contained basic components as 1.8 mM Ca gluconate, 1.8 mM Mg gluconate, 1.8 mM mannitol, and 10 mM HEPES, and the pH was adjusted to 7.5 using Tris. Choline Cl solutions contained basic components as 1.8 mM $CaCl_2$, 1.8 mM $MgCl_2$, 1.8 mM mannitol, and 10 mM HEPES, and the pH was adjusted to 7.5 with Tris. The 48-, 12-, and 6-mM sodium gluconate and choline chloride solutions contained 38-, 63-, and 68-mM Mg gluconate, respectively. Data are presented as means ± SE, *n* = 6–8, from two independent experiments performed on different oocyte batches.

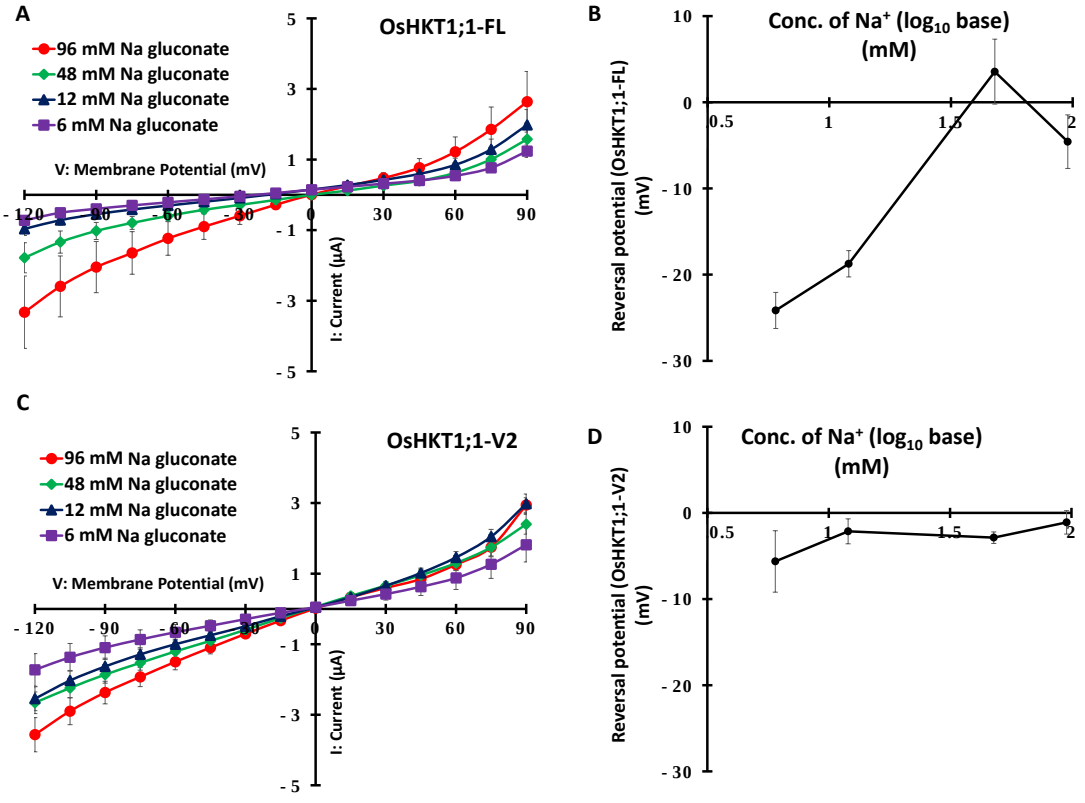

**Figure 2.10.** Sodium concentration dependency of OsHKT1;1-FL and OsHKT1;1-V2 expressed in X. laevis oocytes. (**A**, **C**) Current-voltage relationships from oocytes expressing OsHKT1;1-FL and OsHKT1;1-V2, respectively. (**B**, **D**) Log10 base reversal potential analysis of OsHKT1;1-FL and OsHKT1;1-V2, respectively. A series of sodium gluconate solutions with concentrations ranging from 96 mM to 6 mM was used as the external bath solution. The basic components of the solutions contained 1.8 mM Ca gluconate, 1.8 mM Mg gluconate, 1.8 mM mannitol, and 10 mM HEPES, and the pH was adjusted to 7.5 using Tris. The 48-, 12-, and 6-mM sodium gluconate solutions contained 38-, 63-, and 68-mM Mg gluconate, respectively. Oocytes were isolated and injected with 2.5 ng cRNAs/50 nL and then incubated for about 18 hr for OsHKT1;1-FL or 4 hr for OsHKT1;1-V2 at 18 °C. To obtain current-voltage relationships, voltage steps (2 sec) were applied from +90 to −120 mV in 15 mV decrements. Data are presented as mean ± SE, $n$ = 15–16, from two independent experiments using different batches of oocytes.

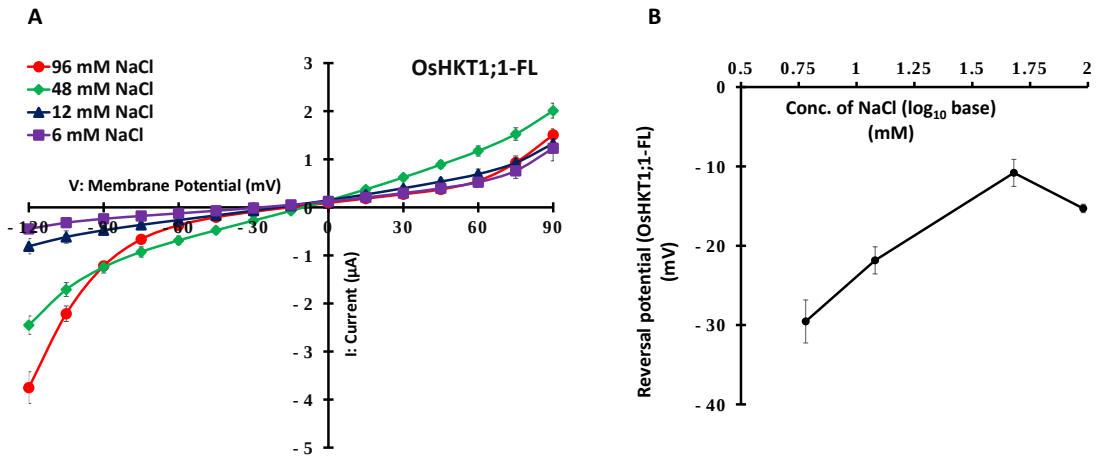


**Figure 2.11.** Sodium concentration dependency of OsHKT1;1-FL, derived from Nipponbare, expressed in *X. laevis* oocytes. (**A**) Current-voltage relationships of oocytes expressing OsHKT1;1-FL. (**B**) Log10 base reversal potential analysis of oocytes expressing OsHKT1;1-FL. A series solution of NaCl from 96 mM to 6 mM was used as an external solution, the background elements of which were 1.8 mM $CaCl_2$, 1.8 mM $MgCl_2$, 1.8 mM mannitol, and 10 mM HEPES (pH 7.5 with Tris). The 48 mM to 6 mM NaCl solutions contained 38-, 63-, or 68-mM gluconic acid of magnesium (II). Oocytes were isolated and injected with 2.5 ng cRNAs/50 nL and then incubated for approximately 18h at 18 °C. To get current-voltage relationships, voltage steps (2 sec) were applied from +90 to −120 mV in 15 mV decrements. Data are presented as means ± SE, $n$ = 10.

## $Cl^-$ Contents in Oocytes

Cl ion accumulation was investigated using oocytes injected with water, *OsHKT1;1-FL* cRNA, or *OsHKT1;1-V2* cRNA, which were incubated in 96 mM

choline chloride-containing medium (Figure 2.12). The total $Cl^-$ content showed that OsHKT1;1-V2-expressing oocytes (2.5 ng cRNA) accumulated significantly more $Cl^-$ than OsHKT1;1-FL-expressing (2.5 ng cRNA) and water-injected oocytes (Figure 2.12). Furthermore, a 10-fold increase in the injection volume of the *OsHKT1;1-V2* cRNA (25 ng) resulted in the accumulation of approximately 6 times more $Cl^-$ (Figure 2.12). To verify that the observed $Cl^-$ increase was specifically due to $Cl^-$ influx and not caused by nonspecific anion accumulation, the same experiment was performed in Na-gluconate medium without $Cl^-$. Under these $Cl^-$-free conditions, all oocytes, including those expressing OsHKT1;1-V2, showed low $Cl^-$ levels (Figure 2.12). These results support that OsHKT1;1-V2 mediates $Cl^-$ influx into the PM of oocytes, as suggested by the TEVC experiments shown in Figures 2.6, 2.8.

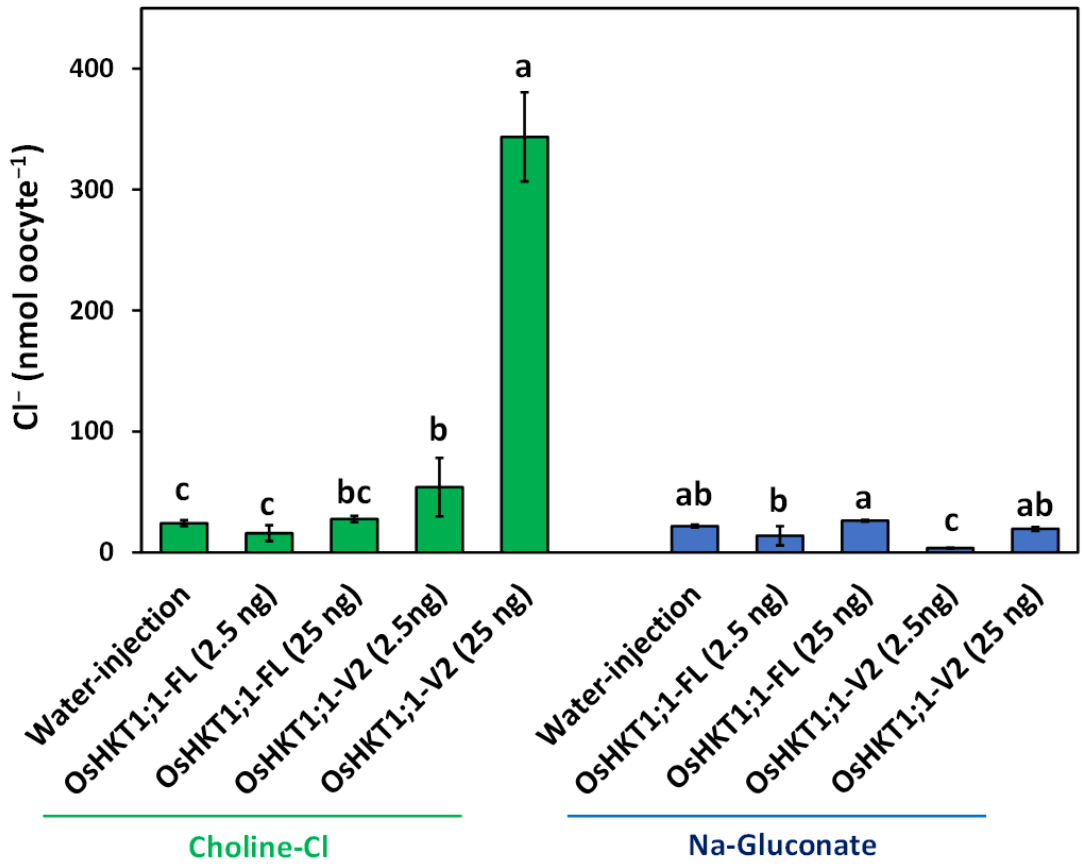


**Figure 2.12.** $Cl^-$ contents of oocytes injected with *OsHKT1;1-FL* cRNA, *OsHKT1;1-V2* cRNA, or water. Oocytes were treated with 96 mM Na-gluconate or 96 mM choline-Cl solution for 6 hr at room temperature. See the Materials and Methods section for details. Data are shown as mean ± SD. 4 to 8 batches of oocytes were used to measure $Cl^-$ contents (note that each batch included 8-10 oocytes): *n* = 8 batches for OsHKT1;1-FL (2.5 ng), 8 for OsHKT1;1-FL (25 ng), 8 for OsHKT1;1-V2 (2.5 ng), 8 for OsHKT1;1-V2 (25 ng), and 8 for water injection in a choline Cl treatment; and *n* = 8 batches for OsHKT1;1-FL (2.5 ng), 4 for OsHKT1;1-FL (25 ng), 4 for

OsHKT1;1-V2 (2.5 ng), 4 for OsHKT1;1-V2 (25 ng), and 8 for water injection in a Na-gluconate treatment. A one-way ANOVA with Tukey post hoc test was used for the Choline-Cl and Na-Gluconate group separately; different lowercase letters indicate statistically significant differences ($p < 0.05$).

**Functional Characterization of OsHKT1;1 Transporters in Yeast**

OsHKT1;1-FL and OsHKT1;1-V2 were introduced into the $Na^+$-sensitive mutant yeast strain G19 to further examine the $Na^+$ transport capacity of OsHKT1;1-FL and OsHKT1;1-V2. No remarkable difference was found in the growth among OsHKT1;1-FL, OsHKT1;1-V2, and empty vector-harboring G19 cells under the control condition (Figure 2.13A). However, the presence of 50 mM NaCl caused severe growth defects in OsHKT1;1-FL-expressing cells. In contrast, cells expressing OsHKT1;1-V2 grew similarly to the vector-harboring control cells (Figure 2.13B). These data indicate that OsHKT1;1-FL, but not OsHKT1;1-V2, possibly accelerated $Na^+$ uptake in yeast cells, leading to toxicity and growth reduction in the cells under NaCl-added conditions. Thus $Na^+$ contents of G19 transformants were determined under no or 50 mM NaCl conditions (Figure 2.13*C*). After 18 and 21 hr incubation, for control and NaCl-added conditions, respectively, in the presence of galactose, G19 cells expressing OsHKT1;1-FL were found to accumulate significantly higher levels of $Na^+$ than the others in both conditions (Figure 2.13C). Whereas $Na^+$ contents of vector control and OsHKT1;1-V2 lines were at similar levels (Figure 2.13C). These results were consistent with the growth phenotype (50 mM NaCl; Figure 2.13B).

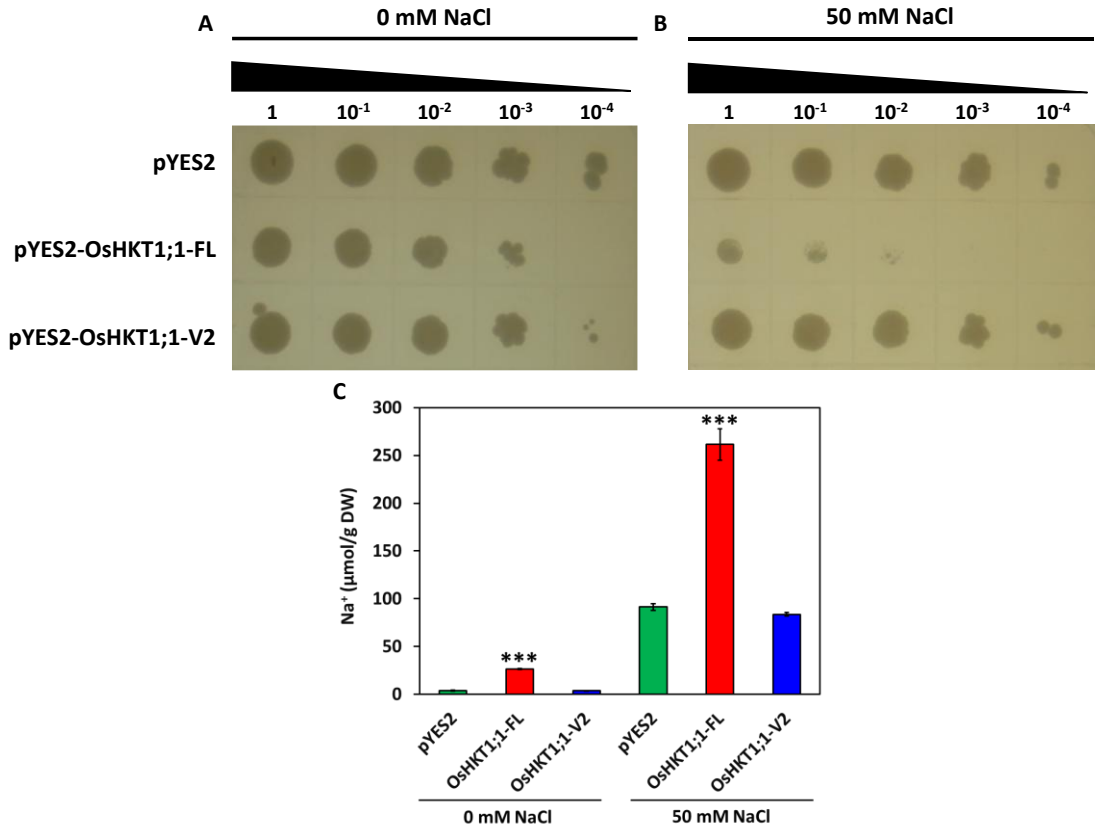


**Figure 2.13.** Functional characterizations of *OsHKT1;1-FL* and *OsHKT1;1-V2* in the G19 yeast strain. Growth of G19 cells transformed with empty vector (pYES2), pYES2-*OsHKT1;1-FL*, and pYES2-*OsHKT1;1-V2*. Each G19 transformant was incubated at 30 °C for 4 days on -Ura medium plates [0.67% (w/v) yeast nitrogen base without amino acids, 0.077% (w/v) drop out mix-Ura, 2% (w/v) galactose, 1% (w/v) raffinose, and 2% agar] containing 0 mM NaCl (**A**) or 50 mM NaCl (**B**). Numbers (1, $10^{-1}$, $10^{-2}$, $10^{-3}$, $10^{-4}$) on the top of each panel indicate the serial dilutions ($OD_{600}$) of yeast cells spotted on the medium. (**C**) $Na^+$ content of G19 transformants that were incubated in liquid synthetic complete (SC) medium supplemented with or without 50 mM NaCl for 18 (control) and 21 (NaCl-treated) hr at 30 °C ($n = 5$, ± SD). Asterisks denote significant differences from control (pYES2 empty vector) (Student's t-test: ***$p < 0.001$).

I later introduced *OsHKT1;1-FL* and *OsHKT1;1-V2* into a $Cl^-$-sensitive mutant yeast strain, *gef1*, to further examine the transport properties of *OsHKT1;1-FL* and *OsHKT1;1-V2*. There is no difference in the growth among *OsHKT1;1-FL*, *OsHKT1;1-V2*, and the empty vector control under the control condition in *gef1* cells (Figures 2.14A, 2.15A). However, *gef1*-expressing *OsHKT1;1-V2* cells showed a slightly better growth performance than pYES2-*gef1* cells in the presence of 1.5 M NaCl (Figure 2.14B). A similar phenomenon was not observed for 1.5 M NMDG-Cl (Figure 2.14C).

In addition, high NaCl (0.8 M and 1.2 M) caused mild growth defects in *OsHKT1;1-V2*-expressing cells compared to the empty vector (Figure 2.15B, C). In contrast, introducing *OsHKT1;1-FL* resulted in severe growth defects in both NaCl conditions (Figure 2.15B, C). Results indicate that *OsHKT1;1-V2* possibly increased $Cl^-$ uptake in high NaCl conditions, and leading to growth defects.

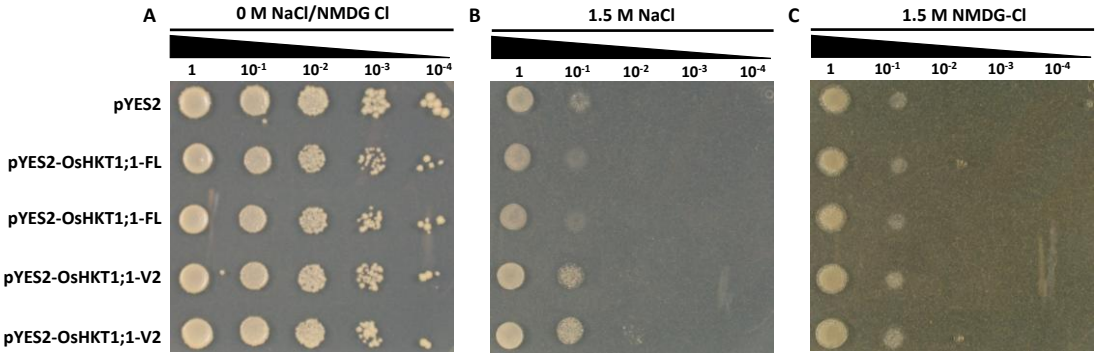


**Figure 2.14.** Functional characterizations of *OsHKT1;1-FL*, and *OsHKT1;1-V2* in *gef1* yeast strain. Growth of *gef1* yeast cells transformed by empty vector (pYES2) control (single), pYSE2-OsHKT1;1-FL (double), or pYSE-OsHKT1;1-V2 (double). Each *gef1* transformants on Ura-induced medium [0.67% (w/v) yeast nitrogen base without amino acids, 0.077% (w/v) drop out mix-Ura, 2% (w/v) galactose, 1% raffinose, and 2% agar] plates containing 0 mM NaCl (**A**), 1.5 M NaCl (**B**), and 1.5 M NMDG-Cl (**C**) were incubated at 30 °C for 11 days. Numbers (1, $10^{-1}$, $10^{-2}$, $10^{-3}$, $10^{-4}$) on the top of each panel indicated serial dilutions of yeast cells placed on the medium.

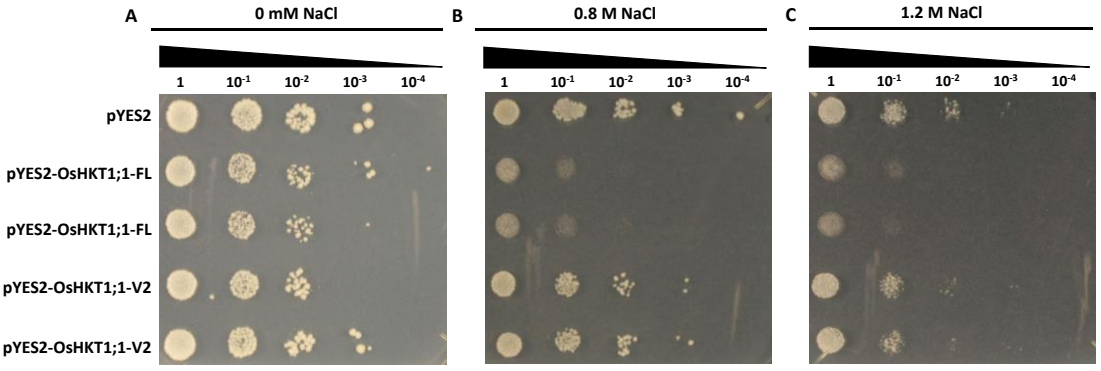


**Figure 2.15.** Functional characterizations of *OsHKT1;1-FL*, and *OsHKT1;1-V2* in *gef1* yeast strain. Growth of *gef1* yeast cells transformed by empty vector (pYES2) control (single), pYSE2-OsHKT1;1-FL (double), or pYSE-OsHKT1;1-V2 (double). Each *gef1* transformants on Ura-induced medium [0.67% (w/v) yeast nitrogen base without amino acids, 0.077% (w/v) drop out mix-Ura, 2% (w/v) galactose, 1% raffinose, and 2% agar] plates containing 0 mM NaCl (**A**), 0.8 M NaCl (**B**), and 1.2 M NaCl (**C**) were incubated at 30 °C for 6 days. Numbers (1, $10^{-1}$, $10^{-2}$, $10^{-3}$, $10^{-4}$) on the top of each panel indicated serial dilutions of yeast cells placed on the medium.

**Transport Properties of OsHKT1;1-FL and Variants from Nipponbare**

In a previous study (Imran et al., 2020) and in Figures 2.2 to 2.12 in the present study, possible *OsHKT1;1* splicing variants, in addition to the full-length cDNA from salt-tolerant *indica* rice, Pokkali, were investigated. Therefore, I attempted to determine whether these *OsHKT1;1* splicing variants could also be found in the salt-sensitive *japonica* rice, Nipponbare, and whether they functioned in a manner similar to those from Pokkali. *OsHKT1;1* cDNAs were isolated from Nipponbare, and their transport properties were examined by TEVC experiments. Eight possible *OsHKT1;1* variants were detected in addition to the full-length cDNA from Nipponbare as Pokkali (Imran et al., 2020). Comparative analysis revealed amino acid substitutions in OsHKT1;1 between the two genotypes (Figure 2.16A–I). However, oocytes expressing Nipponbare (Ni) OsHKT1;1-FL and OsHKT1;1-V6 exhibited inward-rectifying currents in the presence of 96 mM NaCl, with much smaller currents of OsHKT1;1-V6 than OsHKT1;1-FL (Figure 2.17A). In contrast to Ni-OsHKT1;1-V1 and -V4, whose currents were similar to those from water-injected control oocytes (Figure 2.17A), Ni-OsHKT1;1-V2, -V3, -V5, -V7, and-V8 mediated ionic currents in a bidirectional manner, depending on the membrane voltage (Figure 2.17B). There was no remarkable difference in the pattern of elicited currents mediated by these variants between Pokkali and Nipponbare.

Next, oocytes expressing Ni-OsHKT1;1-FL and Ni-OsHKT1;1-V2 were examined in $Cl^-$ solutions (96, 48, 12, and 6 mM as choline chloride) (Figure 2.18). Current-voltage relationships obtained from Ni-OsHKT1;1-FL expressed in oocytes showed small or no currents and no reversal potential shift with changes in $Cl^-$ concentrations in the bath solution (Figure 2.18A, B). In contrast, oocytes injected with *OsHKT1;1-V2* cRNA exhibited both inward and outward currents with apparent reversal potential shifts according to the $Cl^-$ concentration (Figure 2.18C, D). These data suggest that Ni-OsHKT1;1-V2, but not Ni-OsHKT1;1-FL, mediates $Cl^-$ transport, as observed in those transporters from Pokkali.

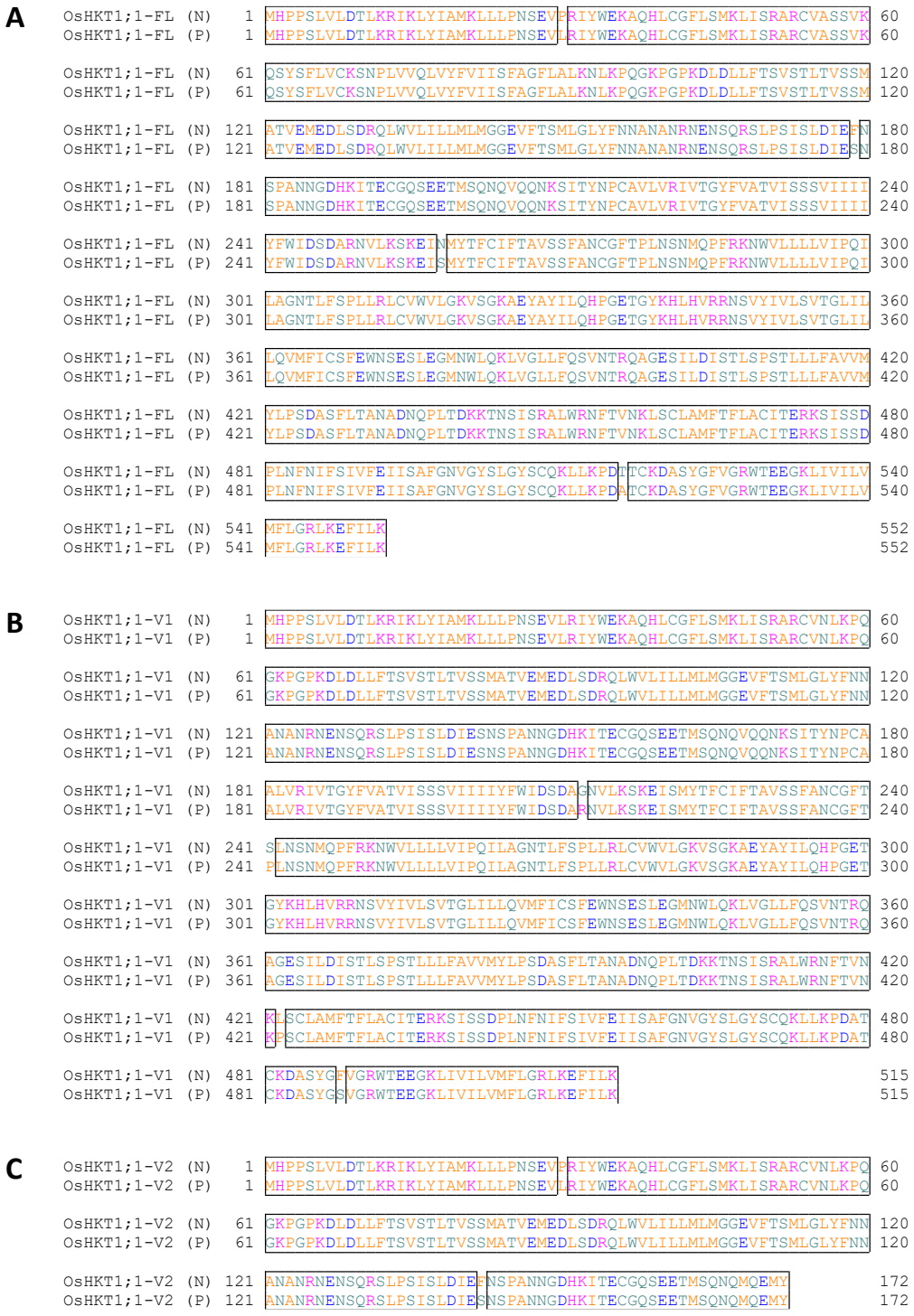
A
OsHKT1;1-FL (N) 1 MHPPSLVLDTLKRIKLYIAMKLLLPNSEVPRIYWEKAQHLCGFLSMKLISRARCVASSVK 60
OsHKT1;1-FL (P) 1 MHPPSLVLDTLKRIKLYIAMKLLLPNSEVLRIYWEKAQHLCGFLSMKLISRARCVASSVK 60
OsHKT1;1-FL (N) 61 QSYSFLVCKSNPLVVQLVYFVIISFAGFLALKNLKPQGKPGPKDLDLLFTSVSTLTVSSM 120
OsHKT1;1-FL (P) 61 QSYSFLVCKSNPLVVQLVYFVIISFAGFLALKNLKPQGKPGPKDLDLLFTSVSTLTVSSM 120
OsHKT1;1-FL (N) 121 ATVEMEDLSDRQLWVLILLMLMGGEVFTSMLGLYFNNANANRNENSQRSLPSISLDIEFN 180
OsHKT1;1-FL (P) 121 ATVEMEDLSDRQLWVLILLMLMGGEVFTSMLGLYFNNANANRNENSQRSLPSISLDIESN 180
OsHKT1;1-FL (N) 181 SPANNGDHKITECGQSEETMSQNQVQQNKSITYNPCAVLVRIVTGYFVATVISSSVIIII 240
OsHKT1;1-FL (P) 181 SPANNGDHKITECGQSEETMSQNQVQQNKSITYNPCAVLVRIVTGYFVATVISSSVIIII 240
OsHKT1;1-FL (N) 241 YFWIDSDARNVLKSKEINMYTFCIFTAVSSFANCGFTPLNSNMQPFRKNWVLLLLVIPQI 300
OsHKT1;1-FL (P) 241 YFWIDSDARNVLKSKEISMYTFCIFTAVSSFANCGFTPLNSNMQPFRKNWVLLLLVIPQI 300
OsHKT1;1-FL (N) 301 LAGNTLFSPLLRLCVWVLGKVSGKAEYAYILQHPGETGYKHLHVRRNSVYIVLSVTGLIL 360
OsHKT1;1-FL (P) 301 LAGNTLFSPLLRLCVWVLGKVSGKAEYAYILQHPGETGYKHLHVRRNSVYIVLSVTGLIL 360
OsHKT1;1-FL (N) 361 LQVMFICSFEWNSESLEGMNWLQKLVGLLFQSVNTRQAGESILDISTLSPSTLLLFAVVM 420
OsHKT1;1-FL (P) 361 LQVMFICSFEWNSESLEGMNWLQKLVGLLFQSVNTRQAGESILDISTLSPSTLLLFAVVM 420
OsHKT1;1-FL (N) 421 YLPSDASFLTANADNQPLTDKKTNSISRALWRNFTVNKLSCLAMFTFLACITERKSISSD 480
OsHKT1;1-FL (P) 421 YLPSDASFLTANADNQPLTDKKTNSISRALWRNFTVNKLSCLAMFTFLACITERKSISSD 480
OsHKT1;1-FL (N) 481 PLNFNIFSIVFEIISAFGNVGYSLGYSCQKLLKPDTTCKDASYGFVGRWTEEGKLIVILV 540
OsHKT1;1-FL (P) 481 PLNFNIFSIVFEIISAFGNVGYSLGYSCQKLLKPDATCKDASYGFVGRWTEEGKLIVILV 540
OsHKT1;1-FL (N) 541 MFLGRLKEFILK 552
OsHKT1;1-FL (P) 541 MFLGRLKEFILK 552
B
OsHKT1;1-V1 (N) 1 MHPPSLVLDTLKRIKLYIAMKLLLPNSEVLRIYWEKAQHLCGFLSMKLISRARCVNLKPQ 60
OsHKT1;1-V1 (P) 1 MHPPSLVLDTLKRIKLYIAMKLLLPNSEVLRIYWEKAQHLCGFLSMKLISRARCVNLKPQ 60
OsHKT1;1-V1 (N) 61 GKPGPKDLDLLFTSVSTLTVSSMATVEMEDLSDRQLWVLILLMLMGGEVFTSMLGLYFNN 120
OsHKT1;1-V1 (P) 61 GKPGPKDLDLLFTSVSTLTVSSMATVEMEDLSDRQLWVLILLMLMGGEVFTSMLGLYFNN 120
OsHKT1;1-V1 (N) 121 ANANRNENSQRSLPSISLDIESNSPANNGDHKITECGQSEETMSQNQVQQNKSITYNPCA 180
OsHKT1;1-V1 (P) 121 ANANRNENSQRSLPSISLDIESNSPANNGDHKITECGQSEETMSQNQVQQNKSITYNPCA 180
OsHKT1;1-V1 (N) 181 ALVRIVTGYFVATVISSSVIIIIYFWIDSDAGNVLKSKEISMYTFCIFTAVSSFANCGFT 240
OsHKT1;1-V1 (P) 181 ALVRIVTGYFVATVISSSVIIIIYFWIDSDARNVLKSKEISMYTFCIFTAVSSFANCGFT 240
OsHKT1;1-V1 (N) 241 SLNSNMQPFRKNWVLLLLVIPQILAGNTLFSPLLRLCVWVLGKVSGKAEYAYILQHPGET 300
OsHKT1;1-V1 (P) 241 PLNSNMQPFRKNWVLLLLVIPQILAGNTLFSPLLRLCVWVLGKVSGKAEYAYILQHPGET 300
OsHKT1;1-V1 (N) 301 GYKHLHVRRNSVYIVLSVTGLILLQVMFICSFEWNSESLEGMNWLQKLVGLLFQSVNTRQ 360
OsHKT1;1-V1 (P) 301 GYKHLHVRRNSVYIVLSVTGLILLQVMFICSFEWNSESLEGMNWLQKLVGLLFQSVNTRQ 360
OsHKT1;1-V1 (N) 361 AGESILDISTLSPSTLLLFAVVMYLPSDASFLTANADNQPLTDKKTNSISRALWRNFTVN 420
OsHKT1;1-V1 (P) 361 AGESILDISTLSPSTLLLFAVVMYLPSDASFLTANADNQPLTDKKTNSISRALWRNFTVN 420
OsHKT1;1-V1 (N) 421 KLSCLAMFTFLACITERKSISSDPLNFNIFSIVFEIISAFGNVGYSLGYSCQKLLKPDAT 480
OsHKT1;1-V1 (P) 421 KPSCLAMFTFLACITERKSISSDPLNFNIFSIVFEIISAFGNVGYSLGYSCQKLLKPDAT 480
OsHKT1;1-V1 (N) 481 CKDASYGFVGRWTEEGKLIVILVMFLGRLKEFILK 515
OsHKT1;1-V1 (P) 481 CKDASYGSVGRWTEEGKLIVILVMFLGRLKEFILK 515
C
OsHKT1;1-V2 (N) 1 MHPPSLVLDTLKRIKLYIAMKLLLPNSEVPRIYWEKAQHLCGFLSMKLISRARCVNLKPQ 60
OsHKT1;1-V2 (P) 1 MHPPSLVLDTLKRIKLYIAMKLLLPNSEVLRIYWEKAQHLCGFLSMKLISRARCVNLKPQ 60
OsHKT1;1-V2 (N) 61 GKPGPKDLDLLFTSVSTLTVSSMATVEMEDLSDRQLWVLILLMLMGGEVFTSMLGLYFNN 120
OsHKT1;1-V2 (P) 61 GKPGPKDLDLLFTSVSTLTVSSMATVEMEDLSDRQLWVLILLMLMGGEVFTSMLGLYFNN 120
OsHKT1;1-V2 (N) 121 ANANRNENSQRSLPSISLDIEFNSPANNGDHKITECGQSEETMSQNQMQEMY 172
OsHKT1;1-V2 (P) 121 ANANRNENSQRSLPSISLDIESNSPANNGDHKITECGQSEETMSQNQMQEMY 172

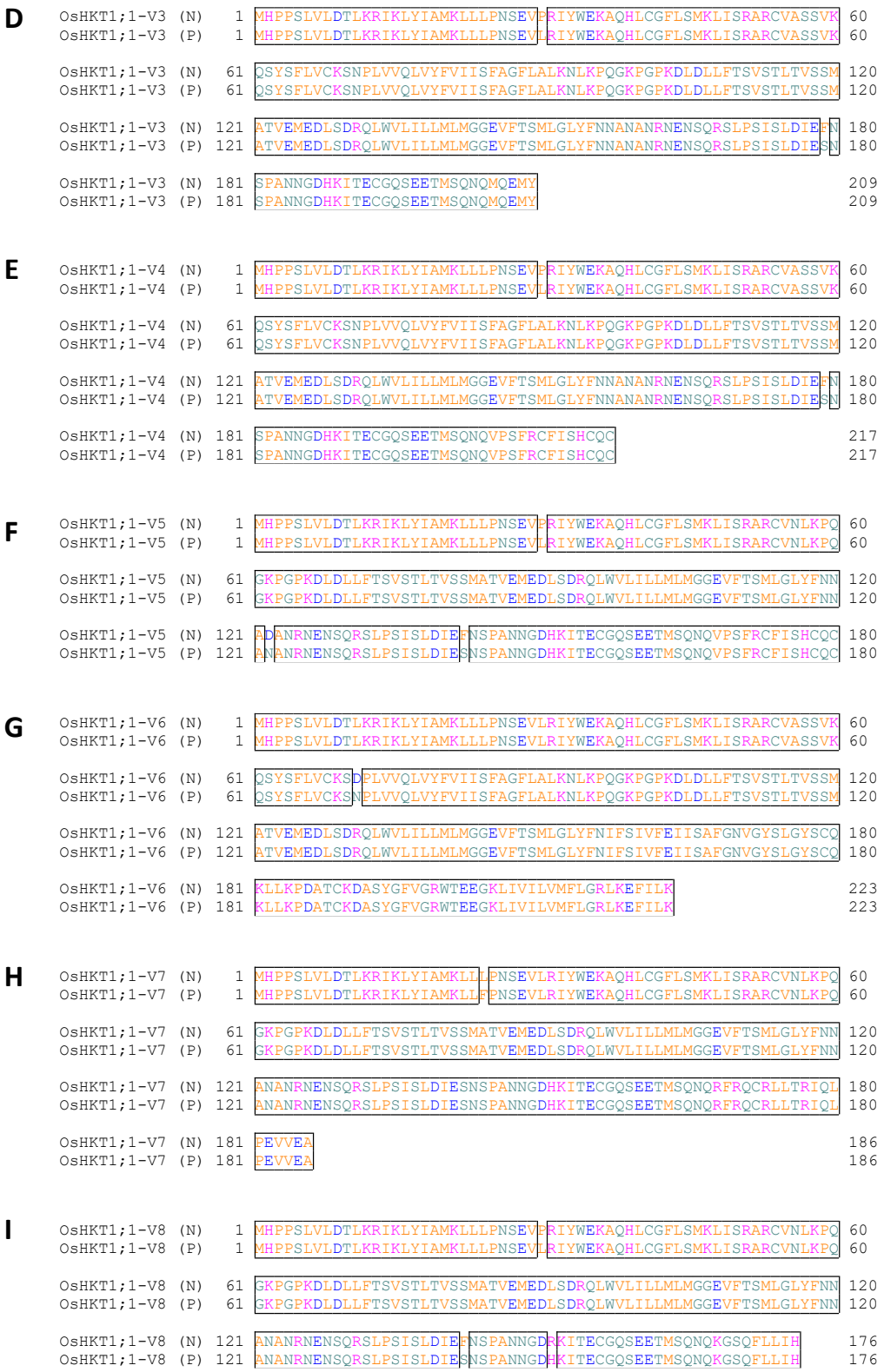


**Figure 2.16.** Comparisons of amino acid sequences of OsHKT1;1-FL and OsHKT1;1 variants between Nipponbare and Pokkali: OsHKT1;1-FL (**A**), OsHKT1;1-V1 (**B**), OsHKT1;1-V2 (**C**), OsHKT1;1-V3 (**D**), OsHKT1;1-V4 (**E**), OsHKT1;1-V5 (**F**), OsHKT1;1-V6 (**G**), OsHKT1;1-V7 (**H**), and OsHKT1;1-V8 (**I**). GENETYX ver. 16 was used.

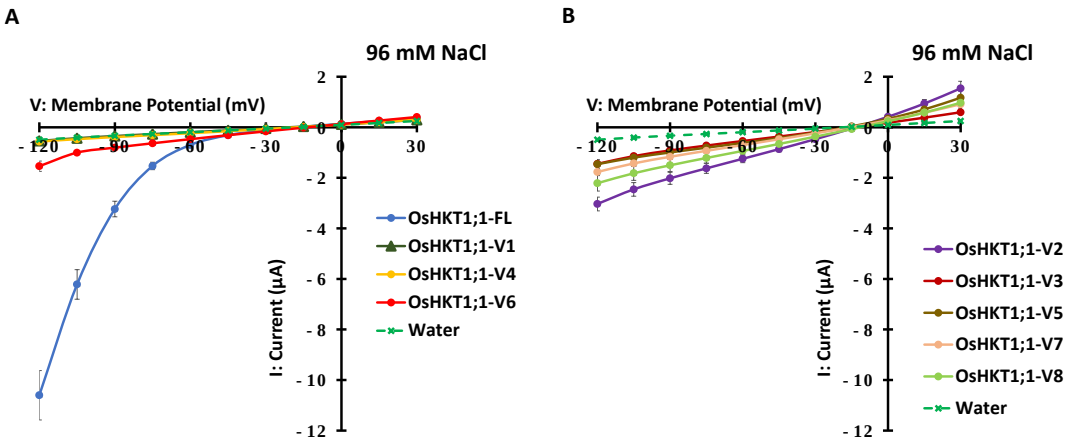


**Figure 2.17.** TEVC recordings of oocytes expressing OsHKT1;1-FL and OsHKT1;1 variants derived from cv. Nipponbare. (**A**) Current-voltage relationships from oocytes expressing OsHKT1;1-FL, -V1, -V4, and-V6 and oocytes injected with water. (**B**) Current-voltage relationships from oocytes expressing OsHKT1;1-V2, -V3, -V5, -V7, and-V8 and oocytes injected with water. The external bath solution contained 96 mM NaCl, 1.8 mM $CaCl_2$, 1.8 mM $MgCl_2$, 1.8 mM mannitol, and 10 mM HEPES (pH 7.5, with Tris). Data are presented as mean ± SE, *n* = 10–18, from two independent experiments using different batches of oocytes.

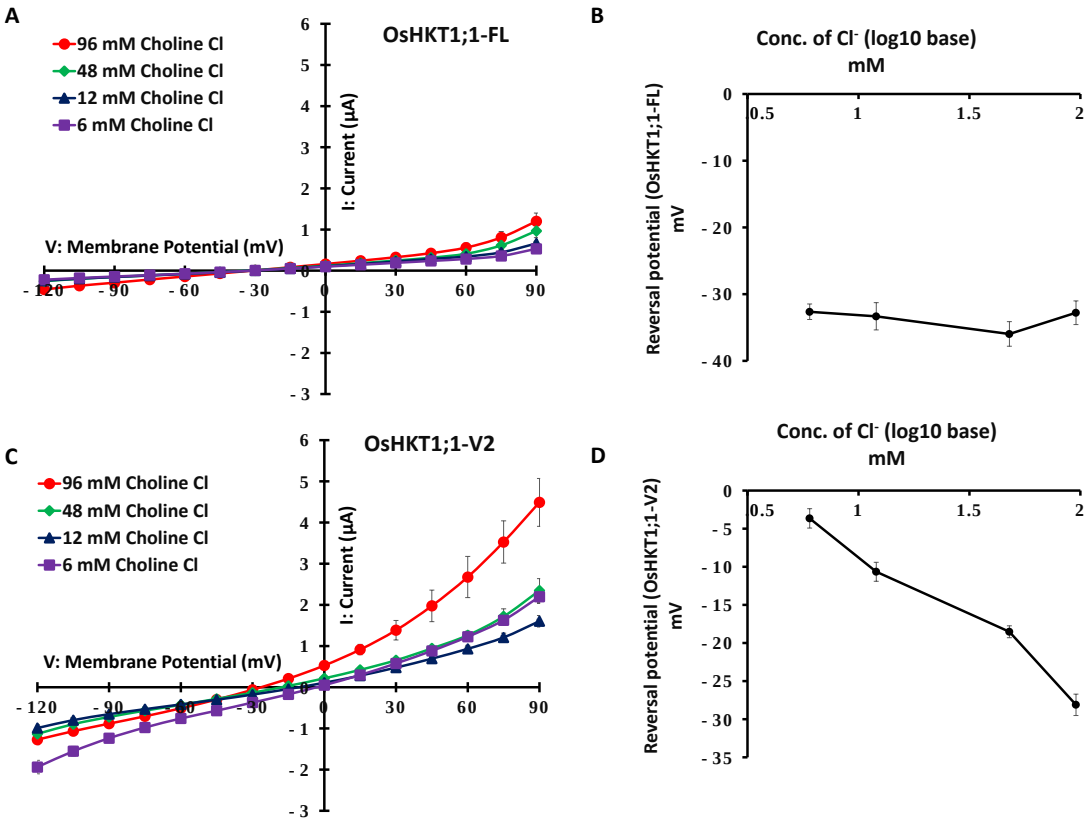


**Figure 2.18.** Chloride concentration dependency of OsHKT1;1-FL and OsHKT1;1-V2, derived from Nipponbare, and expressed in *X. laevis* oocytes. (**A**, **C**) Current-voltage relationships from oocytes expressing OsHKT1;1-FL and OsHKT1;1-V2, respectively. (**B**, **D**) Log10 base reversal potential analysis of OsHKT1;1-FL and OsHKT1;1-V2, respectively. A series of

choline chloride solutions, the concentration of which were from 96 mM to 6 mM, was used as an external bath solution. The basic components of the solutions were 1.8 mM $CaCl_2$, 1.8 mM $MgCl_2$, 1.8 mM mannitol, and 10 mM HEPES, and the pH was adjusted to 7.5 with Tris. 48-, 12-, and 6-mM choline chloride solutions contained 38-, 63-, or 68-mM Mg gluconate, respectively. Oocytes were isolated and injected with 2.5 ng cRNAs/50 nL and then incubated for about 18 hr for OsHKT1;1-FL or 4 hr for OsHKT1;1-V2 at 18 °C. To obtain current-voltage relationships, voltage steps (2 sec) were applied from +90 to −120 mV in 15 mV decrements. Data are presented as means ± SE, $n$ = 8-12.

**Expression Analyses of OsHKT1;1-FL and OsHKT1;1-V2 in Shoots and Roots**

I next investigated the transcript levels of *OsHKT1;1-FL* and *OsHKT1;1-V2* in Pokkali and Nipponbare by conducting RT-qPCR-based absolute quantification. Without stress, Nipponbare plants accumulated approximately five times more *OsHKT1;1-FL* transcripts than Pokkali in shoots (Figure 2.19A). However, in the case of *OsHKT1;1-V2*, the transcript level in shoots was approximately six times higher in Pokkali than in Nipponbare (Figure 2.19A at time 0; note that the scale for transcript amounts is log-10-based). Interestingly, salt stress (100 mM NaCl) temporally increased both *OsHKT1;1-FL* and *OsHKT1;1-V2* transcripts in Nipponbare, peaking at 12 h, whereas those of Pokkali decreased (Figure 2.19A). In roots, the *OsHKT1;1-FL* transcript level was much lower in Pokkali than in Nipponbare, and so was the level of the *OsHKT1;1-V2* transcript under control conditions (Figure 2.19B). The OsHKT1;1-FL transcript level was temporally increased, peaking at 6 hr after salt stress in Nipponbare, but this observation was not applied to Pokkali (Figure 2.19B). The levels of the other transcripts were maintained relatively constant during the periods investigated (Figure 2.19B). These results indicate a differential regulatory mechanism of *OsHKT1;1* gene expression between rice genotypes.

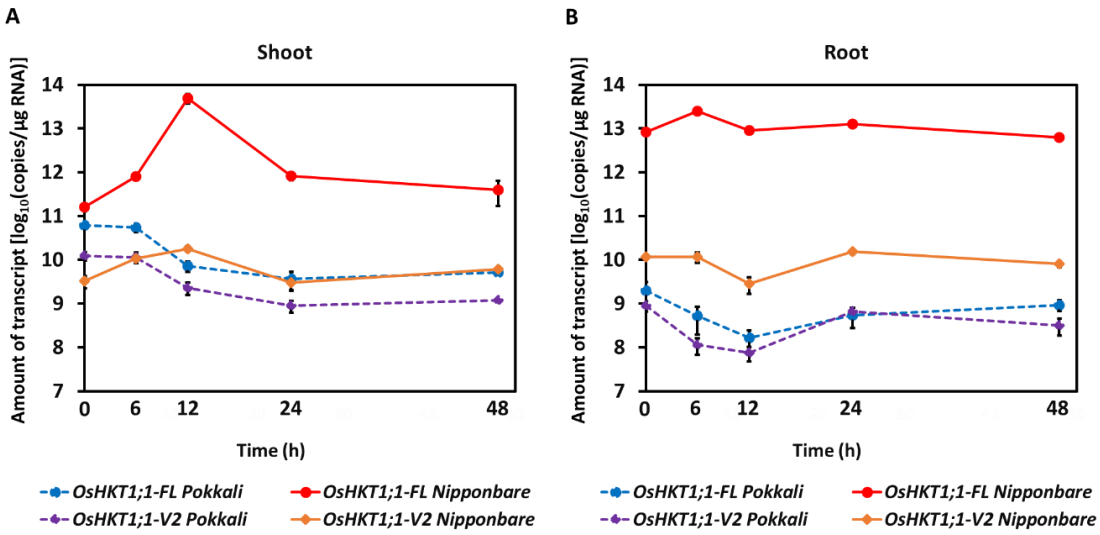


**Figure 2.19.** Absolute quantification of *OsHKT1;1-FL* and *OsHKT1;1-V2* transcript levels in Pokkali and Nipponbare plants with or without salt stress. The number of transcripts is displayed in log10 base in shoots (**A**) and roots (**B**). Fourteen-day-old seedlings of both varieties were treated with or without 100 mM NaCl (6–48 hr) before total RNA extraction. Data are presented as the mean ± SE (n = 6).

## Discussion

HKT membrane proteins are known to be relevant to $Na^+$ homeostasis in plants, including under salinity stress. $Na^+$ exclusion protects photosynthetic tissues from salt-induced damage (Hauser and Horie, 2009), and some of the $Na^+$-selective class 1 HKT (HKT1) transporters play a key role in excluding $Na^+$ from leaves, enhancing salinity tolerance (Mäser et al., 2002; Ren et al., 2005; Sunarpi et al., 2005; Byrt et al., 2007; Munns et al., 2012; Wang et al., 2015a). In rice, OsHKT1;1 and OsHKT1;3 exhibit strong and weak inward rectification for $Na^+$ transport, respectively (Jabnoune et al., 2009; Imran et al., 2020, 2021). Many other studies on the homologue of HKT1;1 from barley, pumpkin, grapevine, blueberry, and wild turf *Sporobolus virginicus* have also revealed $Na^+$-selective transport as OsHKT1;1 (Han et al., 2018; Henderson et al., 2018; Kawakami et al., 2020; Wei et al., 2023a; Song et al., 2024). Campbell et al. (2017) showed that natural allelic variants of *OsHKT1;1* underlie the divergence in root $Na^+$ content between *japonica* and *indica* rice cultivars. They reported three non-synonymous mutations associated with higher OsHKT1;1 activity and $Na^+$ transport efficiency, explaining the genetic basis for the diversity in salt tolerance in rice. This study also provides strong genetic evidence that *OsHKT1;1* plays a central role in $Na^+$ homeostasis and is an important target for improving salinity tolerance through

molecular breeding. Additionally, *OsHKT1;1* interacts with the Salt Overly Sensitive (SOS) pathway and other transporters, implying a complex regulatory network for ion balance and salt stress response (Shi et al., 2000; Horie et al., 2009; Plett et al., 2010; Hasegawa, 2013).

In my previous study, eight *OsHKT1;1* variants (V1-V8) that could be the product of alternative splicing were identified in addition to the full-length *OsHKT1;1-FL* cDNA in the salt-tolerant rice cultivar Pokkali (Imran et al., 2020). In this study, I focused on the variant *OsHKT1;1-V2* as the transcript level was significantly higher than that of *OsHKT1;1-FL* in shoots of Pokkali, and *OsHKT1;1-V2* cRNA-injected oocytes exhibited larger inward and outward currents than other variants in both NaCl and KCl bath solutions (Imran et al., 2020). Although two start codons are present in *OsHKT1;1-V2* mRNA, the present study demonstrated that the first start codon of *OsHKT1;1-V2* is functional (Figure 2.2A, B, C). The plasma membrane localization of FLAG-tagged OsHKT1;1-V2 in oocytes (Figure 2.2E) indicated that the ionic currents elicited by OsHKT1;1-V2 (Figures 2.2, 2.6, 2.8, 2.10) were not artifacts or leaks. In the present study, the co-localization of GFP-fused OsHKT1;1-FL or OsHKT1;1-V2 with the dye FM4-64 in the plasma membrane was further demonstrated in *Arabidopsis* protoplasts (Figure 2.4), supporting the above-mentioned notion.

OsHKT1;1-FL was confirmed to mediate $Na^+$ transport, as reported previously (Imran et al., 2020) (Figures 2.5, 2.13). Interestingly, however, OsHKT1;1-V2 displayed distinct selectivity for $Na^+$ and $Cl^-$: the OsHKT1;1-V2 protein expressed in oocytes was responsive to the changes in the $Cl^-$ concentration but not the $Na^+$ concentration, suggesting a preference for $Cl^-$ transport over $Na^+$ transport (Figures 2.6, 2.7). OsHKT1;1-FL showed a concentration-dependent reversal potential shift only in $Na^+$ bath solutions, whereas OsHKT1;1-V2 showed no concentration-dependent reversal potential shifts in $Na^+$ solutions (Figures 2.10, 2.11). In contrast to the lack of reversal potential shifts in OsHKT1;1-V2-expressing oocytes upon $Na^+$ concentration changes, the observed apparent reversal potential shifts upon $Cl^-$ concentration changes again suggested that OsHKT1;1-V2 is more selective for $Cl^-$ (Figures 2.8, 2.10). This electrophysiological suggestion was further supported by the measurements of $Cl^-$ contents of oocytes expressing OsHKT1;1-V2, which accumulated significantly more $Cl^-$ than the oocytes expressing OsHKT1;1-FL after incubation in the examination solution (Figure 2.12). In fact, oocytes expressing OsHKT1;1-V2 (2.5 ng cRNA) in the medium exhibited an average reversal potential of –17 mV (Figure 2.7A), while the

resting potential of the oocytes was approximately –9 mV (data not shown), which was +8 mV higher than the reversal potential, indicating that $Cl^-$ influx can be triggered under the tested conditions. The obtained results were consistent with those from the TEVC analysis (Figures 2.6, 2.7, 2.8, 2.10). On the other hand, functional assays using the yeast G19 strain supported the notion that OsHKT1;1-FL, but not OsHKT1;1-V2, mediates $Na^+$ uptake (Figure 2.13). In addition to the growth phenotype, quantification of $Na^+$ levels in yeast cells provided evidence that OsHKT1;1-FL but not OsHKT1;1-V2 led to over-accumulation of $Na^+$ even under a control condition where the existence of 1 mM or less $Na^+$ is expected (Figure 2.13C). This result confirms that the growth inhibition observed in OsHKT1;1-FL-expressing G19 strain is attributable to enhanced $Na^+$ uptake. More importantly, the lack of remarkable $Na^+$ accumulation in OsHKT1;1-V2-expressing cells is fully consistent with the electrophysiological analyses in *Xenopus* oocytes (Figures 2.6, 2.10). Consistently, assays in the *gef1* yeast background revealed that OsHKT1;1-V2 did not promote $Na^+$ influx but instead showed slightly better growth in 1.5 M NaCl than in 1.5 M NMDG-Cl (Figure 2.14), suggesting a $Na^+$-dependent role in $Cl^-$ handling rather than direct $Na^+$ transport. The mild growth defects observed in V2-expressing cells further support a modest role in $Cl^-$ uptake, while FL-expressing cells exhibited severe growth inhibition, likely due to excessive $Na^+$ entry driven by OsHKT1;1-FL in combination with the yeast's limited $Na^+$ exclusion capacity (Figure 2.15).

During salt stress, maintenance of $Cl^-$ homeostasis is crucial because excess cytosolic $Cl^-$ can be toxic (Ismail and Horie, 2017; Liu et al., 2023). $Cl^-$ detoxification involves xylem loading, vacuolar sequestration, and efflux from roots (Ismail and Horie, 2017; Wu and Li, 2019). Chloride channels (CLCs) are membrane proteins that mediate $Cl^-$ and $NO_3^-$ transport across plant membranes, contributing to pH regulation and stress tolerance (Nedelyaeva et al., 2020; Subba et al., 2021). Each CLC monomer contains 16–18 transmembrane α-helices that form a self-contained anion pore and a cytosolic CBS domain that regulates gating through conformational and nucleotide-dependent mechanisms (Feng et al., 2010; Subba et al., 2021). The conserved GxGxPE and GKxGPxxH motifs form part of the selectivity filter, where serine or proline residues determine $Cl^-$ versus $NO_3^-$ specificity (Wege et al., 2010). Overexpression of *GmCLC1*, *CsCLC-c*, and *ZmCLC-d* has been reported to enhance salt tolerance by promoting vacuolar $Cl^-$ sequestration and reducing cytosolic accumulation (Wei et al., 2013b, 2016c; Wang et al., 2015b). The plasma membrane transporters NPF2.4 and SLAH1

are proposed to function in regulating $Cl^-$ loading into the xylem (Colmenero-Flores et al., 2019; Zhang et al., 2025), whereas tonoplast-localized CLCs mediate $Cl^-/H^+$ antiport to sequester $Cl^-$ into vacuoles (Ismail et al., 2017; Liu et al., 2023). Additionally, *AtCCC1* functions as a $Na^+$:$K^+$:$Cl^-$ cotransporter essential for maintaining ion balance and osmotic potential (Colmenero-Flores et al., 2007). Loss-of-function mutants of *AtCCC1* and *OsCCC1* exhibit stunted growth and excessive $Cl^-$ accumulation in shoots, indicating that CCC1 participates in $Cl^-$ retrieval and homeostasis (Colmenero-Flores et al., 2007; Chen et al., 2016). Moreover, some ALMT members (*AtALMT9* and *AtALMT12*) facilitate $Cl^-$ transport (Sasaki et al., 2010; De Angeli et al., 2013; Baetz et al., 2016; Liu et al., 2022).

In the present study, I demonstrated that the OsHKT1;1-V2 splice variant encodes a protein of 172 amino acids with a single predicted transmembrane helix (Figure 2.3A). Despite lacking the canonical pore-forming domains of HKTs, TEVC assays revealed robust inward and outward currents, suggesting that OsHKT1;1-V2 may form a self-associated complex that is permeable to $Cl^-$. Sequence inspection of OsHKT1;1-V2 revealed a central hydrophobic stretch (residues 96–118; "LWVLILLMLMGGEVFTSMLGLYF") (Figure 2.3A), likely forming the ion-conducting α-helix, surrounded by charged and polar residues that could stabilize $Cl^-$ within the pore. Notably, OsHKT1;1-V2 contains an upstream GKxGPxx pattern (residues 61–67) that resembles part of the conserved GKxGPxxH selectivity motif present in plant CLC proteins (Figure 2.3A). Although this pattern lacks the canonical histidine present in CLC selectivity filters, it may still contribute to local structural flexibility or pore shaping, providing a residual signature of the anion-interacting architecture. Interestingly, the overall minimal architecture of OsHKT1;1-V2 parallels the basic structural layout of inwardly rectifying $K^+$ (Kir) channels, which are composed of two transmembrane helices (TM1 and TM2) connected by a pore-forming loop and assembled as a tetramer to form a functional channel (Hibino et al., 2010). Kir channels exhibit inward rectification through pore blockage by intracellular $Mg^{2+}$ and polyamines, allowing greater ion influx than efflux (Hibino et al., 2010). By analogy, OsHKT1;1-V2 might represent a minimal anion-conducting module, in which its single transmembrane helix or multimeric assembly provides a rudimentary $Cl^-$ pathway.

Although *Xenopus* oocytes have endogenous anion channels, the following facts minimize the possibility that these channels contributed to the OsHKT1;1-V2-associated currents. First, in contrast to the $Cl^-$-dependent reversal potential changes

seen in OsHKT1;1-V2-expressing oocytes (Figures 2.8C, D, 2.18C, D), water-injected controls showed only small inward and outward currents that did not change with external $Cl^-$ concentration (Figure 2.9B). Second, $Cl^-$ accumulation assays demonstrated that water-injected oocytes consistently showed minimal $Cl^-$ accumulation under all tested conditions, and OsHKT1;1-V2-expressing oocytes showed an increase in Cl− accumulation (Figure 2.12). Note, however, that I cannot exclude the possibility that the OsHKT1;1-V2 variant interacts with other membrane proteins to form a minimal $Cl^-$-selective channel in oocytes. Thus, further mechanistic research will be needed. Approaches such as expressing dominant-negative OsHKT1;1-V2 mutants, testing OsHKT1;1-V2 multimerization biochemically, and reconstituting purified OsHKT1;1-V2 into liposomes or artificial membranes would clarify whether OsHKT1;1-V2 exhibits an inherently channel-forming feature by itself.

Although some amino acid substitutions were detected in the variants of *OsHKT1;1* between Pokkali and Nipponbare (Figure 2.11), the lineup of *OsHKT1;1* transcripts was identical between the two cultivars (Imran et al., 2020). In addition, OsHKT1;1-FL and other OsHKT1;1 variants derived from Nipponbare exhibited transport profiles similar to those of OsHKT1;1 transporters from Pokkali (Figure 2.17) (Imran et al., 2020). Moreover, the similarity in the substrate selectivity of the OsHKT1;1-V2 variants from both rice varieties suggested that the function of OsHKT1;1-V2 in ion homeostasis might be conserved across different genetic backgrounds (Figures 2.8, 2.10, 2.18).

It has been reported that the transcript levels of *OsHKT1;1* in shoots increased significantly, showing a 3- to 5-fold rise after 12 hr of salt treatment, whereas no upregulation was observed in roots (Wang et al., 2015a). In contrast, *HvHKT1;1* was upregulated in roots under salinity stress, with relatively lower expression levels detected in leaves and sheaths (Ismail and Horie, 2017). Similarly, the transcript levels of *HKT1;1* have been analyzed in other plant species, in which the expression level was found to be increased in response to salt stress in both shoots and roots, or only in roots (Sun et al., 2018; Fu et al., 2025; Zhu et al., 2025). However, previous reports have only quantified full-length mRNA and have not considered variants. Absolute quantification of *OsHKT1;1* transcripts in the present and previous studies demonstrated that the expression levels varied among variants and between the cultivars. Nipponbare exhibited higher and more stable expression of *OsHKT1;1-FL* under salt stress (Figure 2.19). As *OsHKT1;1* has been proposed to be a salt-tolerant determinant

in rice (Wang et al., 2015a; Takagi et al., 2015; Campbell et al., 2017), it is intriguing that salt-tolerant Pokkali did not increase *OsHKT1;1* transcripts and maintained a lower level of expression during salt stress compared with those in salt-sensitive Nipponbare (Figure 2.19). These results indicate that *OsHKT1;1* may function to maintain basal ion homeostasis in Pokkali under normal condition and have a limited role in Pokkali under salt stress, although *OsHKT1;1* in a salt-tolerant *indica* rice cultivar Zhenshan 2 was found to play a more essential role in the mechanism of salt tolerance (Campbell et al., 2017). In Pokkali, other specific transporters/channels, including OsHKT1;5 (Singh et al., 2009), may have significant functions under salt stress.

Overall, these results highlight the unexpected characteristics of the *OsHKT1;1* splicing variant OsHKT1;1-V2 in rice, which was suggested to encode a possible $Cl^-$ channel. However, the expression of *OsHKT1;1-V2* was lower than that of *OsHKT1;1-FL* in both Pokkali and Nipponbare. However, important questions remain to be elucidated: (i) Does OsHKT1;1-V2 function as a $Cl^-$ channel in rice? If so, (ii) does OsHKT1;1-V2 contribute to $Cl^-$ homeostasis and salt tolerance? (iii) Does the differential regulation in the expression of *OsHKT1;1-FL* and *OsHKT1;1-V2* between Nipponbare and Pokkali reflect the mechanism of salt tolerance in rice? In addition, further studies are needed to explore the regulatory mechanisms behind the splicing of *OsHKT1;1* and to investigate whether some of the variants other than OsHKT1;1-V2 could also contribute to ion homeostasis in rice plants, including upon salt stress.

**References**

Baetz U, Eisenach C, Tohge T, Martinoia E, De Angeli A. Vacuolar chloride fluxes impact ion content and distribution during early salinity stress. Plant Physiology. **2016**;172(2):1167-1181. https://doi.org/10.1104/pp.16.00183

Byrt CS, Platten JD, Spielmeyer W, James RA, Lagudah ES, Dennis ES, Tester M, Munns R. HKT1; 5-like cation transporters linked to $Na^+$ exclusion loci in wheat, Nax2 and Kna1. Plant Physiology. **2007**;143(4):1918-1928. https://doi.org/10.1104/pp.106.093476

Campbell MT, Bandillo N, Al Shiblawi FR, Sharma S, Liu K, Du Q, Schmitz AJ, Zhang C, Véry AA, Lorenz AJ, Walia H. Allelic variants of OsHKT1;1 underlie the divergence between indica and japonica subspecies of rice (*Oryza sativa*) for root sodium content. PLoS Genetics. **2017**;13(6):e1006823. https://doi.org/10.1371/journal.pgen.1006823

Chen ZC, Yamaji N, Fujii-Kashino M, Ma JF. A cation-chloride cotransporter gene is required for cell elongation and osmoregulation in rice. Plant Physiology. **2016**;171(1):494-507. https://doi.org/10.1104/pp.16.00017

Cheng Q, Zhou Y, Liu Z, Zhang L, Song G, Guo Z, Wang W, Qu X, Zhu Y, Yang D. An alternatively spliced heat shock transcription factor, *OsHSFA2dI*, functions in the heat stress-induced unfolded protein response in rice. Plant Biology. **2015**;17(2):419-429. https://doi.org/10.1111/plb.12267

Chiu WL, Niwa Y, Zeng W, Hirano T, Kobayashi H, Sheen J. Engineered GFP as a vital reporter in plants. Current Biology. **1996**;6(3):325-330. https://doi.org/10.1016/S0960-9822(02)00483-9

Colmenero-Flores JM, Franco-Navarro JD, Cubero-Font P, Peinado-Torrubia P, Rosales MA. Chloride as a beneficial macronutrient in higher plants: new roles and regulation. International Journal of Molecular Sciences. **2019**;20(19):4686. https://doi.org/10.3390/ijms20194686

Colmenero-Flores JM, Martínez G, Gamba G, Vázquez N, Iglesias DJ, Brumós J, Talón M. Identification and functional characterization of cation–chloride cotransporters in plants. The Plant Journal. **2007**;50(2):278-292. https://doi.org/10.1111/j.1365-313x.2007.03048.x

Cotsaftis O, Plett D, Shirley N, Tester M, Hrmova M. A Two-Staged model of $Na^+$ exclusion in rice explained by 3D modeling of HKT transporters and alternative splicing. PloS One. **2012**;7(7):e39865. https://doi.org/10.1371/journal.pone.0039865

De Angeli A, Zhang J, Meyer S, Martinoia E. AtALMT9 is a malate-activated vacuolar chloride channel required for stomatal opening in Arabidopsis. Nature Communication. **2013**;4:1804. https://doi.org/10.1038/ncomms2815

Feng L, Campbell EB, Hsiung Y, MacKinnon R. Structure of a eukaryotic CLC transporter defines an intermediate state in the transport cycle. Science. **2010**;330(6004):635-641. https://doi.org/10.1126/science.1195230

Fu S, Chen X, Jiang Y, Dai S, Zhang H, Feng S, Zhou A. Characterization of the $Na^+$-preferential transporter HKT1.1 from halophyte shrub *Salix linearistipularis*. Physiology and Molecular Biology of Plants. **2025**;31:823-833. https://doi.org/10.1007/s12298-025-01605-2

Ganie SA, Reddy AS. Stress-induced changes in alternative splicing landscape in rice: functional significance of splice isoforms in stress tolerance. Biology. **2021**;10(4):309. https://doi.org/10.3390/biology10040309

Garciadeblás B, Senn ME, Bañuelos MA, Rodríguez-Navarro A. Sodium transport and HKT transporters: the rice model. The Plant Journal. **2003**;34(6):788-801. https://doi.org/10.1046/j.1365-313X.2003.01764.x

Han Y, Yin S, Huang L, Wu X, Zeng J, Liu X, Qiu L, Munns R, Chen ZH, Zhang G. A sodium transporter HvHKT1;1 confers salt tolerance in barley via regulating tissue and cell ion homeostasis. Plant and Cell Physiology. **2018**;59(10):1976-1989. https://doi.org/10.1093/pcp/pcy116

Hasegawa PM. Sodium ($Na^+$) homeostasis and salt tolerance of plants. Environmental and Experimental Botany. **2013**;92:19-31. https://doi.org/10.1016/j.envexpbot.2013.03.001

Hauser F, Horie T. A conserved primary salt tolerance mechanism mediated by HKT transporters: a mechanism for sodium exclusion and maintenance of high $K^+/Na^+$ ratio in leaves during salinity stress. Plant, Cell & Environment. **2010**;33(4):552-565. https://doi.org/10.1111/j.1365-3040.2009.02056.x

Haxim Y, Wang L, Pan Z, Fan X, Ma J. A novel high-affinity potassium transporter SeHKT1;2 from halophyte *Salicornia europaea* shows strong selectivity for $Na^+$ rather than $K^+$. Frontiers in Plant Science. **2023**;14:1104070. https://doi.org/10.3389/fpls.2023.1104070

Henderson SW, Dunlevy JD, Wu Y, Blackmore DH, Walker RR, Edwards EJ, Gilliham M, Walker AR. Functional differences in transport properties of natural HKT1;1 variants influence shoot $Na^+$ exclusion in grapevine rootstocks. New Phytologist. **2018**;217(3):1113-1127. https://doi.org/10.1111/nph.14888

Hibino H, Inanobe A, Furutani K, Murakami S, Findlay IA, Kurachi Y. Inwardly rectifying potassium channels: their structure, function, and physiological roles. Physiological Reviews. **2010**;90(1):291-366. https://doi.org/10.1152/physrev.00021.2009

Horie T, Hauser F, Schroeder JI. HKT transporter-mediated salinity resistance mechanisms in Arabidopsis and monocot crop plants. Trends in Plant Science. **2009**;14(12):660-668. https://doi.org/10.1016/j.tplants.2009.08.009

Imran S, Horie T, Katsuhara M. Expression and ion transport activity of rice OsHKT1;1 variants. Plants. **2020**;9(1):16. https://doi.org/10.3390/plants9010016

Imran S, Tsuchiya Y, Tran ST, Katsuhara M. Identification and characterization of rice OsHKT1;3 variants. Plants. **2021**;10(10):2006. https://doi.org/10.3390/plants10102006

Ismail AM, Horie T. Genomics, physiology, and molecular breeding approaches for improving salt tolerance. Annual Review of Plant Biology. **2017**;68:405-434. https://doi.org/10.1146/annurev-arplant-042916-040936

Jabnoune M, Espeout S, Mieulet D, Fizames C, Verdeil JL, Conéjéro G, Rodríguez-Navarro A, Sentenac H, Guiderdoni E, Abdelly C, Véry AA. Diversity in expression patterns and functional properties in the rice HKT transporter family. Plant Physiology. **2009**;150(4):1955-1971. https://doi.org/10.1104/pp.109.138008

Katsuhara M, Akiyama Y, Koshio K, Shibasaka M, Kasamo K. Functional analysis of water channels in barley roots. Plant and Cell Physiology. **2002**;43(8):885-893. https://doi.org/10.1093/pcp/pcf102

Kawakami Y, Imran S, Katsuhara M, Tada Y. $Na^+$ transporter SvHKT1;1 from a halophytic turf grass is specifically upregulated by high $Na^+$ concentration and regulates shoot $Na^+$ concentration. International Journal of Molecular Sciences. **2020**;21(17):6100. https://doi.org/10.3390/ijms21176100

Liu L, Li X, Wang C, Ni Y, Liu X. The role of chloride channels in plant responses to NaCl. International Journal of Molecular Sciences. **2023**;25(1):19. https://doi.org/10.3390/ijms25010019

Liu RW, Yuan JZ, Li XY, Cui YN, Cai MM, He ZH, Ma Q. Aluminum-activated Malate Transporter 12 is involved in restricting root-to-shoot $Cl^-$ transport in Arabidopsis under $Cl^-$-salt stress. Plant and Soil. **2022**;478:461-478. https://doi.org/10.1007/s11104-022-05484-4

Lv J, Zhou F, Wei Q, Long X, Tian W, Zhai J, Wang J, Zhang Q, Wan D. An alternative 3′ splice site of *PeuHKT1;3* improves the response to salt stress through enhancing affinity to $K^+$ in *Populus*. Plant Physiology and Biochemistry. **2024**;212:108776. https://doi.org/10.1016/j.plaphy.2024.108776

Lv M, Xiong Y, Yang H, Wang J, Zhang L, Zuo K. The interaction complexes of TsHKT1 splicing variants enhance salt tolerance of *Thellungiella salsuginea* by decreasing $Na^+$ uptake. Plant Science. **2025**;23:112678. https://doi.org/10.1016/j.plantsci.2025.112678

Magaraggia F, Solinas G, Valle G, Giovinazzo G, Coraggio I. Maturation and translation mechanisms involved in the expression of a myb gene of rice. Plant molecular biology. **1997**;35(6):1003-1008. https://doi.org/10.1023/A:1005821518242

Mahdieh M, Mostajeran A, Horie T, Katsuhara M. Drought stress alters water relations and expression of PIP-type aquaporin genes in Nicotiana tabacum plants. Plant and Cell Physiology. **2008**;49(5):801-813. https://doi.org/10.1093/pcp/pcn054

Mäser P, Eckelman B, Vaidyanathan R, Horie T, Fairbairn DJ, Kubo M, Yamagami M, Yamaguchi K, Nishimura M, Uozumi N, Robertson W. Altered shoot/root $Na^+$ distribution and bifurcating salt sensitivity in Arabidopsis by genetic disruption of the $Na^+$ transporter AtHKT1. FEBS Letters. **2002**;531(2):157-161. https://doi.org/10.1016/S0014-5793(02)03488-9

Matsukura S, Mizoi J, Yoshida T, Todaka D, Ito Y, Maruyama K, Shinozaki K, Yamaguchi-Shinozaki K. Comprehensive analysis of rice *DREB2*-type genes that encode transcription factors involved in the expression of abiotic stress-responsive genes. Molecular Genetics and Genomics. **2010**;283(2):185-196. https://doi.org/10.1007/s00438-009-0506-y

Meyer S, Mumm P, Imes D, Endler A, Weder B, Al-Rasheid KA, Geiger D, Marten I, Martinoia E, Hedrich R. *At*ALMT12 represents an R-type anion channel required for stomatal movement in Arabidopsis guard cells. The Plant Journal. **2010**;63(6):1054-1062. https://doi.org/10.1111/j.1365-313X.2010.04302.x

Munns R, James RA, Xu B, Athman A, Conn SJ, Jordans C, Byrt CS, Hare RA, Tyerman SD, Tester M, Plett D. Wheat grain yield on saline soils is improved by an ancestral Na+ transporter gene. Nature Biotechnology. **2012**;30(4):360-364. https://doi.org/10.1038/nbt.2120

Munns R, Tester M. Mechanisms of salinity tolerance. Annual Review of Plant Biology. **2008**;59(1):651-681. https://doi.org/10.1146/annurev.arplant.59.032607.092911

Nakamura A, Fukuda A, Sakai S, Tanaka Y. Molecular cloning, functional expression and subcellular localization of two putative vacuolar voltage-gated chloride channels in rice (*Oryza sativa* L.). Plant and Cell Physiology. **2006**;47(1):32-42. https://doi.org/10.1093/pcp/pci220

Nedelyaeva OI, Shuvalov AV, Balnokin YV. Chloride channels and transporters of the CLC family in plants. Russian Journal of Plant Physiology. **2020**;67(5):767-784. https://doi.org/10.1134/S1021443720050106

Plett D, Safwat G, Gilliham M, Skrumsager Møller I, Roy S, Shirley N, Jacobs A, Johnson A, Tester M. Improved salinity tolerance of rice through cell type-specific expression of AtHKT1;1. PloS One. **2010**;5(9):e12571. https://doi.org/10.1371/journal.pone.0012571

Quintero FJ, Garciadeblas B, Rodríguez-Navarro A. The *SAL1* gene of Arabidopsis, encoding an enzyme with 3'(2'), 5'-bisphosphate nucleotidase and inositol polyphosphate 1-phosphatase activities, increases salt tolerance in yeast. The Plant Cell. **1996**;8(3):529-537. https://doi.org/10.1105/tpc.8.3.529

Ren Z, Liu Y, Kang D, Fan K, Wang C, Wang G, Liu Y. Two alternative splicing variants of maize HKT1;1 confer salt tolerance in transgenic tobacco plants. Plant Cell, Tissue and Organ Culture. **2015**;123(3):569-578. https://doi.org/10.1007/s11240-015-0861-9

Ren ZH, Gao JP, Li LG, Cai XL, Huang W, Chao DY, Zhu MZ, Wang ZY, Luan S, Lin HX. A rice quantitative trait locus for salt tolerance encodes a sodium transporter. Nature Genetics. **2005**;37(10):1141-1146. https://doi.org/10.1038/ng1643

Rubio F, Gassmann W, Schroeder JI. Sodium-driven potassium uptake by the plant potassium transporter HKT1 and mutations conferring salt tolerance. Science. **1995**;270(5242):1660-1663. https://doi.org/10.1126/science.270.5242.1660

Rus A, Yokoi S, Sharkhuu A, Reddy M, Lee BH, Matsumoto TK, Koiwa H, Zhu JK, Bressan RA, Hasegawa PM. AtHKT1 is a salt tolerance determinant that controls $Na^+$ entry into plant roots. Proceedings of the National Academy of Sciences. **2001**;98(24):14150-14155. https://doi.org/10.1073/pnas.241501798

Sasaki T, Mori IC, Furuichi T, Munemasa S, Toyooka K, Matsuoka K, Murata Y, Yamamoto Y. Closing plant stomata requires a homolog of an aluminum-activated malate transporter. Plant and cell physiology. **2010**;51(3):354-365. https://doi.org/10.1093/pcp/pcq016

Sasaki T, Tsuchiya Y, Ariyoshi M, Nakano R, Ushijima K, Kubo Y, Mori IC, Higashiizumi E, Galis I, Yamamoto Y. Two members of the aluminum-activated malate transporter family, *SlALMT4* and *SlALMT5*, are expressed during fruit development, and the overexpression of *SlALMT5* alters organic

acid contents in seeds in tomato (*Solanum lycopersicum*). Plant and Cell Physiology. **2016**;57(11):2367-2379. https://doi.org/10.1093/pcp/pcw157

Shabala S, Cuin TA. Potassium transport and plant salt tolerance. Physiologia Plantarum. **2008**;133(4):651-69. https://doi.org/10.1111/j.1399-3054.2007.01008.x

Shi H, Ishitani M, Kim C, Zhu JK. The Arabidopsis thaliana salt tolerance gene SOS1 encodes a putative $Na^+/H^+$ antiporter. Proceedings of the National Academy of Sciences. **2000**;97(12):6896-6901. https://doi.org/10.1073/pnas.120170197

Shibasaka M, Horie T, Katsuhara M. Mechanisms activating latent functions of PIP aquaporin water channels via the interaction between PIP1 and PIP2 proteins. Plant and Cell Physiology. **2021**;62(1):92-99. https://doi.org/10.1093/pcp/pcaa142

Singh RK, Redoña E, Refuerzo L. Varietal Improvement for Abiotic Stress Tolerance in Crop Plants: Special Reference to Salinity in Rice. In Abiotic Stress Adaptation in Plants; Pareek, A., Sopory, S., Bohnert, H., Eds.; Springer: Dordrecht, Germany, **2009**, pp. 387–415. https://doi.org/10.1007/978-90-481-3112-9_18

Song H, Cao Y, Zhao X, Zhang L. Na+-preferential ion transporter HKT1;1 mediates salt tolerance in blueberry. Plant Physiology. **2024**;194(1):511-529. https://doi.org/10.1093/plphys/kiad510

Sopjani M. The AMP activated protein kinase in the regulation of sodium coupled transporters (SGLT1, EAAT3 & EAAT4) and eryptosis, [Ph.D thesis], **2010**, Eberhard Karls Universität Tübingen, Germany.

Subba A, Tomar S, Pareek A, Singla-Pareek SL. The chloride channels: silently serving the plants. Physiologia Plantarum. **2021**;171(4):688-702. https://doi.org/10.1111/ppl.13240

Sun J, Cao H, Cheng J, He X, Sohail H, Niu M, Huang Y, Bie Z. Pumpkin CmHKT1;1 controls shoot $Na^+$ accumulation via limiting $Na^+$ transport from rootstock to scion in grafted cucumber. International Journal of Molecular Sciences. **2018**;19(9):2648. https://doi.org/10.3390/ijms19092648

Sunarpi X, Horie T, Motoda J, Kubo M, Yang H, Yoda K, Horie R, Chan WY, Leung HY, Hattori K, Konomi M. Enhanced salt tolerance mediated by AtHKT1 transporter-induced $Na^+$ unloading from xylem vessels to xylem parenchyma

cells. The Plant Journal. **2005**;44(6):928-938. https://doi.org/10.1111/j.1365-313X.2005.02595.x

Takagi H, Tamiru M, Abe A, Yoshida K, Uemura A, Yaegashi H, Obara T, Oikawa K, Utsushi H, Kanzaki E, Mitsuoka C. MutMap accelerates breeding of a salt-tolerant rice cultivar. Nature Biotechnology. **2015**;33(5):445-449. https://doi.org/10.1038/nbt.3188

Wang R, Jing W, Xiao L, Jin Y, Shen L, Zhang W. The rice high-affinity potassium transporter1;1 is involved in salt tolerance and regulated by an MYB-type transcription factor. Plant Physiology. **2015a**;168(3):1076-1090. https://doi.org/10.1104/pp.15.00298

Wang S, Su SZ, Wu Y, Li SP, Shan XH, Liu HK, Wang S, Yuan YP. Overexpression of maize chloride channel gene *ZmCLC-d* in *Arabidopsis thaliana* improved its stress resistance. Biologia Plantarum. **2015b**;59(1):55-64. https://doi.org/10.1007/s10535-014-0468-8

Wege S, Jossier M, Filleur S, Thomine S, Barbier-Brygoo H, Gambale F, De Angeli A. The proline 160 in the selectivity filter of the Arabidopsis $NO_3^-/H^+$ exchanger AtCLCa is essential for nitrate accumulation in planta. The Plant Journal. **2010**;63(5):861-869. https://doi.org/10.1111/j.1365-313X.2010.04288.x

Wei L, Liu L, Chen Z, Huang Y, Yang L, Wang P, Xue S, Bie Z. CmCNIH1 improves salt tolerance by influencing the trafficking of CmHKT1;1 in pumpkin. The Plant Journal. **2023a**;114(6):1353-68. https://doi.org/10.1111/tpj.16197

Wei P, Wang L, Liu A, Yu B, Lam HM. *GmCLC1* confers enhanced salt tolerance through regulating chloride accumulation in soybean. Frontiers in Plant Science. **2016c**;7:1082. https://doi.org/10.3389/fpls.2016.01082

Wei Q, Liu Y, Zhou G, Li Q, Yang C, Peng SA. Overexpression of *CsCLCc*, a chloride channel gene from *Poncirus trifoliata*, enhances salt tolerance in Arabidopsis. Plant Molecular Biology Reporter. **2013b**;31(6):1548-57. https://doi.org/10.1007/s11105-013-0592-1

Wu FH, Shen SC, Lee LY, Lee SH, Chan MT, Lin CS. Tape-Arabidopsis Sandwich-a simpler Arabidopsis protoplast isolation method. Plant Methods. **2009**;5(1):16. https://doi.org/10.1186/1746-4811-5-16

Wu H, Li Z. The importance of $Cl^-$ exclusion and vacuolar $Cl^-$ sequestration: revisiting the role of $Cl^-$ transport in plant salt tolerance. Frontiers in Plant Science. **2019**;10:1418. https://doi.org/10.3389/fpls.2019.01418

Xue S, Yao X, Luo W, Jha D, Tester M, Horie T, Schroeder JI. AtHKT1;1 mediates nernstian sodium channel transport properties in Arabidopsis root stelar cells. PloS One. **2011**;6(9):e24725. https://doi.org/10.1371/journal.pone.0024725

Yoo SD, Cho YH, Sheen J. *Arabidopsis* mesophyll protoplasts: a versatile cell system for transient gene expression analysis. Nature Protocols. **2007**;2(7):1565-72. https://doi.org/10.1038/nprot.2007.199

Zhang H, Yu C, Zhang Q, Qiu Z, Zhang X, Hou Y, Zang J. Salinity survival: Molecular mechanisms and adaptive strategies in plants. Frontiers in Plant Science. **2025**;16:1527952. https://doi.org/10.3389/fpls.2025.1527952

Zhang Y, Chen Z, Tian H, Wu Y, Kong Y, Wang X, Sui N. Alternative splicing plays a crucial role in the salt tolerance of foxtail millet. Journal of Agricultural and Food Chemistry. **2024**;72(19):10814-10827. https://doi.org/10.1021/acs.jafc.4c00809

Zhang Y, Su J, Duan S, Ao Y, Dai J, Liu J, Wang P, Li Y, Liu B, Feng D, Wang J. A highly efficient rice green tissue protoplast system for transient gene expression and studying light/chloroplast-related processes. Plant Methods. **2011**;7(1):30. https://doi.org/10.1186/1746-4811-7-30

Zhou Y, Li XH, Guo QH, Liu P, Li Y, Wu CA, Yang GD, Huang JG, Zhang SZ, Zheng CC, Yan K. Salt responsive alternative splicing of a RING finger E3 ligase modulates the salt stress tolerance by fine-tuning the balance of COP9 signalosome subunit 5A. PLoS Genetics. **2021**;17(11):e1009898. https://doi.org/10.1371/journal.pgen.1009898

Zhu JK. Salt and drought stress signal transduction in plants. Annual Review of Plant Biology. **2002**;53(1):247-273. https://doi.org/10.1146/annurev.arplant.53.091401.143329

Zhu Z, Liu X, Meng F, Jiang A, Zhou Y, Yuan F, Chen M. LbHKT1;1 negatively regulates salt tolerance of Limonium bicolor by decreasing salt secretion rate of salt glands. Plant, Cell & Environment. **2025**;48(5):3544-3558. https://doi.org/10.1111/pce.15375

# SECTION 2

# Development of Transgenic Rice Lines

## Introduction

The OsHKT1;1 gene, belonging to the high-affinity potassium transporter (HKT) family, plays a vital role in maintaining $Na^+$ and $Cl^-$ homeostasis and conferring salinity tolerance in rice (Wang et al., 2015; Takagi et al., 2015). Recent studies revealed that alternative splicing of OsHKT1;1 generates multiple variants with distinct transport properties and expression profiles (Imran et al., 2020). Among these, the full-length OsHKT1;1-FL mediates $Na^+$-selective transport, while the truncated variant OsHKT1;1-V2 functions as a $Cl^-$-permeable channel despite lacking the canonical HKT pore structure (Imran et al., 2026). Electrophysiological assays using *Xenopus laevis* oocytes demonstrated that OsHKT1;1-V2 produces robust inward and outward $Cl^-$ currents, and $Cl^-$ concentration–dependent reversal potential shifts, confirming its strong $Cl^-$ selectivity (Imran et al., 2026). Consistent with these electrophysiological characteristics, oocytes expressing OsHKT1;1-V2 accumulated significantly more $Cl^-$ content than OsHKT1;1-FL or water-injected controls, providing physiological evidence of its $Cl^-$ transport capacity (Imran et al., 2026). Structural inspection further revealed that OsHKT1;1-V2 has only one transmembrane helix and a GKxGPxx–like motif reminiscent of part of the CLC selectivity filter, suggesting that the variant may assemble as a minimal anion-conducting unit or interact with other membrane components to form a functional $Cl^-$ pathway. Both OsHKT1;1-FL and OsHKT1;1-V2 localize to the plasma membrane, indicating their direct involvement in ion flux regulation at the cell surface. Moreover, the transcript levels of the two isoforms change markedly between salt-tolerant and salt-sensitive rice cultivars, suggesting that alternative splicing of OsHKT1;1 contributes to genotype-specific salt adaptation mechanisms (Imran et al., 2026).

Building on these findings, the present study aims to develop transgenic rice lines expressing OsHKT1;1-FL and OsHKT1;1-V2 under the control of the native OsHKT1;1 promoter to investigate their physiological functions *in planta*. The putative OsHKT1;1 promoter was successfully isolated, cloned, and functionally validated using EGFP reporter assays in rice protoplasts, confirming its transcriptional activity.

Promoter-driven constructs—pEGAD:OsHKT1;1pro.-OsHKT1;1-FL and pEGAD:OsHKT1;1pro.-OsHKT1;1-V2—were introduced into *Oryza sativa* cv. Nipponbare via Agrobacterium-mediated transformation (Wang et al., 2015). These transgenic lines will allow detailed analyses of $Na^+$, $K^+$, and $Cl^-$ accumulation and distribution in tissues, growth performance, and salt tolerance. Ultimately, this work will illuminate the distinct physiological roles, structural features, and regulatory mechanisms of OsHKT1;1 variants in shaping rice salinity adaptation (Imran et al., 2026; Wang et al., 2015).

## Materials and Methods

### Plasmid Construction

Genomic DNA was extracted from rice (*Oryza sativa* L. cv. Nipponbare) seedlings using. The putative promoter region of OsHKT1;1 was amplified from the extracted genomic DNA by PCR using Pro.OsHKT1;1 Fw: CATGTCATCATTCATGCAAAATC and BamHIAgeIOsHKT1;1pro-Rv: GGGGATCCACCGGTTCTTCAACAAATTTTTTGGGCT primers. The promoter was purified from agarose gel using NucleoSpin gel and PCR cleanup kit. The purified product was then digested using SacI (Takara Bio Inc., Japan) and BamHI (Toyobo Co., Ltd., Japan) restriction enzymes for the desired promoter size (789 bp), following a previous study (Wang et al., 2015). The pBluescript KS(−) cloning vector was also digested using the same set of restriction enzymes. The resulting DNA was cloned into a cloning vector, pBluescript KS(−). Next, 2 µL of the cloning product was transformed into E. coli, and DNA was extracted from the grown transformants. The recombinant DNA sequence was confirmed by Sanger sequencing. The pBluescript KS(−) cloning vector containing the putative promoter region of OsHKT1;1 was then digested using SacI (Takara Bio Inc., Japan) and AgeI (Biolabs, USA) restriction enzymes. The pEGAD vector was also digested with the same set of restriction enzymes, and the regions other than the 35S promoter region controlling EGFP expression were separated by agarose gel electrophoresis. The extracted DNA sequence was used as the vector in the subsequent ligation step. The restriction enzyme-digested insert and vector were cleaned up using a spin column and then ligated using the DNA ligation kit Ligation High (Toyobo Co. Ltd., Japan). The putative OsHKT1;1 promoter region was inserted into the pEGAD vector, replacing the 35S promoter region immediately preceding EGFP. This resulted in the preparation of a transfer DNA (T-DNA) plasmid

(pEGAD: OsHKT1;1pro.-EGFP) whose expression is controlled by the OsHKT1;1 promoter (Figure 2.20). After Ligation High treatment, 2 µL of the ligation product was transformed into E. coli, and DNA was extracted from the grown transformants. The recombinant DNA sequence was confirmed by Sanger sequencing.

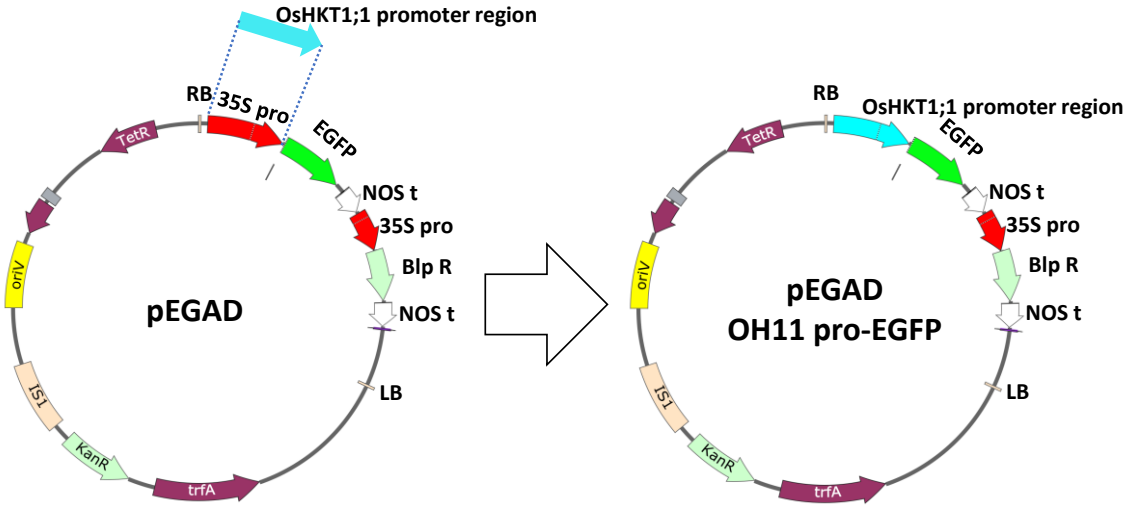


**Figure 2.20.** Schematic diagram of pEGAD and the OsHKT1;1 putative promoter region insertion vector. OsHKT1;1 promoter region indicates the putative OsHKT1;1 promoter sequence, EGFP indicates the EGFP ORF sequence, NOS t indicates the NOS terminator sequence, and 35S pro indicates the 35S promoter sequence. Blp R indicates the bar gene, which is a BASTA resistance gene. Tet R and Kan R indicate the tetracycline resistance gene and kanamycin resistance gene, respectively. RB and LB indicate T-DNA border sequences.

### EGFP Fluorescence Imaging

Rice protoplasts were transfected with constructs containing either the constitutive CaMV 35S promoter (positive control), the OsHKT1;1 promoter (test construct), or no DNA (negative control). The transfection with the polyethylene glycol (PEG 4000) method was carried out according to Yoo et al. (2007) as described previously (Sasaki et al., 2016). Incubation solution (0.5 M mannitol, 20 mM KCl, and 4 mM MES; pH 5.7) was used to re-suspend the protoplasts, which were then left in the dark at 24 °C for 16 hours (Zhang et al., 2011). Confocal microscopy was conducted, and an Olympus FluoView 1000 inverted laser scanning confocal imaging system (Olympus, Japan) was used to capture pictures. GFP was detected using 473 nm excitation with a 490–525 nm bandpass filter, whereas chlorophyll was identified with a 543 nm excitation and a 560–620 nm bandpass filter.

**Preparation of T-DNA Plasmid of OsHKT1;1 Promoter-Controlled OsHKT1;1-FL and OsHKT1;1-V2**

The prepared plasmid was used to generate rice transformants and to prepare T-DNA plasmids expressing OsHKT1;1-FL and OsHKT1;1-V2 under the control of the OsHKT1;1 promoter. OsHKT1;1-FL and OsHKT1;1-V2 were amplified by PCR using AgeI.OsHKT1;1-FL-Fw: ATTTGTTGAAGAACCGGTATGCATCCACCAAGTT and EcoRI.OsHKT1;1-FL-Rv: CTTCTCGAGCCCGGGGAATTCTCATTTCA GGATGAAC; AgeI.OsHKT1;1-V2-Fw: ATTTGTTGAAGAACCGGTATGCAT CCACCAAGTT and EcoRI.OsHKT1;1-V2-Rv: CTTCTCGAGCCCGGGGAA TTCTCAGTACATTTCTTGC primers, respectively, which added restriction enzyme sites at both ends of the OsHKT1;1-FL and OsHKT1;1-V2 sequence. The PCR products of OsHKT1;1-FL and OsHKT1;1-V2 were purified from agarose gel using NucleoSpin gel and PCR cleanup kit. The PCR-amplified OsHKT1;1-FL and OsHKT1;1-V2 sequences were used as an insert in the subsequent ligation reaction. The pEGAD:OsHKT1;1pro.-EGFP vector was digested with the restriction enzymes AgeI (Biolabs, USA) and EcoRI (Takara Bio Inc., Japan), and the region other than the EGFP sequence was separated by agarose gel electrophoresis. The extracted DNA sequence was used as the vector for the subsequent ligation step. After spin column cleanup, the insert and vector were reacted and ligated using the NEBuilder HiFi DNA Assembly Cloning Kit (Biolabs, USA). OsHKT1;1-FL and OsHKT1;1-V2 were inserted into pEGAD:OsHKT1;1pro.-EGFP in place of EGFP, yielding the pEGAD:OsHKT1;1pro.-OsHKT1;1-FL and pEGAD:OsHKT1;1pro.-OsHKT1;1-V2 whose expression is controlled by the OsHKT1;1 promoter (Figure 2.21). After ligation, 2 µL of the ligation product was transformed into E. coli, and DNA was extracted from the grown transformants. The recombinant DNA sequence was confirmed by Sanger sequencing. The prepared plasmid was used to generate rice transformants.

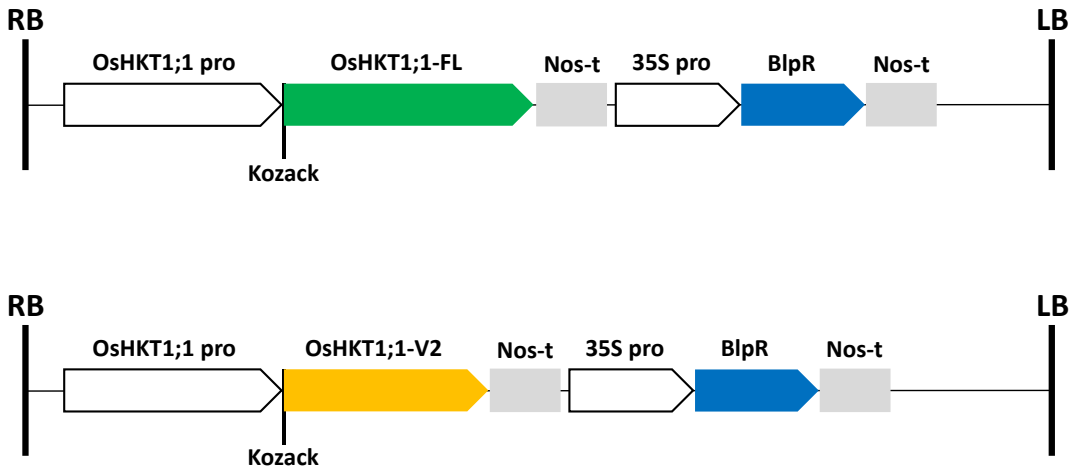


**Figure 2.21.** Schematic diagram of the pEGAD:OsHKT1;1pro.-OsHKT1;1-FL and pEGAD:OsHKT1;1pro.-OsHKT1;1-V2. OsHKT1;1 pro indicates the putative OsHKT1;1 promoter sequence, OsHKT1;1-FL/-V2 indicates the OsHKT1;1-FL/-V2 ORF sequence, Kozack indicates the Kozak sequence, Nos-t indicates the NOS terminator sequence, 35S pro indicates the 35S promoter sequence, and BlpR indicates the bar gene.

### Transformation into Rice Plants

For the actual work of producing transformed rice, I sent the seeds of the rice cultivars to be used and the vector construct to the Akita Prefectural University Biotechnology Center and requested that they carry out the transformation. Knock out (KO) rice line of OsHKT1;1 in the Nipponbare background was transformed with pEGAD:OsHKT1;1pro.-EGFP, pEGAD:OsHKT1;1pro.OsHKT1;1-FL, and pEGAD:OsHKT1;1pro.OsHKT1;1-V2. Transformation was performed using the Agrobacterium method, and the target gene was introduced via T-DNA insertion into calli induced from mature rice seeds. BASTA (a glufosinate herbicide) was used at a concentration of 200 μg $ml^{-1}$ to select regenerated transformants. The regenerated plants of the transformants were sent from the Biotechnology Center and acclimated for 5 days in a chamber with a 12-hour light and 12-hour dark photoperiod at 26°C. After that, they were transferred to Wagner pots and grown hydroponically under the same light/dark conditions as during acclimation. The nutrient solution for hydroponic culture was 4 mM $KNO_3$, 1 mM $NH_4H_2PO_4$, 1 mM $CaCl_2$·2H2O, 0.42 mM $MgSO_4$·$7H_2O$, 9.1 μM $MnCl_2$·$4H_2O$, 0.32 μM $CuSO_4$·$5H_2O$, 0.77 μM $ZnSO_4$·$7H_2O$, 46.3 μM $H_3BO_3$, 97 μM $Na_2MoO_4$, 0.11 mM NaOH, 17.5 μM $FeCl_3$·$6H_2O$, and 19.6 μM citrate (pH 5.5–6.0) in a volume of 3.5 L. The nutrient solution was changed every three days.

**Result and Discussion**

Previous study reported that knockout of OsHKT1;1 (*oshkt1;1*) abolished its expression and caused strong salt sensitivity, with reduced growth, lower chlorophyll, poor survival, and higher $Na^+$ accumulation in shoots, especially leaf blades (Wang et al., 2015). The mutant also showed reduced $Na^+$ in phloem sap and increased $Na^+$ in xylem sap, indicating disrupted $Na^+$ transport and recirculation. However, complementation of OsHKT1;1 fully restored wild-type phenotypes, including normal salt tolerance and shoot $Na^+$ levels (Wang et al., 2015). These results confirm that OsHKT1;1 is essential for limiting $Na^+$ accumulation in shoots and maintaining salt tolerance in rice. Previous study focused only on the full-length OsHKT1;1. However, in the present study, I focused on a splice variant, OsHKT1;1-V2, that generates strong $Cl^-$ currents, exhibits clear $Cl^-$-dependent reversal potential shifts, accumulates high intracellular $Cl^-$ in oocytes, and likely functions as a minimal anion-conducting unit despite lacking the canonical HKT pore. But it is necessary to clarify the physiological significance of this ion transport mechanism in rice plants. In this chapter, I used the *Tos17* insertion KO line as a background to generate rice mutants by introducing OsHKT1;1-FL or OsHKT1;1-V2 together with the putative OsHKT1;1 promoter. Furthermore, to confirm the functionality of OsHKT1;1 promoter, transient expression analysis of the OsHKT1;1 promoter fused with the EGFP reporter gene was analyzed in rice protoplasts. Strong green fluorescence was observed in protoplasts transfected with the 35S promoter-EGFP construct, confirming successful transformation and reporter expression (Figure 2.22A-C). Protoplasts expressing the OsHKT1;1 promoter-EGFP construct exhibited detectable green fluorescence, indicating that the OsHKT1;1 promoter is functional and capable of driving gene expression in rice cells (Figure 2.22D-F). No fluorescence was observed in the negative control, confirming the specificity of the observed signals (Figure 2.22G-I). These results suggest that the putative promoter region of OsHKT1;1 can function as an active promoter, potentially similar to the OsHKT1;1 promoter.

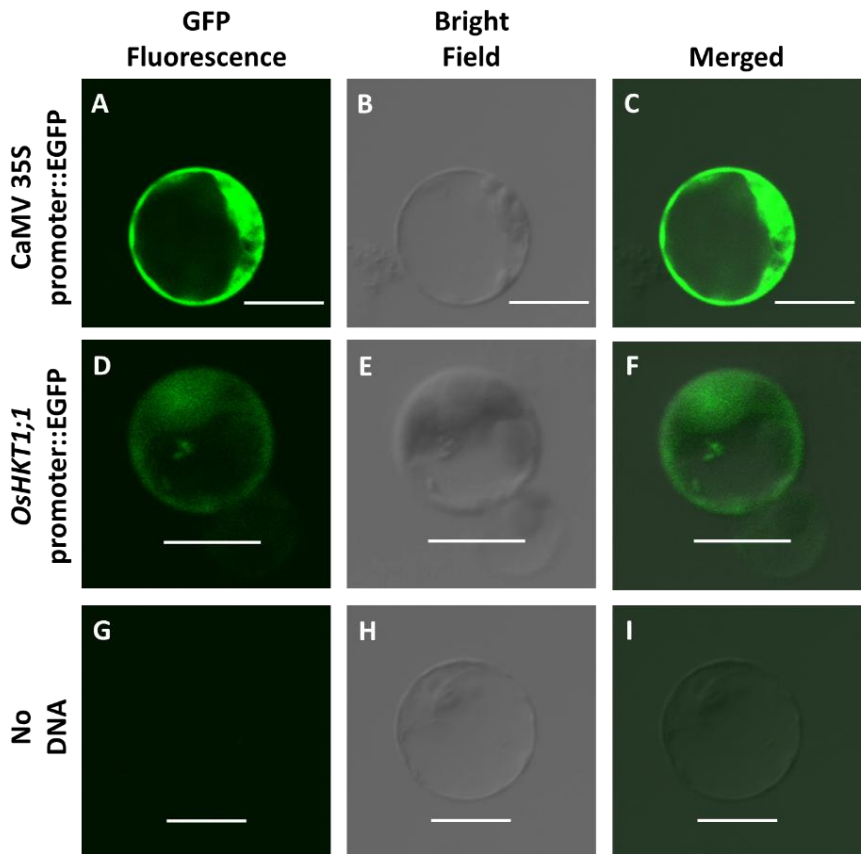


**Figure 2.22.** Expression of EGFP driven by the OsHKT1;1 promoter in rice protoplasts. Rice protoplasts were transiently transfected with constructs containing the (**A-C**): CaMV 35S promoter::EGFP (positive control), (**D-F**) *OsHKT1;1* promoter::EGFP, or (**G-I**) no DNA (negative control). Fluorescence (A, D, G), bright-field (B, E, H), and merged (C, F, I) images were captured using confocal microscopy. Scale bars = 10 μm.

After transformation, plants regenerated from callus were grown in hydroponics for about 2 weeks. For seed production, rice plants of each line were then grown in soil. As a result, for all lines, rice seeds of the next generation ($T_1$) could be obtained from the transformed rice plantlets of the current generation ($T_0$). At the time of writing, $T_0$ plants of transgenic rice were still being grown (Figure 2.23). In this study, I only confirmed that the cloned promoter region functions as the OsHKT1;1 promoter in rice plants.

**Figure 2.23.** Transformant rice during growth.

Furthermore, the T-DNA insertion site in the genomic DNA may vary among individuals during regeneration, potentially resulting in unstable expression at the cellular and tissue levels. Therefore, it is necessary to establish homozygous transgenic lines. After seed collection in the $T_1$ generation, I plan to analyze the genomic DNA from each individual to confirm the presence or absence of transformation, and then use the established lines to analyze physiological function at the plant level. Using these transformants, I plan to investigate the accumulation of $Na^+$, $K^+$, and $Cl^-$, plant growth, and phenotypes under salt stress. This should lead to a deeper understanding of the function and physiological significance of OsHKT1;1-FL and OsHKT1;1-V2 in plants.

**References**

Imran S, Ono S, Horie R, Katsuhara M, Horie T. Chloride-Transporting OsHKT1;1 Splice Variants and Their Expression Profiles under Salinity Stress in Rice. International Journal of Molecular Sciences. **2026**;27(3):1178. https://doi.org/10.3390/ijms27031178

Sasaki T, Tsuchiya Y, Ariyoshi M, Nakano R, Ushijima K, Kubo Y, Mori IC, Higashiizumi E, Galis I, Yamamoto Y. Two members of the aluminum-activated malate transporter family, *SlALMT4* and *SlALMT5*, are expressed during fruit development, and the overexpression of *SlALMT5* alters organic acid contents in seeds in tomato (*Solanum lycopersicum*). Plant and Cell Physiology. **2016**;57(11):2367-2379. https://doi.org/10.1093/pcp/pcw157

Takagi H, Tamiru M, Abe A, Yoshida K, Uemura A, Yaegashi H, Obara T, Oikawa K, Utsushi H, Kanzaki E, Mitsuoka C. MutMap accelerates breeding of a salt-tolerant rice cultivar. Nature Biotechnology. **2015**;33(5):445-449. https://doi.org/10.1038/nbt.3188

Wang R, Jing W, Xiao L, Jin Y, Shen L, Zhang W. The rice high-affinity potassium transporter1;1 is involved in salt tolerance and regulated by an MYB-type transcription factor. Plant Physiology. **2015**;168(3):1076-1090. https://doi.org/10.1104/pp.15.00298

Yoo SD, Cho YH, Sheen J. *Arabidopsis* mesophyll protoplasts: a versatile cell system for transient gene expression analysis. Nature Protocols. **2007**;2(7):1565-1572. https://doi.org/10.1038/nprot.2007.199

Zhang Y, Su J, Duan S, Ao Y, Dai J, Liu J, Wang P, Li Y, Liu B, Feng D, Wang J. A highly efficient rice green tissue protoplast system for transient gene expression and studying light/chloroplast-related processes. Plant Methods. **2011**;7(1):30. https://doi.org/10.1186/1746-4811-7-30

# CHAPTER 3

# Survey of Barley Sodium Transporter HvHKT1;1 Variants and Their Functional Analysis

## Introduction

Salinity, a major environmental factor affecting crop productivity worldwide, especially in drylands, where irrigation practices often contribute to soil salinization (Tarolli et al., 2024). High salinity disrupts plant physiological processes by inducing osmotic stress, ion toxicity, and nutrient imbalance, leading to reduced seed germination, stunted growth, and lower yields (Pandit et al., 2024). Excessive sodium ($Na^+$) and chloride ($Cl^-$) affect essential metabolic functions, impairing photosynthesis and enzymatic activities (Zhou et al., 2024). Barley (*Hordeum vulgare* L.) is an important cereal crop cultivated widely, serving as a staple food, feed, and key ingredient in brewing. Despite its adaptability to diverse climates, barley growth and productivity are significantly limited by soil salinity, a common abiotic stress that adversely affects plant water uptake, nutrient balance, and overall physiological functions (Tarolli et al., 2024). Sodium toxicity is a primary factor in salinity stress, leading to ionic imbalances that disrupt cellular homeostasis and metabolic processes (Zhou et al., 2024).

High-affinity potassium transporters (HKTs) are a category of important membrane proteins essential for maintaining potassium ($K^+$) homeostasis in plants, especially under conditions of low soil $K^+$ availability or salinity stress. These transporters mainly help the absorption and distribution of $K^+$ and $Na^+$, which are crucial for various physiological processes, including osmotic regulation, enzyme activation, and maintaining membrane potential (Horie et al., 2009). HKTs are divided into two subclasses on the basis of their ion selectivity: Subclass I members primarily transport $Na^+$, while Subclass II members are more selective for $K^+$ (Platten et al., 2006). The foremost HKT gene, *HKT1*, was recognized in wheat, where it arbitrates high-affinity $K^+$ uptake and low-affinity $Na^+$ transport (Schachtman and Schroeder, 1994). Further research indicates that HKTs are widely existing across plant species such as Arabidopsis, rice, and barley, with their expression often regulated by environmental factors like salt stress, $K^+$ deficiency, and osmotic stress (Garciadeblás et al., 2003;

Hauser and Horie, 2010). In rice, *OsHKT1;1* controls $Na^+$ exclusion from shoots, enhancing salt tolerance by preserving a favorable $Na^+/K^+$ ratio (Ren et al., 2005). Similarly, in wheat, the homolog *TaHKT1;5-D* is associated with improved $Na^+$ elimination from leaves, aiding salinity tolerance in *Triticum durum* (Munns et al., 2012). In maize, *ZmHKT1;1* influences $Na^+$ uptake and translocation, with its overexpression resulting in increased salt sensitivity (Zhang et al., 2019). The barley *HKT1* gene was further identified as corresponding to *HKT1;1* through phylogenetic analysis and encoded a transporter that is selective for $Na^+$ (Han et al., 2018). Knockdown of *HvHKT1;1* using barley BSMV-induced gene silencing enhanced sensitivity to salt and $Na^+$ buildup in leaves and roots of barley lines, compared to controls, highlighting this gene's crucial role in barley's salt tolerance (Han et al., 2018).

In nearly all previous cases, researchers have focused only on the full-length protein to measure transport activity. However, Imran et al. (2020) reported the presence of several functional mRNA variants in rice *OsHKT1;1*. What about barley *HvHKT1;1*? In this study, I aimed to identify *HvHKT1;1* mRNA variants in a barley cultivar, Haruna-Nijo, and characterized their expression profiles and transport activities using qPCR analyses and two-electrode voltage-clamp (TEVC) experiments with *Xenopus laevis* (*X. laevis*) oocytes.

## Materials and Methods

### Plant Material and Growth Conditions

Barley (*Hordeum vulgare* L., cv. Haruna-Nijo) seeds were treated and grown. Briefly, seeds were sterilized with 10% $H_2O_2$ (10 min), germinated in aerated distilled water (1 day), and hydroponically cultured in 0.25 mM $CaSO_4$ (2 d) followed by nutrient solutions (4 mM $KNO_3$, 1 mM $NaH_2PO_4$, 1 mM $MgSO_4$, 1 mM $CaCl_2$, 1 mg $liter^{-1}$ Fe-citrate and pH 5.5 with NaOH). A five-day-old plant was used to extract total RNA. After that, 17-day-old seedlings were treated with 150 mM NaCl for the gene expression investigation. Plants were sampled at 0 (as a control), 2, 6, 12, and 24 hr following the start of treatment.

### Extraction of DNA, RNA, and Synthesis of cDNA

Barley gDNA was isolated as described in the DNeasy Plant Mini kit (Qiagen, Hilden, Germany). Total RNA was isolated as described in the RNeasy Plant Mini Kit (Qiagen, Hilden, Germany) and then treated with DNase I (Ambion, Austin, TX, USA)

to remove gDNA contamination. Reverse transcription was performed according to the ReverTra Ace qPCR RT Master Mix (TOYOBO, Osaka, Japan).

**Secondary Structure Analysis**

The secondary structure was determined using the online software Protter Ver. 1.0 (http://wlab.ethz.ch/protter/start/, accessed on 02 March 2025) (Wang et al., 2025).

**Expression Analysis**

After preparing the total RNA, DNase treatment was performed to remove any contaminating gDNA. First-strand cDNA synthesis was conducted using a high-capacity cDNA reverse transcription kit (Applied Biosystem by Thermo Fisher Scientific). Once the cDNA was prepared, amplified *HvHKT1;1-FL* and its variants with specific primers (Table 2.1). *HvEF1α* mRNA amplification served as internal control. Absolute quantification was conducted as mentioned previously (Imran et al., 2020), using the real-time PCR machine (model: 7300, Applied Biosystem, Foster City, CA, USA). Specific cDNAs served as standards to quantify every variant.

**Table 2.1.** Gene-specific primer pairs were used for the cloning and in the real-time PCR experiments.

| Primer Name | Sequence for full-length cloning | Sequence for real-time PCR |
|---|---|---|
| HvHKT1;1-F | ATGCATCGATTCAGCTCAGC | |
| HvHKT1;1-R | CTAATTTGCAGCCACCTCTGG | |
| HvHKT1;1-FL-F | | ATGTTCACCTCTGTGTCCACAGT |
| HvHKT1;1-FL-R | | CTGATTCATCGCTTTGCTTTCC |
| HvHKT1;1-V1-F | | GGAACTTGGATCTGATGTTCACC |
| HvHKT1;1-V1-R | | CTACAAGAATCTGATTGTGTGGC |
| HvHKT1;1-V2-F | | CTTGTTTCTGTGACGGTGTCGA |
| HvHKT1;1-V2-R | | CCTACAAGAATCTGATTGTGTGGC |
| HvHKT1;1-V3-F | | CTTGTTTCTGTGACGGTGTCGA |
| HvHKT1;1-V3-R | | GGATTACTGATTCATCGCTTTGC |

**Preparation of cRNA for *X. laevis* Oocytes Heterologous Expression**

The cDNAs of *HvHKT1;1* variants were subcloned into the vector pXβG as described (Imran et al., 2020; 2021). Capped RNAs (cRNAs) were synthesized as

mentioned previously (Imran et al., 2020). The cRNAs at concentrations of 50 ng/50 nL or 50 nL of nuclease-free water for the control were injected into *X. laevis* oocytes. The oocytes after injection were kept at 18 °C in MBS solution until electrophysiological measurements were performed (Imran et al., 2020).

**Electrophysiology**

Measurement of oocytes current using the TEVC technique was conducted 1 d after injection of cRNA as mentioned previously (Imran et al., 2020). Biological replicates were generated from oocytes derived from different frogs and batches, with results representative of two or more independent batches unless otherwise specified.

Across the tested concentrations, conductance was assessed at membrane potentials from −75 to −120 mV. Ion permeability ratios were estimated from reversal potential shifts using a modified Goldman equation (Tran et al., 2025) that excluded $Cl^-$ permeability and accounted solely for monovalent cations such as $Na^+$, $K^+$, $Rb^+$, $Cs^+$, and $Li^+$. The modified Goldman equation at the experimental temperature (20°C) is:

$$E_{rev} = -58\log\left(\frac{Constant}{\alpha[X^+]_{out} + [Na^+]_{out}}\right) \text{ (mV)}$$

Where $E_{rev}$ is the reversal potential (mV); α is ($P_x$, the permeability for the ion $X^+$)/($P_{Na}$, the permeability for $Na^+$); $[X^+]_{out}$ is the extracellular concentration of $X^+$; $[Na^+]$out is the extracellular concentration of $Na^+$. The intracellular concentrations of ions were expected to be constant within a few minutes of the measurements.

Two reversal potentials, $E_{rev(1)}$ and $E_{rev(2)}$, were measured using two different external solutions with the concentrations of $X^+$ and $Na^+$ as follows: External solution (1); $[X^+]_{out(1)}$ and $[Na^+]_{out(1)}$ for $E_{rev(1)}$ ; External solution (2); $[X^+]_{out(2)}$ and $[Na^+]_{out(2)}$ for $E_{rev(2)}$. According to $E_{rev}$ described above,

$$\begin{aligned} E_{rev(1)} - E_{rev(2)} &= -58\log\left(\frac{Constant}{\alpha[X^+]_{out(1)} + [Na^+]_{out(1)}}\right) \\ &+ 58\log\left(\frac{Constant}{\alpha[X^+]_{out(2)} + [Na^+]_{out(2)}}\right) \\ &= -58\log\left(\frac{\alpha[X^+]_{out(2)} + [Na^+]_{out(2)}}{\alpha[X^+]_{out(1)} + [Na^+]_{out(1)}}\right) \text{ (mV)} \end{aligned}$$

Based on the values of $E_{rev(1)}$, $E_{rev(2)}$, $[X^+]_{out(1)}$, $[Na^+]_{out(1)}$, $[X^+]_{out(2)}$, and $[Na^+]_{out(2)}$, the ion permeability ratios α ($P_X/P_{Na}$) were calculated.

**Statistical Analysis**

Statistical analyses were conducted using IBM SPSS Statistics version 25. Data were subjected to a one-way ANOVA. When more than two treatments were compared, Tukey's post hoc test was applied. For comparisons involving only two treatments, post hoc tests were not applicable, and significance was based on the ANOVA *p*-value. In R 4.4.3, "ggplot2" and "minpack.lm" packages were used to analyze ionic conductance.

## Results

### Identification of HvHKT1;1 Variants

Amplified several fragments from cDNAs derived from the barley variety Haruna-Nijo using full-length primers of *HvHKT1;1* (Figure 3.1A). This full-length *HvHKT1;1* clone (*HvHKT1;1-FL*; accession number: LC910891) encodes a 64.7 kDa polypeptide with 576 putative amino acids and consists of 1731 nucleotides (Figures 3.1B, 3.2, 3.3). After sequencing, in addition to the full-length sequence, three splicing variants were identified. These variants, *HvHKT1;1-V1* (accession number: LC910892), -*V2* (accession number: LC910893), and -*V3* (accession number: LC910894), have lengths of 1446, 1301, and 1586 nucleotides, respectively, and encode polypeptides of 54.0, 40.5, and 32.9 kDa, with 481, 362, and 294 deduced amino acids (Figures 3.1B, 3.2, 3.3). Eight transmembrane domains (1–8) were projected using the online program Protter (http://wlab.ethz.ch/protter/start/), as shown in Figure 3.1C.

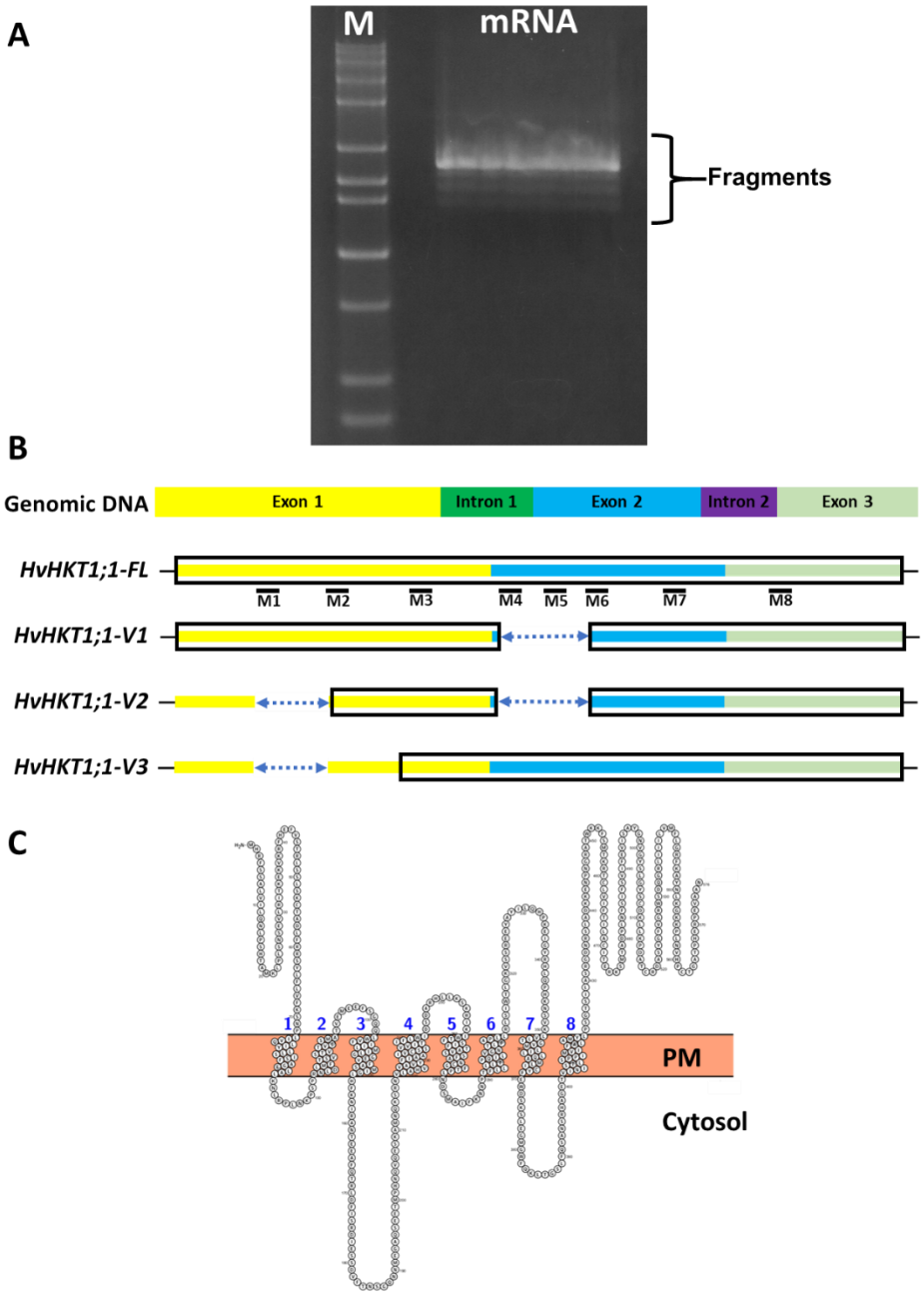


**Figure 3.1.** *HvHKT1;1* variants identified in barley cultivar Haruna-Nijo. (**A**) Gel picture of RT-PCR product that was amplified with primers for *HvHKT1;1*. (**B**) Diagrammatic representations of *HvHKT1;1-FL* and its splice variants. Black boxes designate amino acid regions identical to *HvHKT1;1-FL*; lines represent non-translated regions, and dotted lines show missing nucleotides (gaps) in comparison to the *HvHKT1;1-FL* sequence. (**C**) The transmembrane domain (M1-M8) of HvHKT1;1-FL projected using Protter (http://wlab.ethz.ch/protter/start/) (Wang et al., 2025).

```
HvHKT1;1-FL    1 ATGCATCGATTCAGCTCAGCTCTAGTTATCCTGCAGAATCTGCCATCGCATACAGCCATG 60
HvHKT1;1-V1    1 ATGCATCGATTCAGCTCAGCTCTAGTTATCCTGCAGAATCTGCCATCGCATACAGCCATG 60
HvHKT1;1-V2    1 ATGCATCGATTCAGCTCAGCTCTAGTTATCCTGCAGAATCTGCCATCGCATACAGCCATG 60
HvHKT1;1-V3    1 ATGCATCGATTCAGCTCAGCTCTAGTTATCCTGCAGAATCTGCCATCGCATACAGCCATG 60

HvHKT1;1-FL   61 AAGCTCCCATTATCCAATTCGGAAGTTCTTAGAATCACCAAGGAGAAAGTGAAGCGTTTC 120
HvHKT1;1-V1   61 AAGCTCCCATTATCCAATTCGGAAGTTCTTAGAATCACCAAGGAGAAAGTGAAGCGTTTC 120
HvHKT1;1-V2   61 AAGCTCCCATTATCCAATTCGGAAGTTCTTAGAATCACCAAGGAGAAAGTGAAGCGTTTC 120
HvHKT1;1-V3   61 AAGCTCCCATTATCCAATTCGGAAGTTCTTAGAATCACCAAGGAGAAAGTGAAGCGTTTC 120

HvHKT1;1-FL  121 CATGAGTTTGTGTCCACAAGGCTCAGTTCCCTCTCCAAGTGTACAGCAGATTTGTTCAGA 180
HvHKT1;1-V1  121 CATGAGTTTGTGTCCACAAGGCTCAGTTCCCTCTCCAAGTGTACAGCAGATTTGTTCAGA 180
HvHKT1;1-V2  121 CATGAGTTTGTGTCCACAAGGCTCAGTTCCCTCTCCAAGTGTACAGCAGATTTGTTCAGA 180
HvHKT1;1-V3  121 CATGAGTTTGTGTCCACAAGGCTCAGTTCCCTCTCCAAGTGTACAGCAGATTTGTTCAGA 180
                                                                      M1
HvHKT1;1-FL  181 CGCTCTTACTTGTTTCTGGTATTCAAAAGCAATCCTTTGATAGTCCAGCTTATTTACCTT 240
HvHKT1;1-V1  181 CGCTCTTACTTGTTTCTGGTATTCAAAAGCAATCCTTTGATAGTCCAGCTTATTTACCTT 240
HvHKT1;1-V2  181 CGCTCTTACTTGTTTCT---------------------------------------------- 197
HvHKT1;1-V3  181 CGCTCTTACTTGTTTCT---------------------------------------------- 197

HvHKT1;1-FL  241 TTGTCAATATCATTTGCTGGTTTCCTTGCTCTGAAGAACCTCAGGCCACTGAATAAGCCA 300
HvHKT1;1-V1  241 TTGTCAATATCATTTGCTGGTTTCCTTGCTCTGAAGAACCTCAGGCCACTGAATAAGCCA 300
HvHKT1;1-V2  197 ------------------------------------------------------------ 197
HvHKT1;1-V3  197 ------------------------------------------------------------ 197
                                                  M2
HvHKT1;1-FL  301 TCTCCAAGGAACTTGGATCTGATGTTCACCTCTGTGTCCACAGTGACGGTGTCGAGCATG 360
HvHKT1;1-V1  301 TCTCCAAGGAACTTGGATCTGATGTTCACCTCTGTGTCCACAGTGACGGTGTCGAGCATG 360
HvHKT1;1-V2  198 ----------------------------------------GTGACGGTGTCGAGCATG 215
HvHKT1;1-V3  198 ----------------------------------------GTGACGGTGTCGAGCATG 215
                                                             M3
HvHKT1;1-FL  361 GCAACAGTTGAGATGGAGGAATTCTCTGGCCAGCAGCTCTGGGTTTTCATCATACTGATG 420
HvHKT1;1-V1  361 GCAACAGTTGAGATGGAGGAATTCTCTGGCCAGCAGCTCTGGGTTTTCATCATACTGATG 420
HvHKT1;1-V2  216 GCAACAGTTGAGATGGAGGAATTCTCTGGCCAGCAGCTCTGGGTTTTCATCATACTGATG 275
HvHKT1;1-V3  216 GCAACAGTTGAGATGGAGGAATTCTCTGGCCAGCAGCTCTGGGTTTTCATCATACTGATG 275

HvHKT1;1-FL  421 ATATTGGGAGGAGAAGTGTTCGCTTCAATGATAGGGCTGCATTTCAAAAATATTCGGGCC 480
HvHKT1;1-V1  421 ATATTGGGAGGAGAAGTGTTCGCTTCAATGATAGGGCTGCATTTCAAAAATATTCGGGCC 480
HvHKT1;1-V2  276 ATATTGGGAGGAGAAGTGTTCGCTTCAATGATAGGGCTGCATTTCAAAAATATTCGGGCC 335
HvHKT1;1-V3  276 ATATTGGGAGGAGAAGTGTTCGCTTCAATGATAGGGCTGCATTTCAAAAATATTCGGGCC 335

HvHKT1;1-FL  481 AACACCGAGGAGGCCTTCCAGACAAGATTGGATTTTATAAGCAGGGACATCGAATCCTCT 540
HvHKT1;1-V1  481 AACACCGAGGAGGCCTTCCAGACAAGATTGGATTTTATAAGCAGGGACATCGAATCCTCT 540
HvHKT1;1-V2  336 AACACCGAGGAGGCCTTCCAGACAAGATTGGATTTTATAAGCAGGGACATCGAATCCTCT 395
HvHKT1;1-V3  336 AACACCGAGGAGGCCTTCCAGACAAGATTGGATTTTATAAGCAGGGACATCGAATCCTCT 395

HvHKT1;1-FL  541 GATGTTTTCACCAACAGCGGTCAGAATAATATGGAAGGCGCCCAGTCAGAGGAAACCATG 600
HvHKT1;1-V1  541 GATGTTTTCACCAACAGCGGTCAGAATAATATGGAAGGCGCCCAGTCAGAGGAAACCATG 600
HvHKT1;1-V2  396 GATGTTTTCACCAACAGCGGTCAGAATAATATGGAAGGCGCCCAGTCAGAGGAAACCATG 455
HvHKT1;1-V3  396 GATGTTTTCACCAACAGCGGTCAGAATAATATGGAAGGCGCCCAGTCAGAGGAAACCATG 455

HvHKT1;1-FL  601 CCACACAATCAGGTACAGGAAAGCAAAGCGATGAATCAGAAATCCCGCAATGTTTTGGCT 660
HvHKT1;1-V1  601 CCACACAATCA------------------------------------------------- 611
HvHKT1;1-V2  456 CCACACAATCA------------------------------------------------- 466
HvHKT1;1-V3  456 CCACACAATCAGGTACAGGAAAGCAAAGCGATGAATCAGTAATCCCGCAATGTTTTGGCT 515
                                                  M4
HvHKT1;1-FL  661 CATGTAGTAGCTGTCTATTTCATAGCAGCAATAGTTTGCAGCTCTGTAGTCATTACCATC 720
HvHKT1;1-V1  611 ------------------------------------------------------------ 611
HvHKT1;1-V2  466 ------------------------------------------------------------ 466
HvHKT1;1-V3  516 CATGTAGTAGCTGTCTATTTCATAGCAGCAATAGTTTGCAGCTCTGTAGTCATTACCATC 575

HvHKT1;1-FL  721 TTCCTATGGATTGACTCCGATGCAAGGCATCTACTGAAGAGTAAACATATCAAAATTTGG 780
HvHKT1;1-V1  611 ------------------------------------------------------------ 611
HvHKT1;1-V2  466 ------------------------------------------------------------ 466
HvHKT1;1-V3  576 TTCCTATGGATTGACTCCGATGCAAGGCATCTACTGAAGAGTAAACATATCAAAATTTGG 635
                                                  M5
HvHKT1;1-FL  781 ACATTCTCAATCTTCACAGCAGTATCATCATTTGCAAACTGCGGCTTCACTCCGTTGAAT 840
HvHKT1;1-V1  611 ------------------------------------------------------------ 611
HvHKT1;1-V2  466 ------------------------------------------------------------ 466
HvHKT1;1-V3  636 ACATTCTCAATCTTCACAGCAGTATCATCATTTGCAAACTGCGGCTTCACTCCGTTGAAT 695
                                                                      M6
HvHKT1;1-FL  841 GATAGCATGGCAATTTTCAAAAATAACCCAACTTTCCTTCTTCTGCTTACCCCACAGATT 900
HvHKT1;1-V1  612 ----------------------------------------------------------GATT 615
HvHKT1;1-V2  467 ----------------------------------------------------------GATT 470
HvHKT1;1-V3  696 GATAGCATGGCAATTTTCAAAAATAACCCAACTTTCCTTCTTCTGCTTACCCCACAGATT 755
```


**Figure 3.2.** Nucleotide sequence alignment of HvHKT1;1 and its variants using GENETYX ver. 16. M1–M8 indicate transmembrane domains predicted using previously registered data from the GeneBank database.

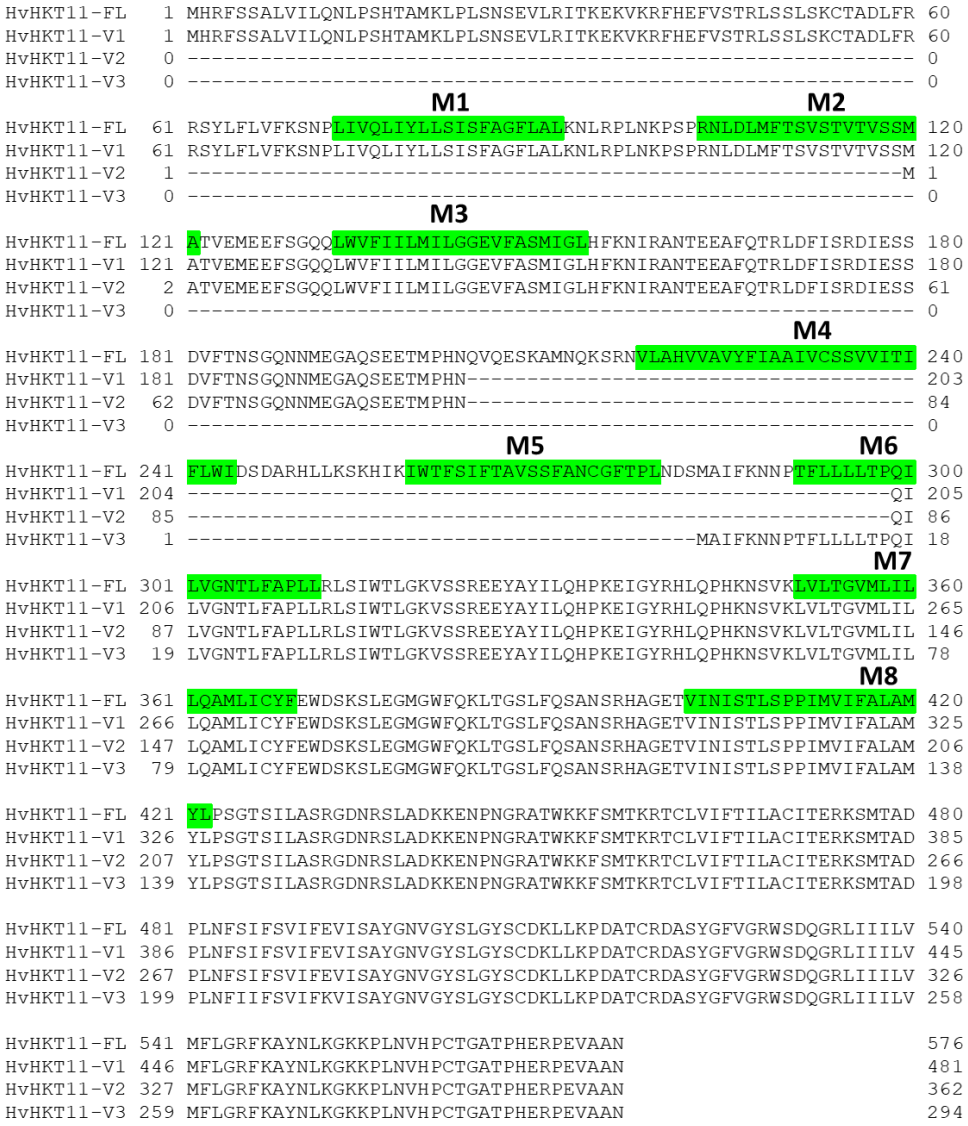


**Figure 3.3.** Protein sequence alignment of HvHKT1;1 and its variants using GENETYX ver. 16. M1–M8 indicate transmembrane domains predicted using previously registered data from the GeneBank database.

## Expression Profiling of HvHKT1;1-FL and Its Variants

Barley plants at 17 days old were examined to evaluate the tissue-specific expression profile of *HvHKT1;1* grown under normal conditions. The full-length *HvHKT1;1-FL* shows significantly highest expression in all tissues, especially in the leaf, followed by the sheath and root (Figure 3.4A-C). However, *HvHKT1;1-V1* shows moderate expression levels, mainly in the leaf and sheath, with minimal presence in the root, while *HvHKT1;1-V2* exhibits relatively low expression across all tissues, with the lowest abundance among the variants (Figure 3.4A-C). Interestingly, *HvHKT1;1-V3* showed significantly high expression in the leaf, with a moderate level in the root and

sheath, indicating its potential tissue preference distinct from the other variants. (Figure 3.4A-C).

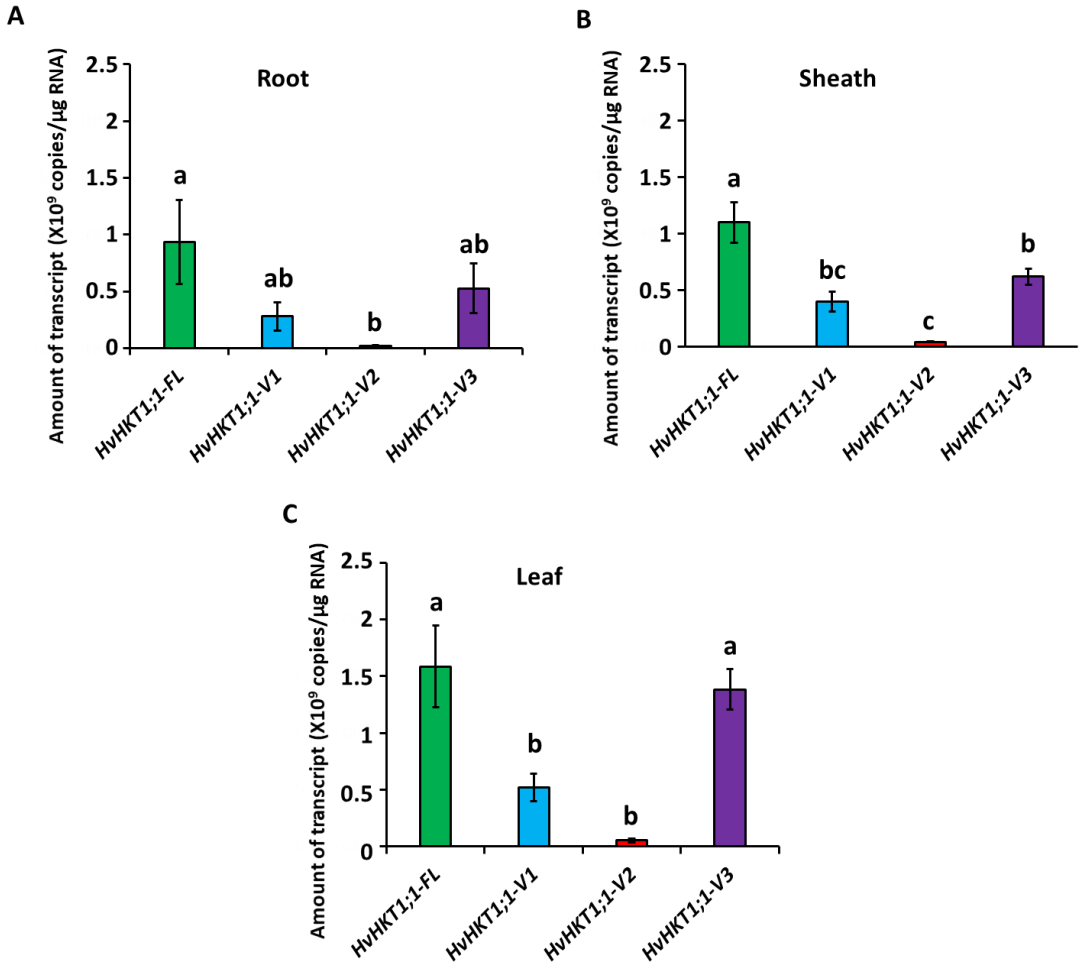


**Figure 3.4.** qPCR analyses of *HvHKT1;1-FL* and its variants' transcripts in the barley cultivar Haruna-Nijo grown under normal conditions. Expression of *HvHKT1;1-FL* and its variants in the roots (**A**), sheaths (**B**), and leaves (**C**) of 17-day-old plants was measured by absolute quantification. Data represent means of three samples ± SE ($n$ = 3). Three separate experiments were conducted, yielding similar results. Different letters indicate significant differences ($p$ < 0.05).

Next, I investigated the expression profiles of *HvHKT1;1-FL* and its variants in barley across different tissues — leaf, sheath, and root — under 150 mM salinity stress (Figures 3.5, 3.6). *HvHKT1;1-FL* reached peak expression at 2 hr in the leaf, with maximum sheath expression at 12 hr, while root expression peaked at 2 hr and stayed low throughout the time course (Figure 3.6A). However, *HvHKT1;1-V1* also showed peak expression in the leaf at 2 hr, and sheath at 12 hr, although transcript levels were

lower than FL, and root expression was minimal (Figure 3.6B). In contrast, *HvHKT1;1-V2* and *HvHKT1;1-V3* exhibited a sharp peak in leaf expression at 2 hr, followed by moderate sheath expression and minimal root expression (Figure 3.6C, D). These findings suggest a coordinated, tissue-specific, and time-dependent regulation of *HvHKT1;1-FL* and its variants in response to salinity, with leaves and sheaths playing key roles in $Na^+$ transport and homeostasis during early stress adaptation.

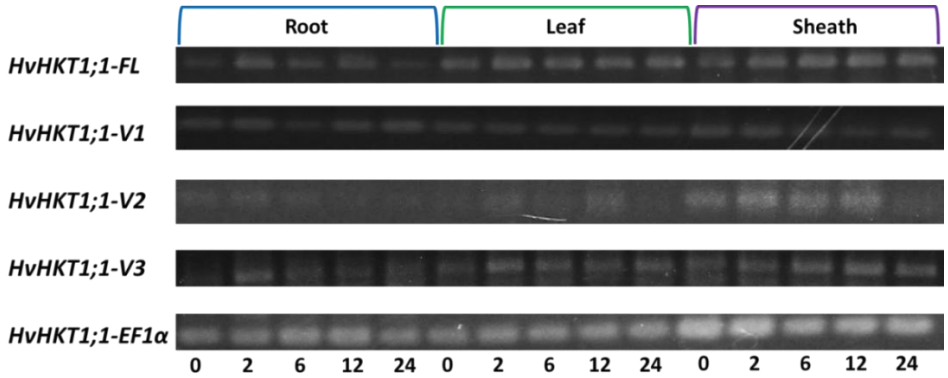


**Figure 3.5.** Expression analysis of *HvHKT1;1-FL* and its variants in root, leaf, and sheath of barley plants grown under stress conditions by reverse transcription polymerase chain reaction (RT-PCR). *HvHKT1;1-EF1α* was used as an internal control.

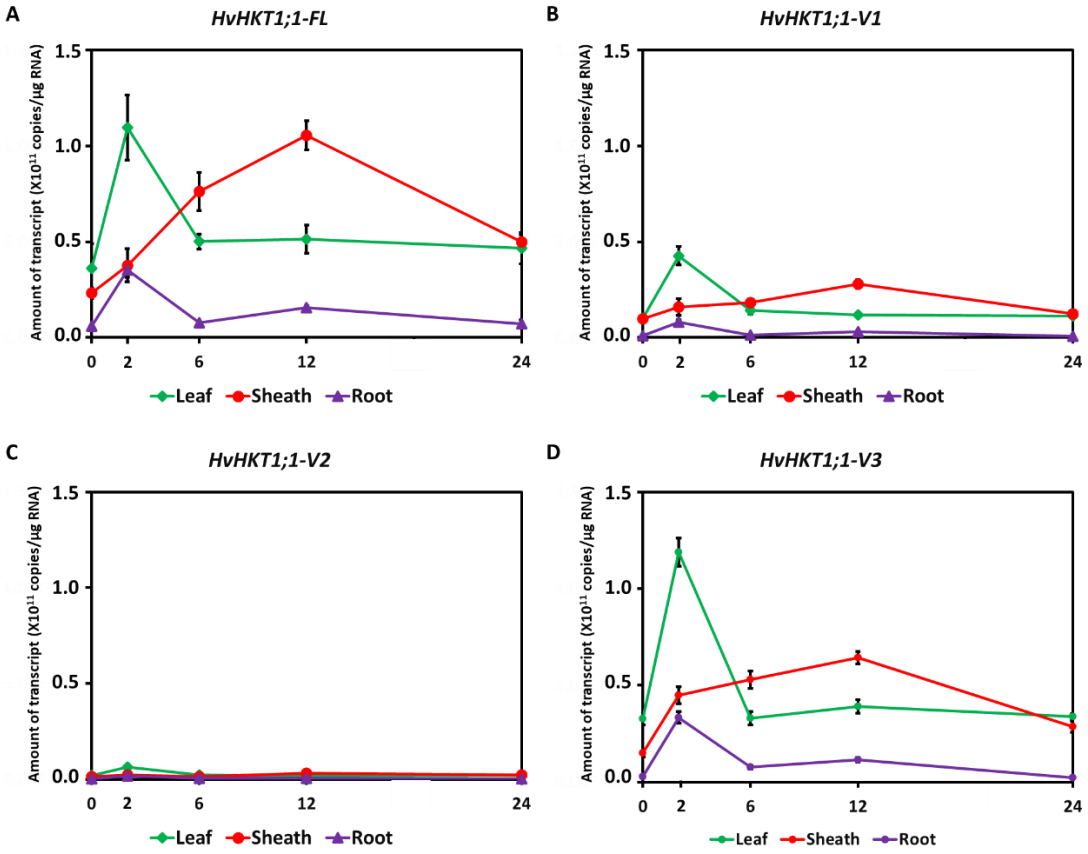


**Figure 3.6.** RT-qPCR analysis of *HvHKT1;1* transcripts in the barley cultivar Haruna-Nijo grown under saline conditions. Expression of *HvHKT1;1-FL* and every variant in root, sheath,

and leaf was measured through absolute quantification. Seventeen-day-old Haruna-Nijo plants were grown with 150 mM NaCl solution for 0, 2, 6, 12, or 24 hr before the extraction of total RNA. (**A**) *HvHKT1;1-FL*, (**B**) *HvHKT1;1-V1*, (**C**) *HvHKT1;1-V2*, and (**D**) *HvHKT1;1-V3*. Absolute transcript amounts (copies/µg RNA) are displayed. Data are means of three samples ± SE ($n$ = 3). Three separate experiments were conducted, yielding similar results.

**Ion Transport Properties of HvHKT1;1-FL and Its Variants**

The figure presents TEVC measurements showing the ion transport properties of HvHKT1;1 and its splice variants from barley under different ionic conditions (96 mM NaCl, KCl, LiCl, CsCl, and RbCl) (Figure 3.7). HvHKT1;1-FL (full-length) exhibited strong inward rectifying currents in a 96 mM $Na^+$ bath solution while producing minimal currents akin to water-injected control oocytes in 96 mM $K^+$, $Li^+$, $Rb^+$, and $Cs^+$-containing bath solutions, indicating strong $Na^+$ selectivity (Figure 3.7A). In contrast, conductance analysis reveals a high *V*max (333 µS) and low *K*m (41 mM), indicating efficient $Na^+$ transport with low affinity (Figure 3.8A, B). On the other hand, HvHKT1;1-V1, -V2, and -V3 expression in oocytes showed reduced $Na^+$ currents compared to the full-length, with minimal $K^+$, $Li^+$, $Rb^+$, and $Cs^+$ currents, demonstrating weaker transport capacity and decreased selectivity compared to HvHKT1;1-FL (Figure 3.7B-D). Moreover, HvHKT1;1-V1, -V2, and -V3 showed progressively lower *V*max (46 µS, 56 µS, and 111 µS, respectively) and higher *K*m (89 mM, 122 mM, and 286 mM, respectively) values, suggesting reduced $Na^+$ transport efficiency (Figure 3.8C-H).

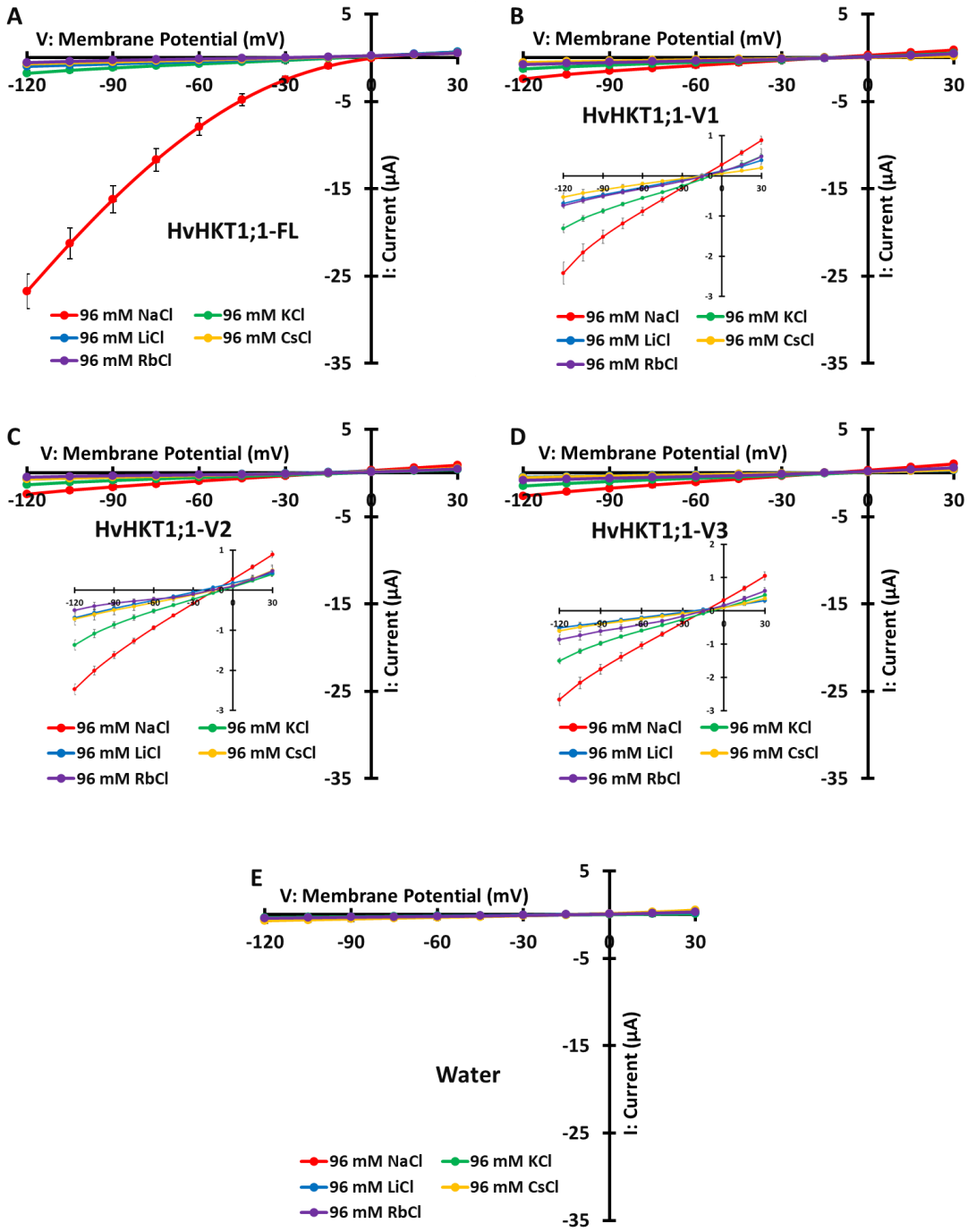


**Figure 3.7.** Monovalent alkaline cation selectivity of HvHKT1;1-FL and its variants. Current–voltage (I–V) curves from oocytes injected with 50 ng of HvHKT1;1-FL cRNA (**A**), HvHKT1;1-V1 cRNA (**B**), HvHKT1;1-V2 cRNA (**C**), HvHKT1;1-V3 cRNA (**D**), or 50 nL water (**E**) are present. External bath solutions comprised chloride salts of $Na^+$, $K^+$, $Cs^+$, $Rb^+$, or $Li^+$ (each at 96 mM). The bath solution's basic components included 1.8 mM $MgCl_2$, 1.8 mM $CaCl_2$, 1.8 mM mannitol, and 10 mM HEPES (pH 7.5 with Tris). Voltage steps ranged from −120 to +30 mV with 15 mV increments. Data are presented as mean ± SE ($n$ = 5–14 for **A**–**D** and $n$ = 5–10 for **E**). Insets display variants with low currents.

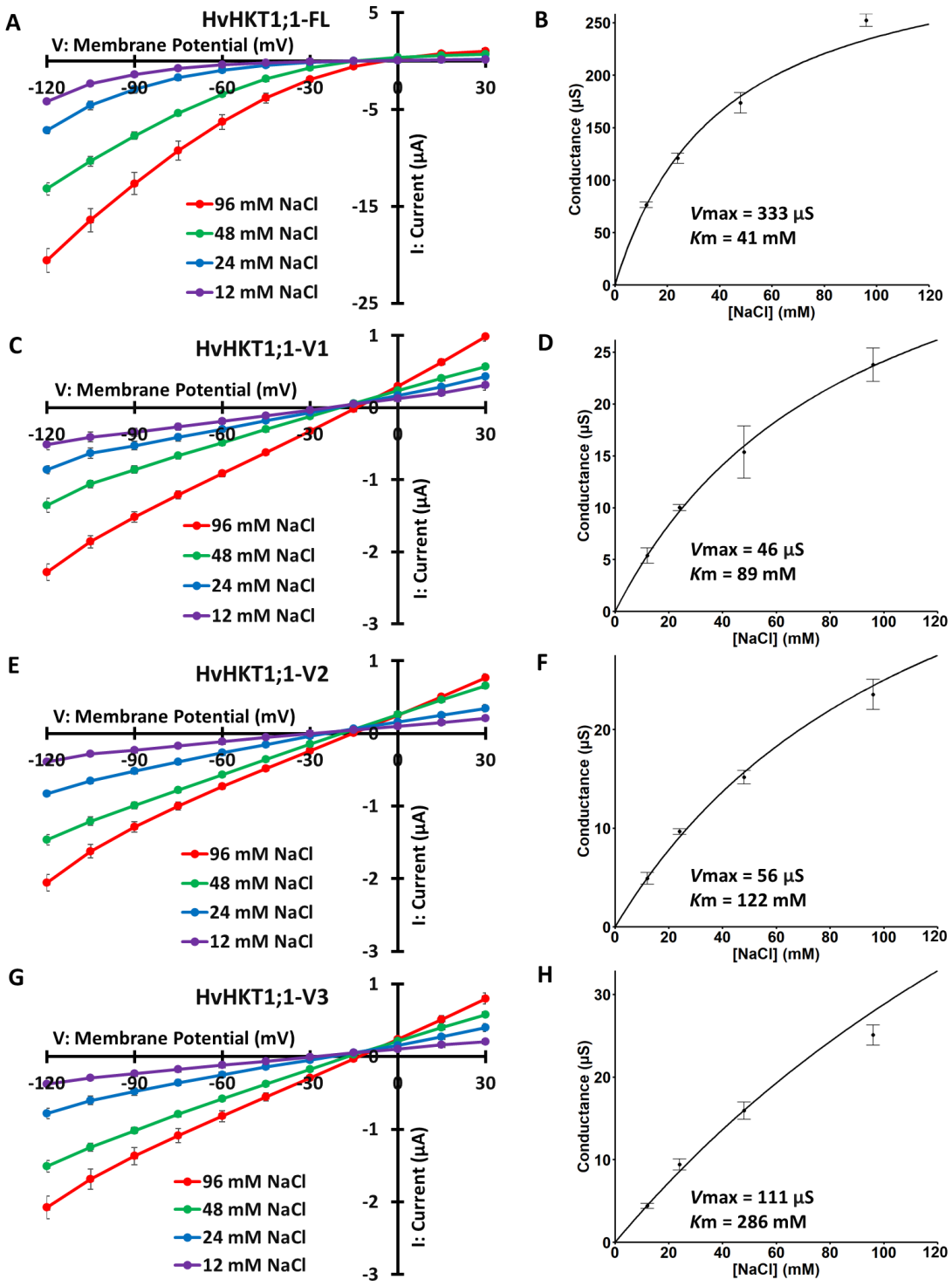


**Figure 3.8.** $Na^+$ transport activity of HvHKT1;1-FL and its variants under different $Na^+$ concentrations. Current–voltage relationships (I–V curves) obtained from oocytes injected with either 50 ng of HvHKT1;1-FL cRNA (**A**), HvHKT1;1-V1 cRNA (**C**), HvHKT1;1-V2 cRNA (**E**), HvHKT1;1-V3 cRNA (**G**). $Na^+$ concentration-dependent ionic conductance analysis for HvHKT1;1-FL (**B**), HvHKT1;1-V1 (**D**), HvHKT1;1-V2 (**F**), HvHKT1;1-V3 (**H**). External bath solutions contained 12, 24, 48, and 96 mM NaCl. 96 mM NaCl solution contains background elements as 1.8 mM $CaCl_2$, 1.8 mM $MgCl_2$, 1.8 mM mannitol, and 10 mM HEPES (pH 7.5

with Tris). 48 mM to 12 mM NaCl solutions contain background elements as 1.8 mM $CaCl_2$, 1.8 mM $MgCl_2$, 96-, 144-, or 168-mM mannitol, and 10 mM HEPES (pH 7.5 with Tris). Voltage steps ranged from −120 to +30 mV with 15 mV increments. Data are shown as means ± SE ($n$ = 6-10).

The reversal potential of HvHKT1;1-FL, -V1, -V2, and -V3-expressing oocytes in a 96 mM NaCl solution was approximately 4 mV, −15 mV, −14 mV, and −14 mV, respectively (Figure 3.7A-D). Their reversal potentials in a 96 mM KCl solution were −11 mV, −8 mV, −8 mV, and −9 mV; in a 96 mM CsCl solution, −22 mV, −14 mV, −15 mV, and −16 mV; in a 96 mM RbCl solution, −35 mV, −12 mV, −15 mV, and −14 mV; and in a 96 mM LiCl solution, −20 mV, −17 mV, −24 mV, and −23 mV, respectively (Figure 3.7A-D). Based on these values, the ion permeability ratios of HvHKT1;1-FL, -V1, -V2, and -V3 were assessed using the modified Goldman equation as shown in Table 1. For HvHKT1;1-FL, the highest $P_{ion}/P_{Na}$ ratio was obtained using $Na^+$-derived data, while the lowest was for $Rb^+$. Conversely, the $P_{ion}/P_{Na}$ ratio is around 1 for all monovalent cations with a large variation in HvHKT1;1-V1, -V2, and -V3. The current in oocytes expressing these variants is also low. These results suggest that HvHKT1;1-V1, -V2, and -V3 have low selectivity for monovalent cations and exhibit weak transport activity (Table 2.2).

**Table 2.2.** Ion permeability ratios of HvHKT1;1-FL, -V1, -V2, and -V3. Ratios were assessed based on the shift of reversal potential recorded in solutions of 96 mM NaCl, KCl, CsCl, RbCl, or LiCl using the modified Goldman equation, which ignored the $Cl^-$permeability.

| | **Ion** | **$Na^+$** | **$K^+$** | **$Cs^+$** | **$Rb^+$** | **$Li^+$** |
|---|---|---|---|---|---|---|
| **HvHKT1;1-FL** | **$P_{ion}/P_{Na}$** | 1 | 0.56 | 0.35 | 0.21 | 0.39 |
| **HvHKT1;1-V1** | **$P_{ion}/P_{Na}$** | 1 | 1.31 | 1.03 | 1.14 | 0.90 |
| **HvHKT1;1-V2** | **$P_{ion}/P_{Na}$** | 1 | 1.25 | 0.94 | 0.96 | 0.66 |
| **HvHKT1;1-V3** | **$P_{ion}/P_{Na}$** | 1 | 1.25 | 0.92 | 1.01 | 0.71 |

**HvHKT1;1-FL and Its Variants Are Selective for $Na^+$**

To assess the affinity for $Na^+$, the reversal potential shift of HvHKT1;1-FL and its variants (-V1, -V2, and -V3) was examined in response to decreasing extracellular $Na^+$ concentration (Figures 3.9, 3.10). The current-voltage relationships indicated that

HvHKT1;1-FL generated significantly larger currents in Na gluconate than in Choline-Cl, confirming HvHKT1;1-FL's strong preference for $Na^+$ (Figures 3.9A, 3.10A). Similarly, the variants (-V1, -V2, and -V3) also showed a preference for $Na^+$ by producing larger currents in Na gluconate than in Choline-Cl (Figures 3.9C, E, G, 3.10C, E, G). A decrease in extracellular $Na^+$ concentration caused a more negative reversal potential, demonstrating that HvHKT1;1-FL and its variants efficiently transport $Na^+$, while the more negative reversal potentials in Choline-Cl solutions indicated no permeability to $Cl^-$ (Figures 3.9B, D, F, H, 3.10B, D, F, H). Collectively, these results confirm that HvHKT1;1-FL and its variants are $Na^+$-selective transporters with similar ion selectivity profiles across different ionic conditions.

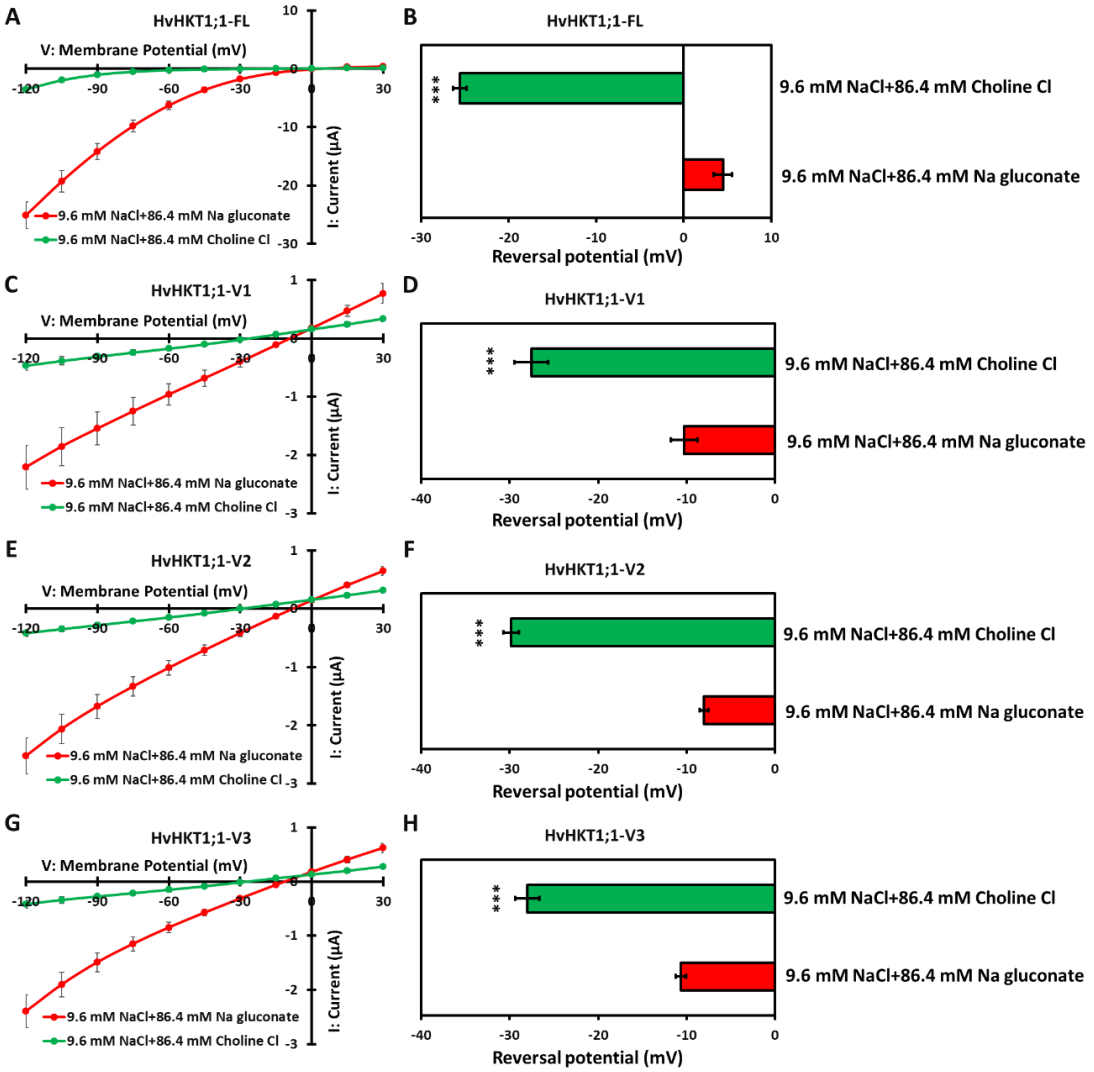


**Figure 3.9.** $Na^+$ selectivity of HvHKT1;1-FL and its variants. Current–voltage (I–V) curves were recorded from oocytes injected with 50 ng of HvHKT1;1-FL cRNA (**A**), HvHKT1;1-V1 cRNA (**C**), HvHKT1;1-V2 cRNA (**E**), and HvHKT1;1-V3 cRNA (**G**). Reversal potential shifts were analyzed by changing the external $Na^+$ concentration from 96 mM to 9.6 mM for

HvHKT1;1-FL (**B**), HvHKT1;1-V1 (**D**), HvHKT1;1-V2 (**F**), and HvHKT1;1-V3 (**H**). External bath solutions contained 9.6 mM NaCl plus 86.4 mM Na gluconate or Choline-Cl. Basic elements in the bath solution included 1.8 mM $MgCl_2$, 1.8 mM $CaCl_2$, 1.8 mM mannitol, and 10 mM HEPES (pH 7.5 with Tris). Voltage steps ranged from −120 to +30 mV with 15-mV increments. Data are shown as means ± SE ($n$ = 6). Asterisks denote values significantly different from 9.6 mM NaCl + 86.4 mM Na gluconate as determined by one-way ANOVA (***$p < 0.001$). Post hoc tests were not applicable because only two groups were compared.

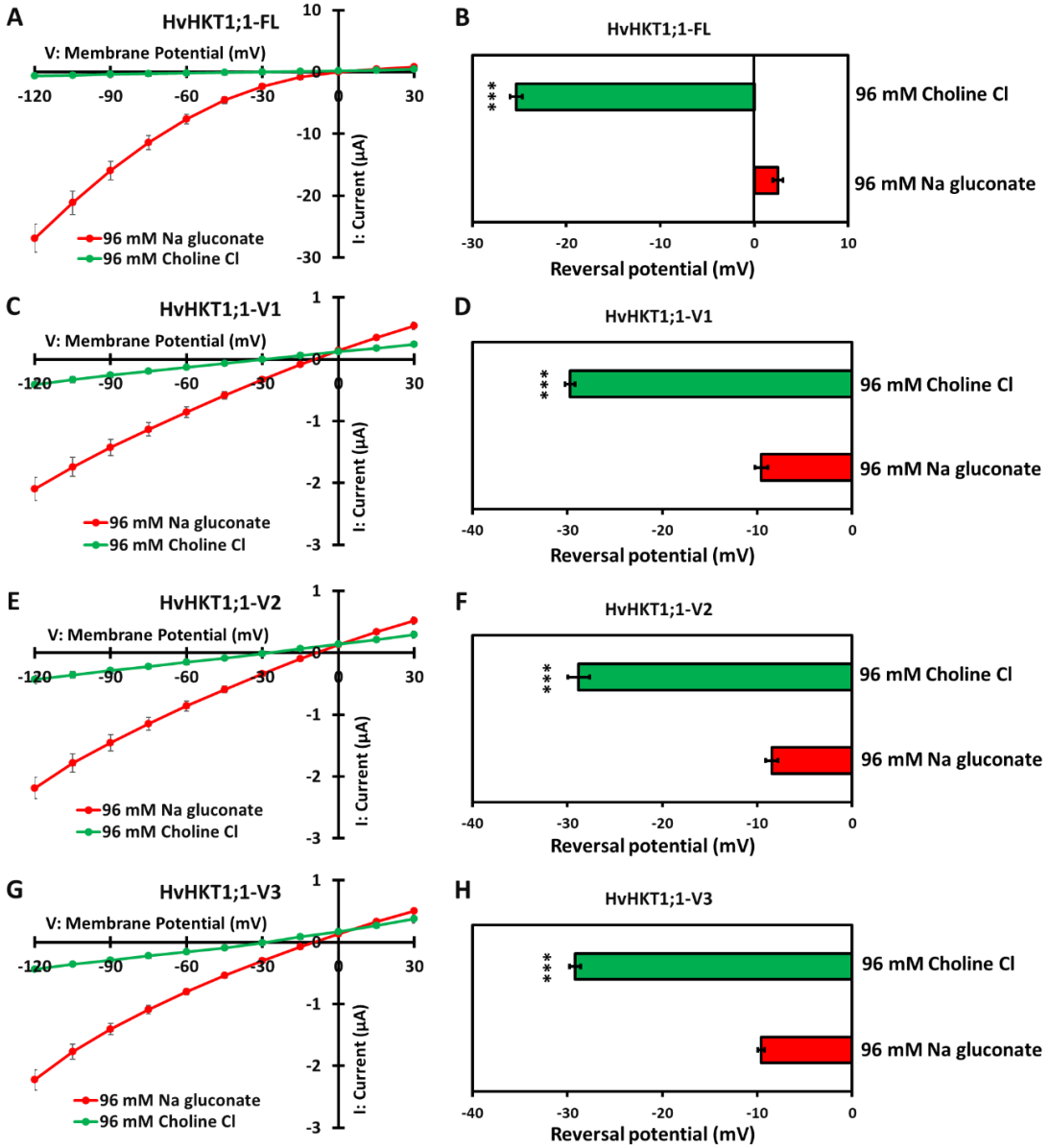


**Figure 3.10.** $Na^+$ selectivity of HvHKT1;1 and its variants. The TEVC experiment using *X. laevis* oocytes was conducted. Current–voltage relationships (I–V curves) obtained from oocytes injected with either 50 ng of HvHKT1;1-FL cRNA (**A**), HvHKT1;1-V1 cRNA (**C**), HvHKT1;1-V2 cRNA (**E**), HvHKT1;1-V3 cRNA (**G**). Reversal potential shift analysis conducted by changing the external $Na^+$ concentration from 96 mM to 0 mM for HvHKT1;1-

FL (**B**), HvHKT1;1-V1 (**D**), HvHKT1;1-V2 (**F**), HvHKT1;1-V3 (**H**). External bath solutions contained 96 mM Na gluconate and 96 mM Choline-Cl. Basic background elements in the bath solution are 1.8 mM $CaCl_2$, 1.8 mM $MgCl_2$, 1.8 mM mannitol, and 10 mM HEPES (pH 7.5 with Tris). Voltage steps ranged from −120 to +30 mV with 15 mV increments. Data are shown as means ± SE ($n = 10$). Asterisks denote values significantly different from 96 mM Na gluconate as determined by one-way ANOVA (***$P < 0.001$). Post hoc tests were not applicable because only two groups were compared.

## Discussion

The HKTs play a crucial role in salinity tolerance of plants by regulating the homeostasis of $Na^+$ and $K^+$, which is important for maintaining cellular functions in salty environments (Horie et al., 2009; Hauser and Horie, 2010; Almeida et al., 2013). HKTs mainly facilitate $Na^+$ and $K^+$ selective transport across cell membranes, helping to reduce the toxic effects of excess $Na^+$ in plant tissues (Riedelsberger et al., 2021). Specifically, HKT1-type transporters, localized in the plasma membrane of root cells, help remove $Na^+$ from the xylem sap, decreasing its movement to the shoots and protecting photosynthetic tissues from salt damage (Horie et al., 2009. Additionally, HKTs contribute to osmotic adjustment and ion balance, which are essential for supporting growth and productivity during salt stress (Almeida et al., 2013).

HKT subfamily 1 transporters play a key role in plant salinity tolerance by facilitating $Na^+$ transport, preventing toxic ion buildup, and redistributing $Na^+$ to vacuoles or less sensitive tissues (Munns et al., 2012). A key function of these transporters is $Na^+$ retrieval from the xylem, reducing its excessive accumulation in shoots and maintaining ionic balance (Hauser and Horie, 2010). *AtHKT1;1*, a passive $Na^+$ transporter, is primarily expressed in xylem parenchyma, where it helps in $Na^+$ unloading, thus enhancing salt tolerance (Horie et al., 2009; Sunarpi et al., 2005). Its presence in leaf phloem suggests an additional role in $Na^+$ recirculation from shoots to roots (Berthomieu et al., 2003). In durum wheat, $Na^+$ removal from leaves is a key function for salt stress adaptation, controlled by the loci *Nax1* and *Nax2*, which encode $Na^+$-selective transporters *TmHKT1;4-A2* and *TmHKT1;5* (Munns et al., 2012; Byrt et al., 2014; Tounsi et al., 2016). Similarly, *OsHKT1;5* in rice regulates unloading $Na^+$ from the xylem and phloem to protect young leaves under salt stress (Ren et al., 2005; Jabnoune et al., 2009; Kobayashi et al., 2017). It has also reported that *OsHKT1;1* is involved in $Na^+$ exclusion from shoots and recirculation to roots (Wang et al., 2015;

Campbell et al., 2017). In *X. laevis* oocytes, HvHKT1;1 exhibited $Na^+$-selective transport, further confirming the specificity of HKT transporters in regulating $Na^+$ homeostasis (Han et al., 2018). Previously, it has been reported that *OsHKT1;1* produced several mRNA splicing variants (Imran et al., 2020). However, only a few studies have reported on *HvHKT1;1*, and its detailed physiological functions and variants have not yet been studied. I assume that, like *OsHKT1;1*, other *HKT1;1* may also produce variants. Based on this assumption, in this study, several variants of *HvHKT1;1* (-*V1*, -*V2*, and -*V3*) were confirmed in addition to the *HvHKT1;1* full-length (*HvHKT1;1-FL*) in a salt-tolerant barley cultivar, Haruna-Nijo (Figures 3.1, 3.2, 3.3).

In this study, HvHKT1;1-FL expressed in *Xenopus* oocytes exhibited higher inward rectifying currents in 96 mM $Na^+$ (Figure 3.7A), as previously mentioned (Han et al., 2018), with little or no currents similar to the water-injected negative control in 96 mM $K^+$, $Li^+$, $Cs^+$, or $Rb^+$ solutions (Figure 3.7A). Additionally, analysis of reversal potential, ion permeability ratio, and high *V*max, low *K*m values indicated efficient $Na^+$ transport by HvHKT1;1-FL with low affinity (Table 2.2; Figure 3.8A, B). Moreover, reversal potential analysis confirmed the effective transport of $Na^+$ by HvHKT1;1-FL, but not $Cl^-$ (Figures 3.9A, B, 3.10A, B). In contrast, oocytes expressing HvHKT1;1-V1, -V2, and -V3 also showed notable $Na^+$ currents, though with more moderate inward currents compared to HvHKT1;1-FL, and minimal transport of other ions (Figure 3.7B to D). Additionally, the low *V*max and high *K*m values of these splice variants suggest reduced $Na^+$ transport efficiency, implying alternative ion selectivity or decreased functionality relative to the full-length HvHKT1;1 (Figure 3.8C- H). Furthermore, reversal potential analysis and ion permeability ratios indicated that HvHKT1;1 variants (-V1, -V2, -V3) functioned as $Na^+$ channels (Table 2.2; Figures 3.9C- H, 3.10C-H), but their selectivity was less than that of HvHKT1;1-FL.

It has been reported that *AtHKT1;1* shows higher expression in roots than in shoots (Uozumi et al., 2000). However, *OsHKT1;1* is highly expressed after 12 hr of salt stress treatment in shoots and shows no difference in expression in roots (Wang et al., 2015). Additionally, Imran et al. (2020) reported a gradual decline in *OsHKT1;1* expression in shoots following salt stress exposure, with no clear pattern in roots. Moreover, Ali et al. (2018) observed that *EpHKT1;1* transcript upregulated more slowly in response to salt treatment. It has been demonstrated that *CmHKT1;1* transcript level in roots exceeds that in the control, peaking at 6 hr (Sun et al., 2018). Moreover,

*LbHKT1;1* exhibited the greatest expression levels in both shoots and roots under salt stress conditions (Zhu et al., 2025). Similarly, in *S. linearistipularis*, exposure to NaCl increased the expression of *SlHKT1.1* in both roots and shoots (Fu et al., 20250. A previous study reported increased *HvHKT1;1* expression in roots under salt stress conditions (Han et al., 2018). In this study, the *HvHKT1;1-FL* mRNA was the most abundant among the identified variants in roots, sheath, and leaves (Figure 3.4). Furthermore, all variants, including the full-length, showed higher expression in the leaves of Haruna-Nijo (Figure 3.4). Under salt stress, *HvHKT1;1-FL* and *HvHKT1;1-V3* display high transcript levels in leaves at 2 hr and in sheaths at 12 hr, with minimal root expression (Figure 3.6A, D). *HvHKT1;1-V1* follows a similar pattern but at lower levels (Figure 3.6B). In contrast, *HvHKT1;1-V2* shows the lowest expression across tissues (Figure 3.6C). Though the variants are missing a partial or a full transmembrane domain, this missing domain does not affect the expression, as also reported in the case of *OsHKT1;1* and *OsHKT1;3* variants (Imran et al., 2020, 2021). Overall, transcript levels are highest in sheaths over time, while root expression remains low across all variants, indicating tissue-specific and time-dependent regulation of *HvHKT1;1* in barley. In conclusion, this study offers a comprehensive analysis of barley *HvHKT1;1* and its splice variants, revealing distinct expression patterns and $Na^+$ transport properties. *HvHKT1;1-FL* exhibits the highest expression and transport efficiency, whereas the variants display reduced $Na^+$ transport, implying regulatory roles in sodium homeostasis. Expression profiling under salinity stress highlights tissue-specific and time-dependent regulation. Comparative studies among cereals reveal both conserved and divergent features of HKT1 transporters. In rice, OsHKT1;1 and OsHKT1;3 produce multiple splice variants that are stress-responsive and may fine-tune $Na^+$ transport under salinity (Imran et al., 2020, 2021; Wang et al., 2015). Some OsHKT1;1 variants are upregulated during early salt exposure and show reduced ion conductance, suggesting a potential role in $Na^+$ uptake temporally rather than being non-functional by-products. Similarly, wheat transporters such as TaHKT1;5-D and TmHKT1;4-A2 are single full-length isoforms, but their alleles lead to differences in $Na^+$ exclusion capabilities and salt tolerance levels (Munns et al., 2012; Byrt et al., 2014; Tounsi et al., 2016). In contrast, the barley HvHKT1;1 variants identified here appear to share $Na^+$ selectivity with OsHKT1;1 variants but display distinct expression timing and tissue specificity, implying a species-specific regulatory mechanism. Their induction at early time points under salinity (especially in leaves) suggests possible adaptive modulation

rather than transcriptional noise. However, functional attenuation (lower *V*max, higher *K*m) may also reflect partial loss of transport capacity, consistent with non-essential or regulatory variant roles. Therefore, the barley HvHKT1;1 variants may represent a combination of adaptive and functionally reduced forms, a pattern that aligns with OsHKT1;1's stress-induced splicing diversity but diverges from the more stable single-gene expression observed in wheat HKT1;5. These findings enhance my understanding of $Na^+$ transport in barley and offer insights for enhancing salinity tolerance in crops. Although my electrophysiological and expression data clarify variant-specific transport functions, I did not evaluate their effects on whole-plant $Na^+/K^+$ homeostasis or growth under salinity. However, previous studies have shown that *HvHKT1;1* regulates tissue-level $Na^+$ distribution and contributes to salt tolerance in barley (Han et al., 2018). But the previous report didn't consider HvHKT1;1 variants, which were characterized in the present study, may differentially affect plant performance under saline conditions. Future research should investigate the physiological roles of these variants and their potential applications in crop breeding and genetic engineering to enhance stress resilience.

**References**


Ali A, Khan IU, Jan M, Khan HA, Hussain S, Nisar M, Chung WS, Yun DJ. The high-affinity potassium transporter EpHKT1;2 from the extremophile *Eutrema parvula* mediates salt tolerance. Frontiers in Plant Science. **2018**;9:1108. https://doi.org/10.3389/fpls.2018.01108

Almeida P, Katschnig D, De Boer AH. HKT transporters—state of the art. International Journal of Molecular Sciences. **2013**;14(10):20359-20385. https://doi.org/10.3390/ijms141020359

Berthomieu P, Conéjéro G, Nublat A, Brackenbury WJ, Lambert C, Savio C, Uozumi N, Oiki S, Yamada K, Cellier F, Gosti F. Functional analysis of *AtHKT1* in Arabidopsis shows that $Na^+$ recirculation by the phloem is crucial for salt tolerance. The EMBO Journal. **2003**;22(9):2004-2014. https://doi.org/10.1093/emboj/cdg207

Byrt CS, Xu B, Krishnan M, Lightfoot DJ, Athman A, Jacobs AK, Watson-Haigh NS, Plett D, Munns R, Tester M, Gilliham M. The $Na^+$ transporter, TaHKT1;5-d, limits shoot $Na^+$ accumulation in bread wheat. The Plant Journal. **2014**;80(3):516-526. https://doi.org/10.1111/tpj.12651

Campbell MT, Bandillo N, Al Shiblawi FR, Sharma S, Liu K, Du Q, Schmitz AJ, Zhang C, Véry AA, Lorenz AJ, Walia H. Allelic variants of OsHKT1;1 underlie the divergence between indica and japonica subspecies of rice (*Oryza sativa*) for root sodium content. PLoS Genetics. **2017**;13(6):e1006823. https://doi.org/10.1371/journal.pgen.1006823

Fu S, Chen X, Jiang Y, Dai S, Zhang H, Feng S, Zhou A. Characterization of the $Na^+$-preferential transporter HKT1.1 from halophyte shrub *Salix linearistipularis*. Physiology and Molecular Biology of Plants. **2025**;31(5):823-833. https://doi.org/10.1007/s12298-025-01605-2

Garciadeblás B, Senn ME, Bañuelos MA, Rodríguez-Navarro A. Sodium transport and HKT transporters: the rice model. The Plant Journal. **2003**;34(6):788-801. https://doi.org/10.1046/j.1365-313X.2003.01764.x

Han Y, Yin S, Huang L, Wu X, Zeng J, Liu X, Qiu L, Munns R, Chen ZH, Zhang G. A sodium transporter HvHKT1;1 confers salt tolerance in barley via regulating tissue and cell ion homeostasis. Plant and Cell Physiology. **2018**;59(10):1976-1989. https://doi.org/10.1093/pcp/pcy116

Hauser F, Horie T. A conserved primary salt tolerance mechanism mediated by HKT transporters: a mechanism for sodium exclusion and maintenance of high $K^+/Na^+$ ratio in leaves during salinity stress. Plant, Cell & Environment. **2010**;33(4):552-565. https://doi.org/10.1111/j.1365-3040.2009.02056.x

Horie T, Hauser F, Schroeder JI. HKT transporter-mediated salinity resistance mechanisms in Arabidopsis and monocot crop plants. Trends in Plant Science. **2009**;14(12):660-668. https://doi.org/10.1016/j.tplants.2009.08.009

Imran S, Horie T, Katsuhara M. Expression and ion transport activity of rice *OsHKT1;1* variants. Plants. **2020**;9(1):16. https://doi.org/10.3390/plants9010016

Imran S, Tsuchiya Y, Tran STH, Katsuhara M. Identification and characterization of rice *OsHKT1;3* variants. Plants. **2021**;10(10):2006. https://doi.org/10.3390/plants10102006

Jabnoune M, Espeout S, Mieulet D, Fizames C, Verdeil JL, Conéjéro G, Rodríguez-Navarro A, Sentenac H, Guiderdoni E, Abdelly C, Véry AA. Diversity in expression patterns and functional properties in the rice HKT transporter family. Plant Physiology. **2009**;150(4):1955-1971. https://doi.org/10.1104/pp.109.138008

Kobayashi NI, Yamaji N, Yamamoto H, Okubo K, Ueno H, Costa A, Tanoi K, Matsumura H, Fujii-Kashino M, Horiuchi T, Nayef MA. OsHKT1;5 mediates $Na^+$ exclusion in the vasculature to protect leaf blades and reproductive tissues from salt toxicity in rice. The Plant Journal. **2017**;91(4):657-670. https://doi.org/10.1111/tpj.13595

Munns R, James RA, Xu B, Athman A, Conn SJ, Jordans C, Byrt CS, Hare RA, Tyerman SD, Tester M, Plett D. Wheat grain yield on saline soils is improved by an ancestral $Na^+$ transporter gene. Nature Biotechnology. **2012**;30(4):360-364. https://doi.org/10.1038/nbt.2120

Pandit K, Chandni, Kaur S, Kumar M, Bhardwaj R, Kaur S. Salinity stress: impact on plant growth. Advances in Food Security and Sustainability. **2024**;9:145-160. https://doi.org/10.1016/bs.af2s.2024.07.002

Platten JD, Cotsaftis O, Berthomieu P, Bohnert H, Davenport RJ, Fairbairn DJ, Horie T, Leigh RA, Lin HX, Luan S, Mäser P. Nomenclature for HKT transporters, key determinants of plant salinity tolerance. Trends in Plant Science. **2006**;11(8):372-374. https://doi.org/10.1016/j.tplants.2006.06.001

Ren ZH, Gao JP, Li LG, Cai XL, Huang W, Chao DY, Zhu MZ, Wang ZY, Luan S, Lin HX. A rice quantitative trait locus for salt tolerance encodes a sodium transporter. Nature Genetics. **2005**;37(10):1141-1146. https://doi.org/10.1038/ng1643

Riedelsberger J, Miller JK, Valdebenito-Maturana B, Piñeros MA, González W, Dreyer I. Plant HKT channels: an updated view on structure, function and gene regulation. International Journal of Molecular Sciences. **2021**;22(4):1892. https://doi.org/10.3390/ijms22041892

Schachtman DP, Schroeder JI. Structure and transport mechanism of a high-affinity potassium uptake transporter from higher plants. Nature. **1994**;370(6491):655-658. https://doi.org/10.1038/370655a0

Sun J, Cao H, Cheng J, He X, Sohail H, Niu M, Huang Y, Bie Z. Pumpkin CmHKT1;1 controls shoot $Na^+$ accumulation via limiting $Na^+$ transport from rootstock to scion in grafted cucumber. International Journal of Molecular Sciences. **2018**;19(9):2648. https://doi.org/10.3390/ijms19092648

Sunarpi X, Horie T, Motoda J, Kubo M, Yang H, Yoda K, Horie R, Chan WY, Leung HY, Hattori K, Konomi M. Enhanced salt tolerance mediated by AtHKT1 transporter-induced $Na^+$ unloading from xylem vessels to xylem parenchyma

cells. The Plant Journal. **2005**;44(6):928-938. https://doi.org/10.1111/j.1365-313X.2005.02595.x

Tarolli P, Luo J, Park E, Barcaccia G, Masin R. Soil salinization in agriculture: mitigation and adaptation strategies combining nature-based solutions and bioengineering. iScience. **2024**;27(2):108830. https://doi.org/10.1016/j.isci.2024.108830

Tounsi S, Ben Amar S, Masmoudi K, Sentenac H, Brini F, Véry AA. Characterization of two HKT1;4 transporters from *Triticum monococcum* to elucidate the determinants of the wheat salt tolerance *Nax1* QTL. Plant and Cell Physiology. **2016**;57(10):2047-2057. https://doi.org/10.1093/pcp/pcw123

Tran ST, Katsuhara M, Mito Y, Onishi A, Higa A, Ono S, Paul NC, Horie R, Harada Y, Horie T. OsPIP2;4 aquaporin water channel primarily expressed in roots of rice mediates both water and nonselective $Na^+$ and $K^+$ conductance. Scientific Reports. **2025**;15(1):12857. https://doi.org/10.1038/s41598-025-96259-1

Uozumi N, Kim EJ, Rubio F, Yamaguchi T, Muto S, Tsuboi A, Bakker EP, Nakamura T, Schroeder JI. The *Arabidopsis HKT1* gene homolog mediates inward $Na^+$ currents in *Xenopus laevis* oocytes and $Na^+$ uptake in *Saccharomyces cerevisiae*. Plant Physiology. **2000**;122(4):1249-1260. https://doi.org/10.1104/pp.122.4.1249

Wang R, Jing W, Xiao L, Jin Y, Shen L, Zhang W. The rice high-affinity potassium transporter1;1 is involved in salt tolerance and regulated by an MYB-type transcription factor. Plant Physiology. **2015**;168(3):1076-1090. https://doi.org/10.1104/pp.15.00298

Wang Y, Kamau S, Song S, Zhang Y, Zhang X. Identification of high-affinity nicotinic acid transporter genes from *Verticillium dahliae* and functional analysis based on HIGS technology. Journal of Cotton Research. **2025**;8(1):20. https://doi.org/10.1186/s42397-025-00215-3

Zhang M, Liang X, Wang L, Cao Y, Song W, Shi J, Lai J, Jiang C. A HAK family $Na^+$ transporter confers natural variation of salt tolerance in maize. Nature Plants. **2019**;5(12):1297-1308. https://doi.org/10.1038/s41477-019-0565-y

Zhou H, Shi H, Yang Y, Feng X, Chen X, Xiao F, Lin H, Guo Y. Insights into plant salt stress signaling and tolerance. Journal of Genetics and Genomics. **2024**;51(1):16-34. https://doi.org/10.1016/j.jgg.2023.08.007

Zhu Z, Liu X, Meng F, Jiang A, Zhou Y, Yuan F, Chen M. *LbHKT1;1* negatively regulates salt tolerance of Limonium bicolor by decreasing salt secretion rate of salt glands. Plant, Cell & Environment. **2025**;48(5):3544-3558. https://doi.org/10.1111/pce.15375

# CHAPTER 4

# OsCNGC2 as a $Na^+$, $K^+$ Non-Selective Channel, Triggered by Co-Existence of $Na^+$ and $K^+$

## Introduction

Ion transport and signaling mechanisms are essential to plant adaptation and survival under fluctuating environmental conditions. Among the broad range of membrane transport proteins that are involved in ion homeostasis and signaling, cyclic nucleotide-gated channels (*CNGCs*) are non-selective cation channels that play a crucial role in plant growth, development, and stress responses (Jha et al., 2016; Duszyn et al., 2019). The first CNGCs were identified in animal sensory systems, such as photoreceptor and olfactory neurons (Fesenko et al. 1985; Nakamura and Gold, 1987). Their plant counterparts have since attracted significant interest for their unique regulatory mechanisms and physiological functions. In plants, CNGCs are primarily located in the plasma membrane and facilitate the influx of calcium ($Ca^{2+}$), potassium ($K^+$), and sodium ($Na^+$) ions, making them essential in signaling pathways related to abiotic stress tolerance (Duszyn et al., 2019; Ma et al., 2006; Hua et al., 2003; Bridges et al., 2005; Leng et al., 2002). These channels are activated by the direct binding of cyclic nucleotides such as cyclic adenosine monophosphate (cAMP) or cyclic guanosine monophosphate (cGMP) (Leng et al., 1999; Leng et al., 2002; Wang et al., 2013; Mori et al., 2018; Zhang et al., 2019; Dietrich et al., 2020). However, plant CNGCs show lower cyclic nucleotide sensitivity than their animal counterparts (Isner and Maathuis, 2018; Jarratt-Barnham et al., 2021). Additionally, calmodulin-binding domains within plant *CNGCs* point to a complex regulation by calcium-calmodulin feedback mechanisms (Kaplan et al., 2007; Ungerer et al., 2011).

Several *CNGC* genes have been identified in various plant species, with approximately 20 found in *Arabidopsis thaliana* (Mäser et al., 2001), 16 in *Oryza sativa* (Nawaz et al., 2014), and 9 in *Hordeum vulgare* (Mori et al., 2018). These channels have diverse physiological roles, ranging from development and nutrient uptake to responses to biotic and abiotic stressors, including salinity, drought, and pathogen attack (Kaplan et al., 2007; Sherman et al., 2009). Although most our current knowledge of plant *CNGCs* is derived from studies in Arabidopsis, *CNGCs* in

monocotyledonous crops like rice remain less characterized. Only a few *CNGCs* have been functionally characterized using electrophysiological approaches. It has been reported that Arabidopsis root voltage-independent cation channels were non-selective cation channels whose open probability was reduced by cytosolic cAMP or cGMP (Frans et al., 2001). Electrophysiological analyses showed that cGMP activated inward $Ca^{2+}$-permeable currents in wild-type guard cells, which were absent in *cngc5 cngc6* mutants, confirming that *CNGC5* and *CNGC6* encode plasma membrane channels mediating cGMP-dependent $Ca^{2+}$ influx (Wang et al., 2013). Although detailed electrophysiological characteristics of plant *CNGCs* remain largely unexplored, a growing body of genetic and molecular biological evidence continues to highlight their important physiological roles in various plant processes. Studies in *Arabidopsis* have demonstrated the diverse functional repertoire of *CNGCs*. For example, *AtCNGC2* and *AtCNGC4* are well known for their roles in pathogen defense and $Ca^{2+}$ signaling (Chin et al., 2013). Loss-of-function mutations in *AtCNGC2* (also known as the dnd1 mutant) result in constitutive defense activation and impaired $Ca^{2+}$ influx (Clough et al., 2000). Similarly, *AtCNGC11* and *AtCNGC12* are required for basal resistance to bacterial pathogens and also participate in reproductive development (Urquhart et al., 2011). Several *CNGCs* also exhibit ion selectivity or preference, although the consensus is that most CNGCs are non-selective cation channels. For instance, AtCNGC10 plays a role in regulating cellular $K^+$ homeostasis across the plasma membrane, and disruptions in this $K^+$ gradient can influence a wide range of plant growth and developmental processes (Borsics et al., 2007). Meanwhile, *AtCNGC19* and *AtCNGC20* are upregulated under salt stress and contribute to $Na^+$ influx in root epidermal cells (Oranab et al., 2021). The functional overlap and redundancy among *CNGCs* suggest that they form heteromeric complexes, which might modulate their ion selectivity and activation properties *in vivo* (Kaplan et al., 2007). In tobacco (*Nicotiana tabacum*), NtCBP4, a CNGC-like protein, is involved in $Pb^{2+}$ uptake and localizes to the plasma membrane, further supporting the role of *CNGCs* in heavy metal transport and stress signaling (Arazi et al., 1999). In rice, several *OsCNGC* genes have been associated with stress responses and hormone signaling. For example, *OsCNGC13* and *OsCNGC16* are transcriptionally responsive to salinity, drought, and phytohormones (Nawaz et al., 2014). However, functional data on ion selectivity and physiological roles of rice *CNGCs* are sparse, limiting our ability to exploit them for crop improvement. Among the sixteen *OsCNGC* genes in rice, *OsCNGC2* was selected for further

electrophysiological analysis based on its expression characteristics reported in previous studies. Genome-wide expression profiling revealed that *OsCNGC2* is expressed across multiple rice tissues, including leaves and roots, suggesting a constitutive physiological role within the plant (Wang et al., 2023). Additionally, expression datasets with recent analyses of rice *CNGCs* also showed *OsCNGC2* expression in vegetative tissues (Chang et al., 2024). Despite this consistent expression, the transport properties of *OsCNGC2* remain unknown due to the lack of electrophysiological characterization. These expression patterns, therefore, provided a clear rationale for selecting *OsCNGC2* for detailed functional investigation.

Therefore, in the present study, I characterized the electrophysiological properties of rice *OsCNGC2* using two-electrode voltage-clamp analysis in *X. laevis* oocytes. To further understand its physiological role, I also examined its subcellular localization using fluorescent tagging and evaluated its gene expression profiles across tissues and stress conditions.

## Materials and Methods

### Plant Material and Growth Conditions

Seeds of Nipponbare (*Oryza sativa* L. ssp. japonica), a salt-sensitive rice cultivar, were sterilized, germinated, and grown hydroponically as described previously (Imran et al., 2020). Briefly, seeds were germinated and grown at 28 °C and 25 °C for 12 hr in the day (250 μmol $m^{-2}$ $s^{-1}$ illumination) and 12 hr at night, respectively, for 5 days, and transferred to 3.5 L pots with a nutrient solution. The nutrient solution contained 4 mM $KNO_3$, 1 mM $NH_4H_2PO_4.2H_2O$, 1 mM $CaCl_2.2H_2O$, 1 mM $MgSO_4.7H_2O$, and micronutrients (1 ppm Fe, 0,5 ppm B, 0.5 ppm Mn, 0.05 ppm Zn, 0.02 ppm Cu, and 0.01 ppm Mo). The pH of the nutrient solution was adjusted to 5.5 with NaOH. Fourteen-day-old plants were sampled for RNA isolation. For the gene expression study, 14-day-old plants were subjected to 100 mM NaCl stress for 0 hr (control), 6 hr, 12 hr, 24 hr, and 48 hr, after which the roots, stems, and leaf blades were collected separately.

### Extraction of RNA, and cDNA Synthesis

Total RNA was extracted, and its quality and integrity were evaluated before synthesizing cDNA, following the protocol described in the materials and methods of Chapter 2. The full-length *OsCNGC2* cDNA was then amplified with a pair of primers,

FW: GGAAAATGATGATGGGAAGAGAGG, RV: GAACTACTGCTCTTCTG CAGCA, and subsequently inserted into a pCR4 topo vector (Invitrogen, Carlsbad, CA, USA).

**Expression Analysis**

Total RNA samples were isolated from the roots, stems, and leaf blades of control and 100 mM NaCl-stressed plants, and the first-strand cDNA was reverse-transcribed using a high-capacity cDNA reverse transcription kit (Applied Biosystems, Foster City, CA, USA). cDNA fragments of *OsCNGC2* were amplified with a set of primers, OsCNGC2FW: TTCATACAAGCAGCCTGGCA and OsCNGC2RV: GCTGAGAGTTGTAGCACCGT. Absolute quantification was performed in the quantitative real-time PCR analysis using the 7300 real-time PCR machine (Applied Biosystem, Foster City, CA, USA) as described in (Mahdieh et al., 2008) to analyze the expression level of *OsCNGC2*. Specific cDNA was used as a standard to quantify the OsCNGC2.

**Subcellular Localization Analysis in Plant Cells using *Arabidopsis* Protoplasts**

The subcellular localization of the OsCNGC2 protein was analyzed by fusing its coding sequences with GFP at both the N- and C-termini under the control of the CaMV 35S promoter in the pTH2 vector (Chiu et al., 1996) with modifications. The GFP-fused OsCNGC2s were transiently expressed in protoplasts prepared from *Arabidopsis* leaves as described previously (Wu et al., 2009). The transfection procedure employed the polyethylene glycol (PEG 4000) method of Yoo et al. (2007), as previously described (Sasaki et al., 2016). The protoplasts were re-suspended in incubation (WI) solution (0.5 M mannitol, 20 mM KCl, and 4 mM MES; pH 5.7) and were kept in the dark at 23 °C for 16 hr (Wu et al., 2009). Confocal microscopy was performed, and images were obtained using an Olympus FluoView 1000 inverted laser scanning confocal imaging system (Olympus, Japan). GFP fluorescence was detected with a 490–525 nm bandpass filter using 473 nm excitation.

**Preparation of cRNA for *X. laevis* Oocytes Heterologous Expression**

The cDNA of *OsCNGC2* was cloned into a pXβG vector, and capped RNA (cRNA) synthesis was performed according to the procedure outlined in the materials and methods of Chapter 2. *X. laevis* Oocytes were collected and injected with cRNA at concentrations of 50 ng/50 nL or with 50 nL of nuclease-free water for the negative

control group. The oocytes were then incubated at 18 °C in a modified Barth's solution (MBS) until the electrophysiological measurements were performed (Katsuhara et al., 2002).

**Electrophysiology**

Oocytes injected with water or *OsCNGC2* cRNA were incubated in MBS supplemented with 10 μM (final concentration) 8-bromoadenosine cyclic monophosphate (8Br-cAMP, Sigma B5386, St Louis, MO, USA), 10 μM 8-bromoguanosine cyclic monophosphate (8Br-cGMP, Sigma B1381), or without supplementation of a nucleoside 3′,5′-cyclic monophosphate (cNMP) for 30 min before the two-electrode voltage-clamp (TEVC) measurement. 8-bromo-derivatives are used because they act as membrane-permeable, stable activators of CNGCs (Podda and Grassi, 2014). The TEVC recordings and subsequent data analysis were carried out with an Axoclamp 900A amplifier, Axon Instruments Digidata 1440A, and pCLAMP 10 software (Molecular Devices, USA). The bath solutions were prepared with a baseline concentration of 1.8 mM $MgCl_2$, 1.8 mM $CaCl_2$, and 10 mM HEPES at pH 7.5 with Tris, and chloride salts of monovalent cations were used, otherwise mentioned. D-mannitol was added as needed to keep the osmolality of external solutions between 200 and 220 mOsm in all measurements. To get current-voltage relationships, voltage steps (2 sec) were applied from +30 to −120 mV in 15 mV decrements.

**Statistical Analysis**

Statistical analyses were performed using IBM SPSS Statistics version 25. Significant differences were identified using a one-way analysis of variance followed by a Tukey HSD ($p < 0.05$) (Figures 4.1, 4.2, 4.4, 4.5, 4.6, 4.8). Data in Figures 4.3 to 4.6 were subjected to a t-test (*$p < 0.05$, **$p < 0.01$, ***$p < 0.001$).

**Results**

**Co-presence of $Na^+$ and $K^+$ Activates OsCNGC2**

Ion currents in *X. laevis* oocytes were measured using TEVC in medium containing 96 mM NaCl or 96 mM KCl, and ionic conductance was analyzed (Figure 4.1). The oocytes injected with *OsCNGC2* cRNA showed similar current–voltage (*I–V*) relationships and conductance values to water-injected controls, either in the presence or absence of 8Br-cAMP or 8Br-cGMP in bath solution containing 96 mM

NaCl (Figure 4.1A, B). Similarly, no significant difference in currents and ionic conductance was observed while oocytes were injected with water or *OsCNGC2* cRNA, either in the presence or absence of 8Br-cAMP or 8Br-cGMP under bath solution containing 96 mM KCl (Figure 4.1C, D). The absence of significant differences among treatments (+8Br-cAMP, +8Br-cGMP, +8Br-cAMP/cGMP, and water) indicates that *OsCNGC2* remains inactive in single-ion environments and that neither $Na^+$ nor $K^+$ alone is sufficient to trigger channel activity.

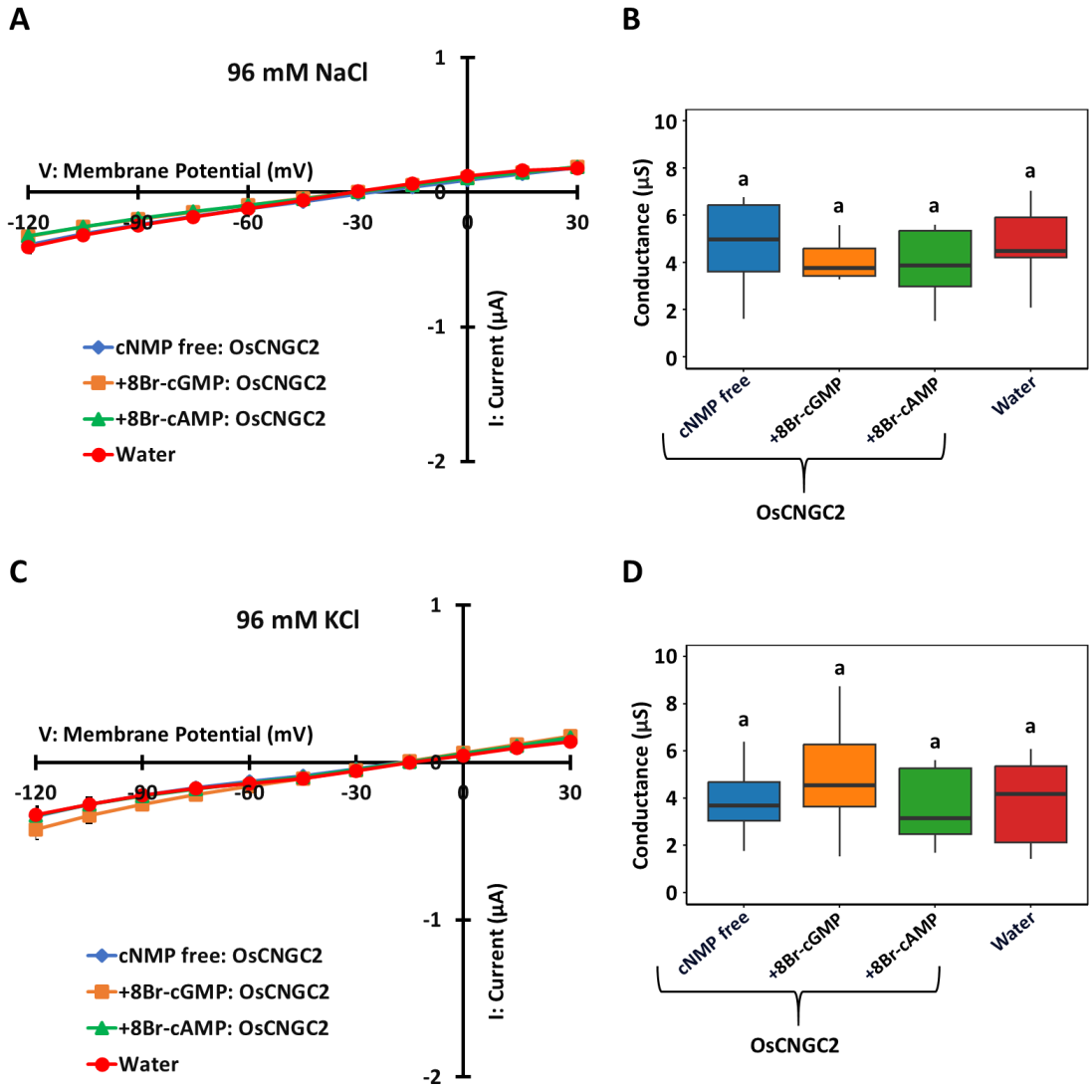


**Figure 4.1.** Current voltage relationship of oocytes expressing OsCNGC2 in the bath solution containing 96 mM NaCl (**A**) and 96 mM KCl (**C**). Currents were recorded by a TEVC system. Conductance analysis of measured current in 96 mM NaCl (**B**) and 96 mM KCl (**D**). *OsCNGC2* cRNA-injected oocytes were treated with or without 8Br-cAMP (10 μM) and 8Br-cGMP (10 μM) for 30 minutes before TEVC measurement. All external solutions contained 1.8 mM $CaCl_2$, 1.8 mM $MgCl_2$, 1.8 mM mannitol, and 10 mM HEPES (pH 7.5 with Tris) as background elements. Oocytes were injected with 50 ng cRNAs/50 nL, and then incubated for about 24 hr

at 18 °C before TEVC measurements. Small letters (in panel B and D) indicate significant differences ($p < 0.05$), accessed through one-way ANOVA with Tukey's HSD test. Data represent means ± SE, $n$ = 9–10, from two independent experiments performed with different batches of oocytes.

In contrast, results demonstrate that when both $Na^+$ and $K^+$ were present (48 mM NaCl + 48 mM KCl), 8Br-cAMP-treated OsCNGC2-injected oocytes exhibited a clear increase in inward current (Figure 4.2A), and the corresponding box plot showed significantly higher conductance (Figure 4.2B). In addition to the current produced by +8Br-cAMP-treated OsCNGC2-injected oocytes, oocytes injected with OsCNGC2 produced a similar current to water-injected control oocytes in the presence of 8Br-cGMP or in the absence of 8Br-cAMP or 8Br-cGMP in the same bath solution (Figure 4.2). This result suggests that OsCNGC2 requires the co-presence of $Na^+$ and $K^+$ for functional activation.

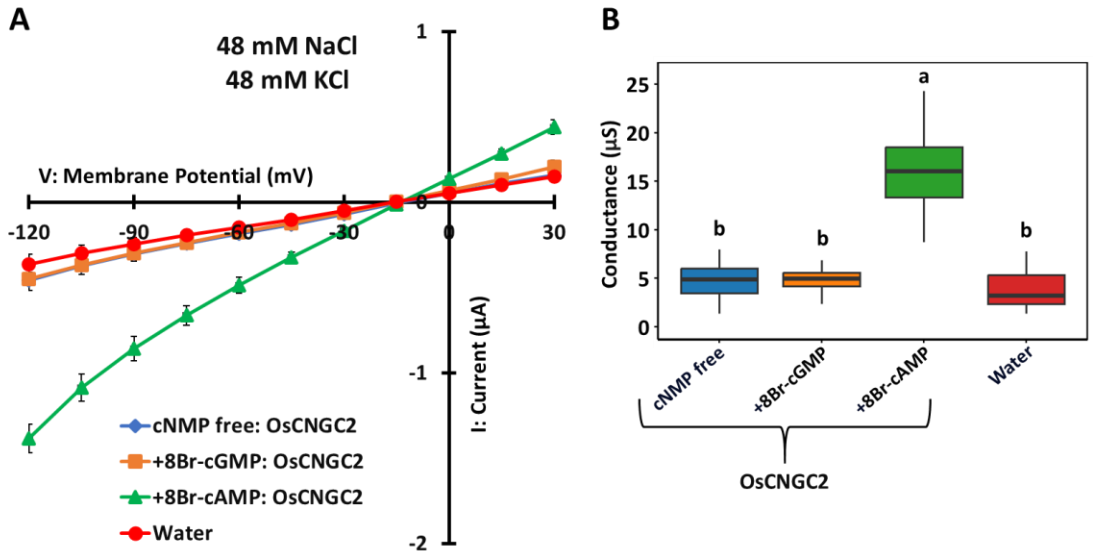


**Figure 4.2.** Current voltage relationship of oocytes expressing OsCNGC2 in the bath solution containing 1:1 mixture of $Na^+$ and $K^+$ media. Currents were recorded using a TEVC system. (**A**) current/voltage curve; (**B**) conductance analysis of measured current. *OsCNGC2* cRNA-injected oocytes were treated with or without 8Br-cAMP (10 µM) and 8Br-cGMP (10 µM) for 30 minutes before TEVC measurement. The external solution used was 48 mM NaCl, 48 mM KCl, 1.8 mM $CaCl_2$, 1.8 mM $MgCl_2$, 1.8 mM mannitol, and 10 mM HEPES (pH 7.5 with Tris). Oocytes were injected with 50 ng cRNAs/50 nL, and then incubated for about 24 hr at 18 °C before TEVC measurements. Small letters (in panel B) indicate significant differences ($p < 0.05$), accessed through one-way ANOVA with Tukey's HSD test. Data represent means ± SE, $n$ = 10–17, from two independent experiments performed with different batches of oocytes.

**OsCNGC2 was not Permeable to $Cl^-$**

To analyze $Cl^-$ permeability by OsCNGC2, we measured the currents after treating OsCNGC2-injected oocytes with 8Br-cAMP and analyzed the reversal potential shift in a bathing solution containing 48 mM Na gluconate + 48 mM KCl, where half of the $Cl^-$ was replaced with gluconate, compared to solutions containing 48 mM NaCl + 48 mM KCl, and 9.6 mM NaCl + 9.6 mM KCl + 76.8 mM Choline Cl, in which every solution contains 96 mM $Cl^-$ (Figure 4.3). *OsCNGC2* cRNA-injected oocytes essentially produced similar currents (Figure 4.3A) and reversal potential in 48 mM NaCl + 48 mM KCl (−14.37±0.56 mV) and 48 mM Na gluconate + 48 mM KCl (−12.31±1.26 mV) bath solutions (Figure 4.3B). However, *OsCNGC2* cRNA-injected oocytes showed currents similar to water-injected control oocytes in 9.6 mM NaCl + 9.6 mM KCl + 76.8 mM Choline Cl bath solution (Figure 4.3A). Additionally, the reversal potential determined in the bath solution containing 9.6 mM NaCl + 9.6 mM KCl + 76.8 mM Choline Cl was −39.66 ± 3.61 mV (Figure 4.3B). No significant reversal potential shift in 48 mM KCl + 48 mM Na gluconate solution compared to 48 mM NaCl + 48 mM KCl solution, and the significant negative shift of the reversal potential in 9.6 mM NaCl + 9.6 mM KCl+76.8 mM Choline Cl solution compared to 48 mM NaCl + 48 mM KCl solution indicates that $Cl^-$ was not permeable by OsCNGC2.

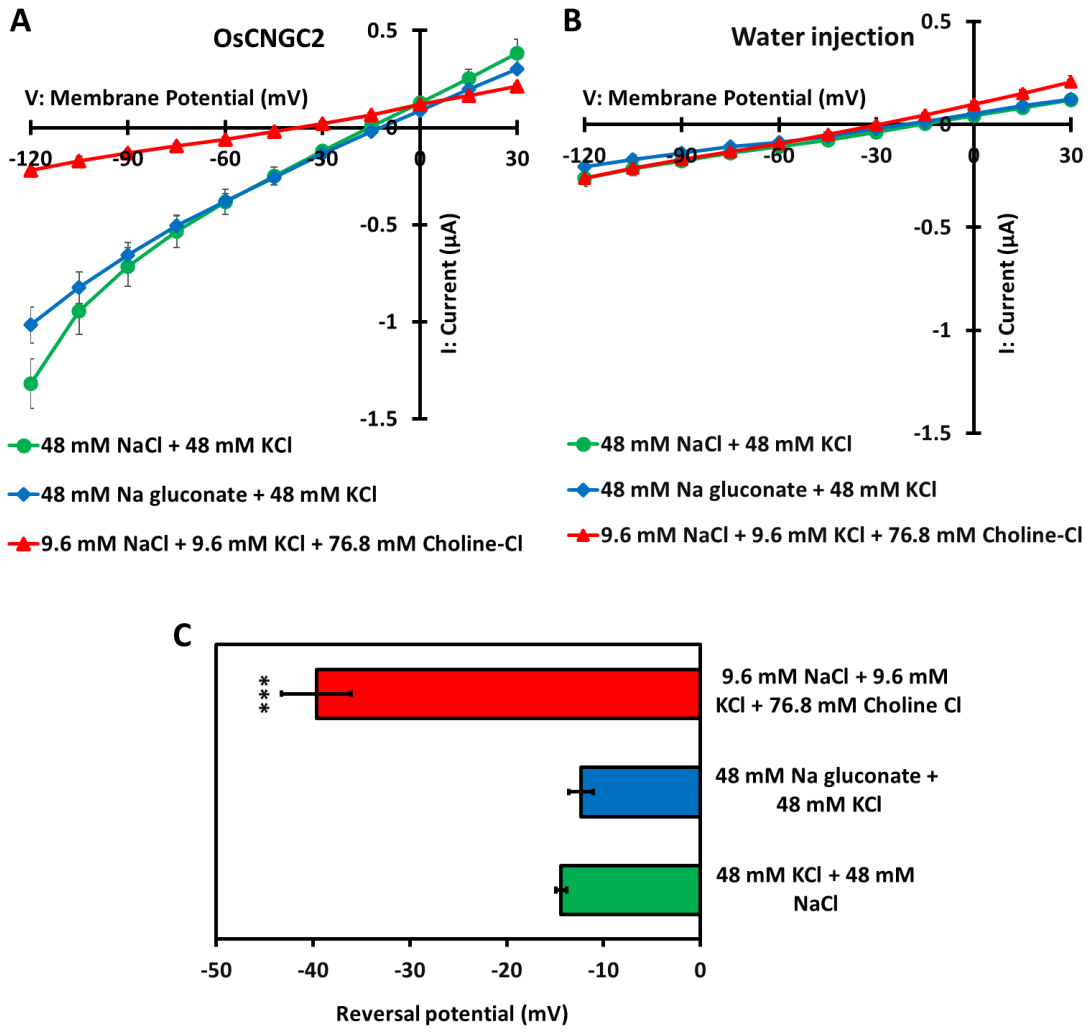


**Figure 4.3.** Current voltage relationship of oocytes expressing OsCNGC2 (**A**) and water-injected negative control (**B**) in the bath solution containing 48 mM NaCl + 48 mM KCl, 48 mM Na gluconate + 48 mM KCl, and 9.6 mM NaCl + 9.6 mM KCl + 76.8 mM Choline Cl. Currents were recorded by a TEVC system. (**C**) Reversal potential shift analysis of measured current from panel A. *OsCNGC2* cRNA-injected oocytes were treated with 8Br-cAMP (10 µM) for 30 minutes before TEVC measurement. External solutions contained 1.8 mM $CaCl_2$, 1.8 mM $MgCl_2$, 1.8 mM mannitol, and 10 mM HEPES (pH 7.5 with Tris) as background elements. Oocytes were injected with 50 ng cRNAs/50 nL, and then incubated for about 24 hr at 18 °C before TEVC measurements. Asterisks (in panel C) denote that the values were significantly different from those of 48 mM NaCl + 48 mM KCl by *t*-test (***$p < 0.001$). Data represent means ± SE, $n = 6–13$, from two independent experiments performed with different batches of oocytes.

**OsCNGC2 Function as $Na^+$, $K^+$ Non-Selective Channel**

To determine the cation selectivity of OsCNGC2, currents were measured, and reversal potential shifts were analyzed under the bath solutions containing different ratios of $Na^+/K^+$ (Figure 4.4). As shown in Figure 4.4A, *OsCNGC2* cRNA-injected oocytes exhibited similar inward currents in bath solutions containing 48 mM NaCl + 48 mM KCl, 19.2 mM NaCl + 76.8 mM KCl, or 76.8 mM NaCl + 19.2 mM KCl. The water-injected control oocytes exhibited minimum or no currents in the same bath solutions (Figure 4.4B). Additionally, the ionic conductance also showed significantly higher values in the same bath solutions compared to water-injected control oocytes (Figure 4.4C). The reversal potential in the bath solution 48 mM NaCl + 48 mM KCl was −16.04±1.17 mV. The slight reversal potential shifted positively (−12.06±0.83 mV) in the case of 19.2 mM NaCl + 76.8 mM KCl bath solution and negatively (−20.21±0l.57 mV) in the case of 76.8 mM NaCl + 19.2 mM KCl bath solution compared to 48 mM NaCl + 48 mM KCl bath solution (Figure 4.4D), suggesting almost non-selective with slight $K^+$-preference.

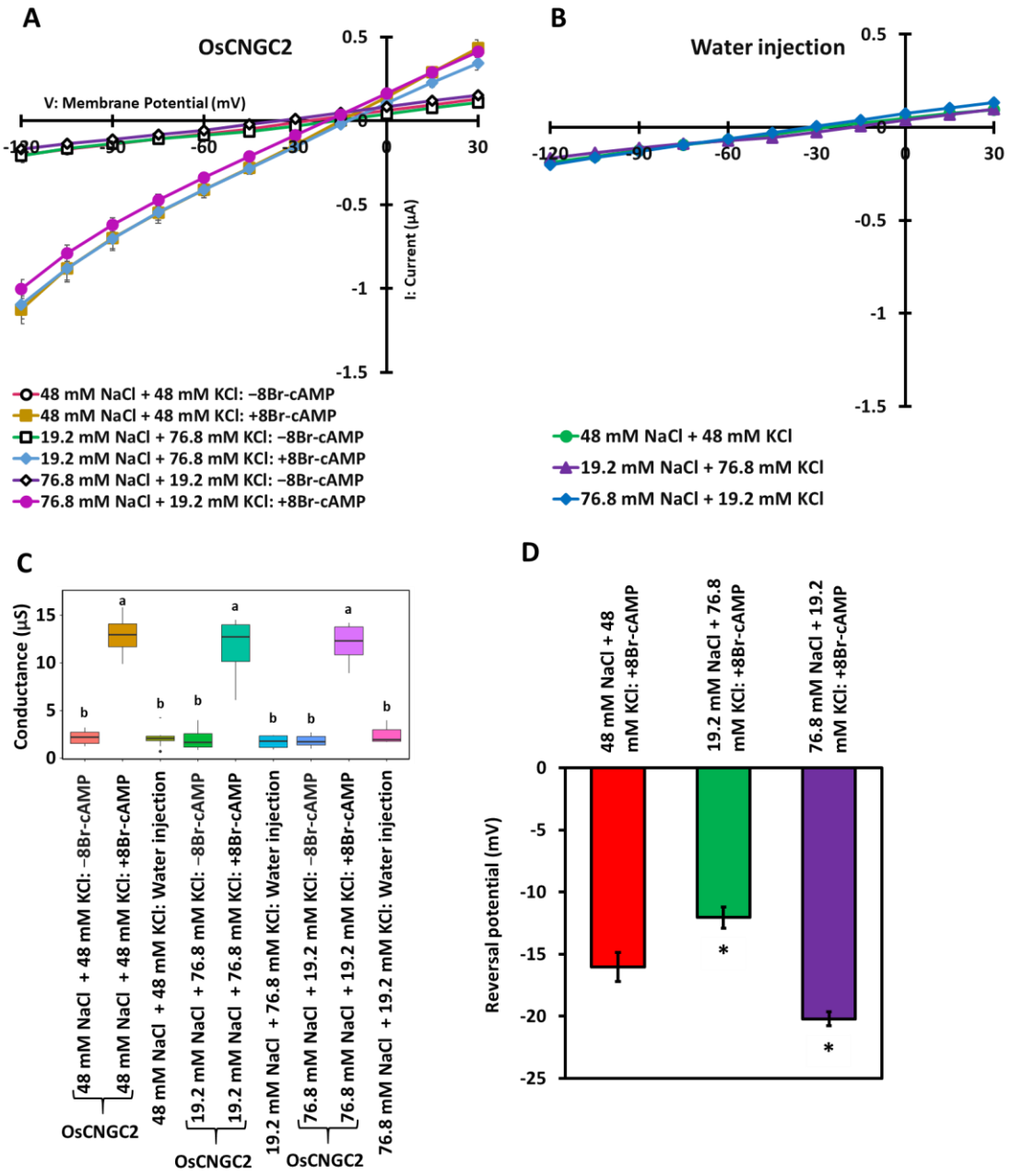


**Figure 4.4.** Current voltage relationship of oocytes expressing OsCNGC2 (**A**) and water-injected negative control (**B**) in the bath solution containing 48 mM NaCl + 48 mM KCl, 19.2 mM NaCl + 76.8 mM KCl, and 76.8 mM NaCl + 19.2 mM KCl. Currents were recorded by a TEVC system. (**C**) Conductance analysis of measured currents; (**D**) Reversal potential shift analysis by OsCNGC2 in 48 mM NaCl + 48 mM KCl, 19.2 mM NaCl + 76.8 mM KCl, and 76.8 mM NaCl + 19.2 mM KCl bath solutions. *OsCNGC2* cRNA-injected oocytes were treated with or without 8Br-cAMP (10 μM) for 30 minutes before TEVC measurement. External solutions contained 1.8 mM $CaCl_2$, 1.8 mM $MgCl_2$, 1.8 mM mannitol, and 10 mM HEPES (pH 7.5 with Tris) as background elements. Oocytes were injected with 50 ng cRNAs/50 nL, and then incubated for about 24 hr at 18 °C before TEVC measurements. Small letters (in panel C) indicate significant differences ($p < 0.05$), accessed through one-way ANOVA with Tukey's

HSD test. Asterisks (in panel D) denote that the values were significantly different from those of 48 mM NaCl + 48 mM KCl by *t*-test (*$p < 0.05$). Data represent means ± SE, $n = 8–13$, from two independent experiments performed with different batches of oocytes.

### OsCNGC2 Facilitates $Ca^{2+}$ Permeation

Ion currents in *X. laevis* oocytes were measured using TEVC in medium containing 18 mM $Ca^{2+}$ or 1.8 mM $Ca^{2+}$, and ionic conductance was analyzed (Figure 4.5). The oocytes injected with *OsCNGC2* cRNA showed similar I–V relationships and conductance values to water-injected controls, either in the presence or absence of 8Br-cAMP under bath solution containing 18 mM $Ca^{2+}$ or 1.8 mM $Ca^{2+}$ (Figure 4.5A, B). However, *OsCNGC2* cRNA-injected oocytes exhibited larger currents and significantly higher ionic conductance than water-injected oocytes in the presence of 8Br-cAMP in the $Ca^{2+}$ containing bath solutions. Current of *OsCNGC2* cRNA-injected oocytes in the 18 mM $Ca^{2+}$ containing bath solution was higher than in the 1.8 mM $Ca^{2+}$ containing bath solution in the presence of 8Br-cAMP (Figure 4.5A, B). This indicates that OsCNGC2 is activated by cAMP, which triggers channel activity that transports $Ca^{2+}$. Next, we analyzed the reversal potential shift of OsCNGC2 in bath solutions containing 18 mM $Ca^{2+}$ and 1.8 mM $Ca^{2+}$ (Figure 4.5C). A tenfold reduction in $Ca^{2+}$ concentration caused a negative shift of 11.5 mV in the reversal potential of OsCNGC2 (Figure 4.5C). Collectively, these results demonstrated that OsCNGC2 functions as a $Ca^{2+}$-permeable channel responsible for $Ca^{2+}$ transport.

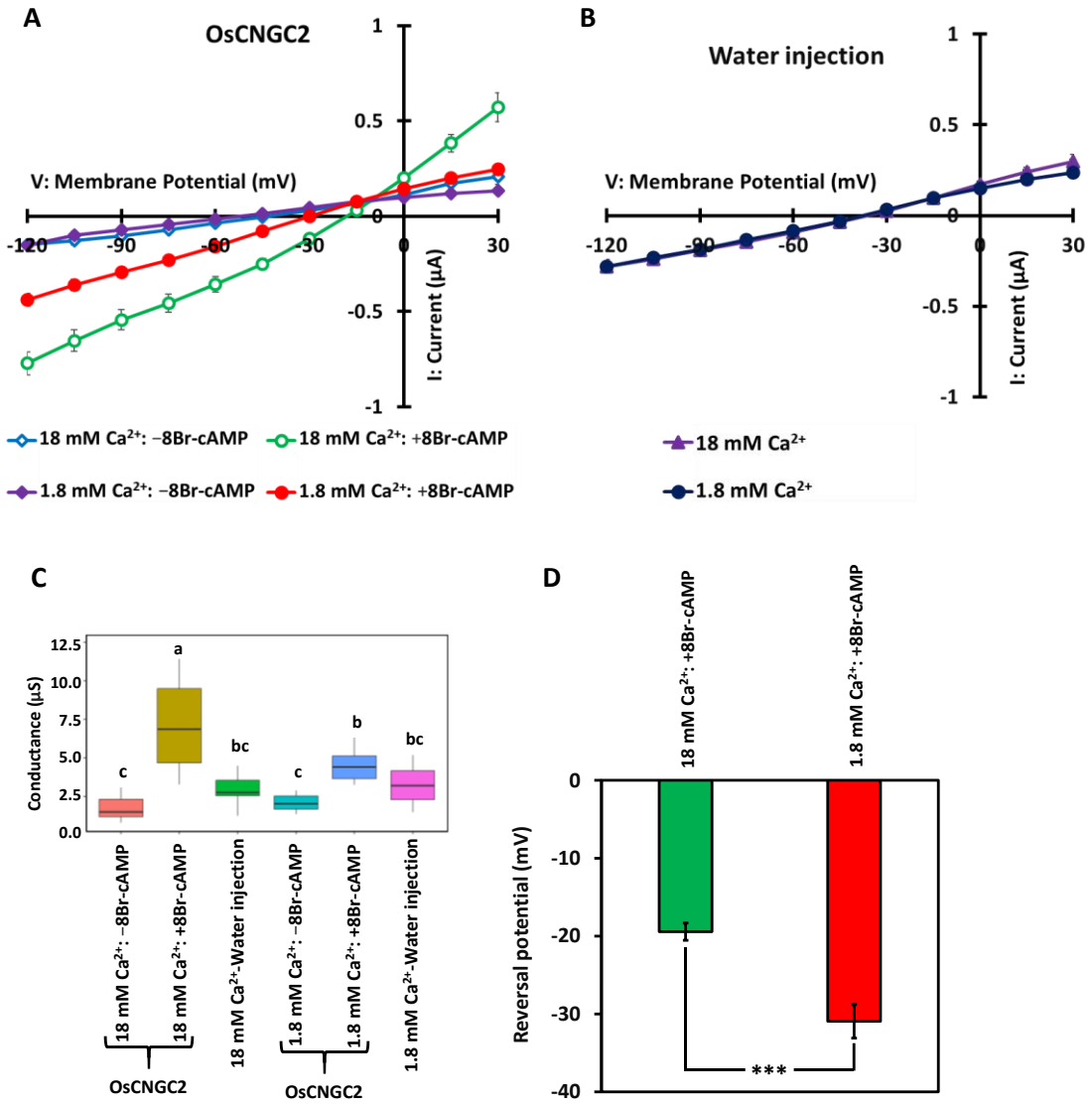


**Figure 4.5.** Current voltage relationship of oocytes expressing OsCNGC2 (**A**) and water-injected negative control (**B**) in the bath solution containing 1.8 mM $Ca^{2+}$ and 18 mM $Ca^{2+}$. Currents were recorded using a TEVC system. (**C**) Conductance analysis of measured currents; (**D**) Reversal potential shift analysis by OsCNGC2 in 1.8 mM $Ca^{2+}$ and 18 mM $Ca^{2+}$ bath solutions. *OsCNGC2* cRNA-injected oocytes were treated with or without 8Br-cAMP (10 µM) for 30 minutes before TEVC measurement. External solutions contained 1.8 mM $CaCl_2$, 1.8 mM $MgCl_2$, 160 mM mannitol, and 10 mM HEPES (pH 7.5 with Tris); and 18 mM $CaCl_2$, 1.8 mM $MgCl_2$, 120 mM mannitol, and 10 mM HEPES (pH 7.5 with Tris) as background elements. Mannitol was added to keep the osmolality of external solutions between 200 and 220 mOsm. Oocytes were injected with 50 ng cRNAs/50 nL, and then incubated for about 24 hr at 18 °C before TEVC measurements. Small letters (in panel C) indicate significant differences ($p < 0.05$), accessed through one-way ANOVA with Tukey's HSD test. Asterisks (in panel D) denote significantly different by *t*-test (***$p < 0.001$). Data represent means ± SE, $n$ = 8–18, from two independent experiments performed with different batches of oocytes.

**Effect of $Ca^{2+}$ on $Na^{+}$ and $K^{+}$ Permeation by OsCNGC2**

The effect of higher $Ca^{2+}$ on $Na^{+}$ and $K^{+}$ permeation was analyzed, and ionic currents were measured using bath solutions containing 48 mM NaCl + 48 mM KCl + 1.8 mM $Ca^{2+}$ or 48 mM NaCl + 48 mM KCl + 18 mM $Ca^{2+}$. Results showed that with 1.8 mM $Ca^{2+}$, OsCNGC2-injected oocytes exhibited higher inward currents in a bath solution containing 48 mM NaCl + 48 mM KCl + 1.8 mM $Ca^{2+}$ than water-injected negative control oocytes (Figure 4.6A, B). However, a tenfold increase in external $Ca^{2+}$ (18 mM $Ca^{2+}$) reduces OsCNGC2-mediated currents in a bath solution containing 48 mM NaCl + 48 mM KCl + 18 mM $Ca^{2+}$ (Figure 4.6A). Conductance analysis also showed a significant reduction when $Ca^{2+}$ concentration increased from 1.8 mM to 18 mM, indicating substantial competitive inhibition (Figure 4.6C). Next, we analyzed the reversal potential shift of OsCNGC2 in bath solutions containing 48 mM NaCl + 48 mM KCl + 1.8 mM $Ca^{2+}$ and 48 mM NaCl + 48 mM KCl + 18 mM $Ca^{2+}$ (Figure 4.6D). It has been demonstrated that a 10-fold increase in $Ca^{2+}$ concentration caused a significant negative shift of 5.5 mV in the reversal potential of OsCNGC2 (Figure 4.6D). The change in reversal potential indicated that $Ca^{2+}$ competes with $Na^{+}$ and $K^{+}$ for permeation when present in higher concentrations.

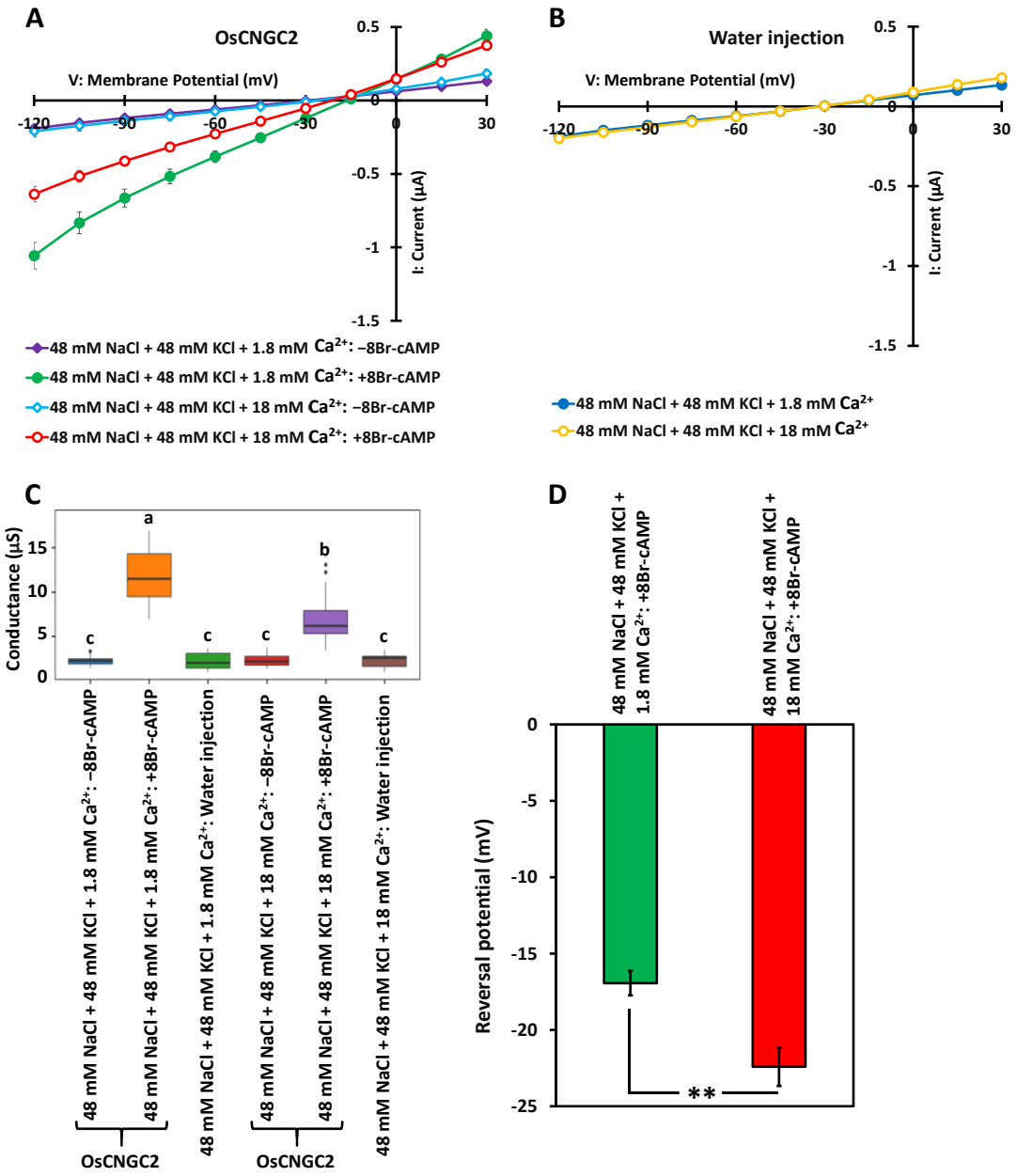


**Figure 4.6.** Current voltage relationship of oocytes expressing OsCNGC2 (**A**) and water-injected negative control (**B**) in the bath solution containing 48 mM NaCl + 48 mM KCl + 1.8 mM $Ca^{2+}$ and 48 mM NaCl + 48 mM KCl + 18 mM $Ca^{2+}$. Currents were recorded using a TEVC system. (**C**) Conductance analysis of measured currents; (**D**) Reversal potential shift analysis by OsCNGC2 in 48 mM NaCl + 48 mM KCl + 1.8 mM $Ca^{2+}$ and 48 mM NaCl + 48 mM KCl + 18 mM $Ca^{2+}$ bath solutions. *OsCNGC2* cRNA-injected oocytes were treated with or without 8Br-cAMP (10 μM) for 30 minutes before TEVC measurement. External solutions contained 1.8 mM $MgCl_2$, 1.8 mM mannitol, and 10 mM HEPES (pH 7.5 with Tris) as background elements. Oocytes were injected with 50 ng cRNAs/50 nL, and then incubated for about 24 hr at 18 °C before TEVC measurements. Small letters (in panel C) indicate significant differences ($p < 0.05$), accessed through one-way ANOVA with Tukey's HSD test. Asterisks (in panel D)

denote significantly different by *t*-test (**$p < 0.01$). Data represent means ± SE, $n = 9–16$, from two independent experiments performed with different batches of oocytes.

### Subcellular Localization of GFP-fused OsCNGC2 in Plant Cells

To study the transient expression assay in plant cells, green fluorescence protein (GFP) was fused with OsCNGC2 at both the N- and C-termini. DNA constructs to express either GFP, GFP-CNGC2, or OsCNGC2-GFP were introduced into *Arabidopsis* leaf protoplasts (Wu et al. 2009). Cells expressing GFP showed strong fluorescence in the cytosol, which did not match the plasma-membrane marker FM4-64 fluorescence (Figure 4.7A- E). GFP fluorescence was observed at the cell periphery when cells expressing GFP-OsCNGC2, which overlapped with the FM4-64 fluorescence (Figure 4.7F- J). A similar overlap of GFP and FM4-64 fluorescence was observed in cells expressing OsCNGC2-GFP (Figure 4.7K-O). These results suggest the plasma-membrane localization of OsCNGC2.

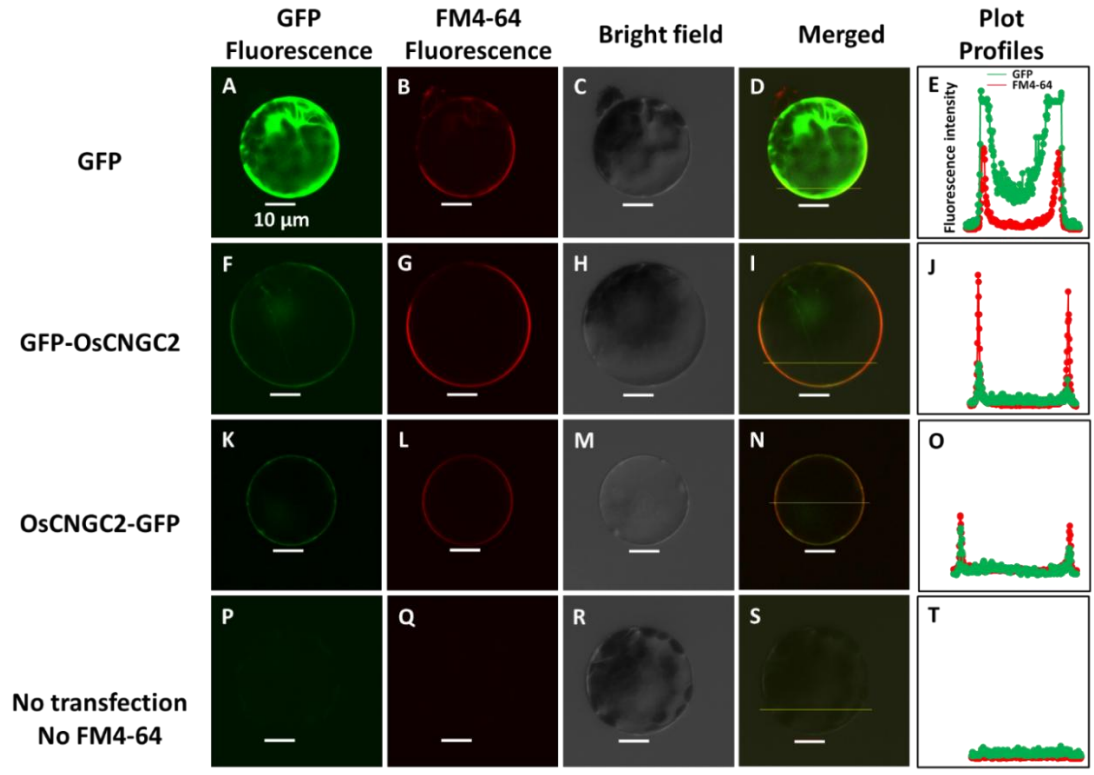


**Figure 4.7.** Subcellular localization of GFP-fused OsCNGC2 transporter in *Arabidopsis*. GFP (**A–D**), GFP-OsCNGC2 (**F–I**), or OsCNGC2-GFP (**K–N**) was transiently overexpressed in *Arabidopsis* leaf protoplasts. Cells were incubated with FM4-64, a PM marker. Protoplasts that were not transfected and not treated with FM4-64 (**P–S**) served as a negative control. The plot-profile fluorescence intensity analysis of protoplasts expressing the different constructs (red

and green colors represent fluorescence from FM4-64 and GFP, respectively): GFP (**E**), GFP-OsCNGC2 (**J**), OsCNGC2-GFP (**O**), and untransfected and no FM4-64-treated protoplast (**T**).

**Expression Analysis of OsCNGC2 in Rice**

The expression profile of *OsCNGC2* showed clear temporal and tissue-specific changes in response to salt treatment (Figure 4.8). Under control conditions (0 hr), *OsCNGC2* transcripts were detected in all tissues, with the stem exhibiting significantly higher transcript levels than the root and leaf, as indicated by different letters. Upon exposure to 100 mM NaCl, expression in both root and leaf remained stable throughout the 48 hr period, with similar letters indicating no significant changes over time. In contrast, stem expression decreased significantly at 6 hr compared to the control, after which it remained statistically unchanged through 24 hr. Although stem expression increased again at 48 hr, the shared letters indicate that this increase was not statistically significant relative to earlier time points. Overall, these patterns suggest that *OsCNGC2* is predominantly regulated in the stem during salt stress, while its expression in roots and leaves remains largely unaffected.

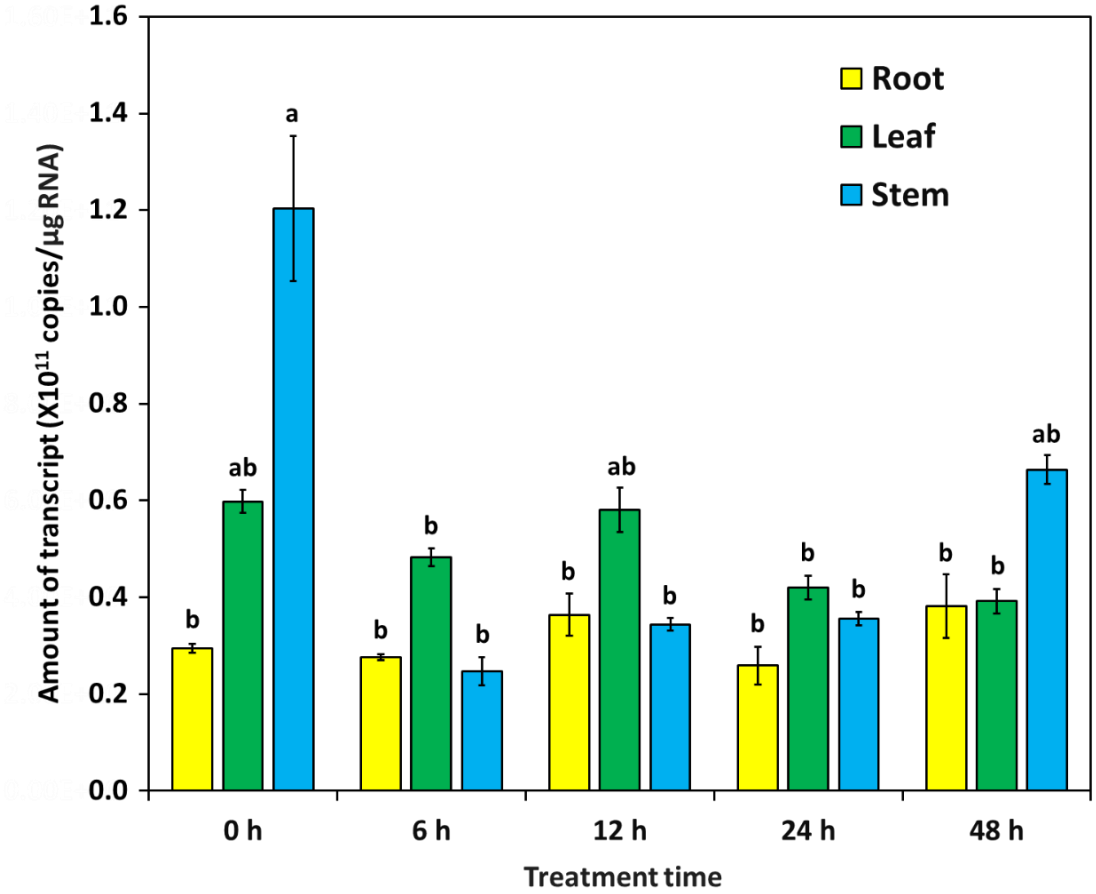

**Figure 4.8.** Absolute quantification of the amount of *OsCNGC2* transcripts in Nipponbare plants with or without salt stress. Fourteen-day-old seedlings were treated with or without 100 mM NaCl (6 to 48 hr) before the total RNA extraction. Absolute transcript amounts (copies/μg RNA) are displayed. Small letters indicate significant differences ($p < 0.05$), accessed through one-way ANOVA with Tukey's HSD test. Data represent the mean ± SE ($n = 9$).

## Discussion

In plant growth and stress adaptation, cyclic nucleotide-gated channels (CNGCs) play a critical role in controlling ion transport, especially that of cations like $Ca^{2+}$, $K^{+,}$ and/or $Na^{+}$ (Leng et al., 2002; Jha et al., 2016; Mori et al., 2018; Dietrich et al., 2020; Jarratt-Barnham et al., 2021). They mediate $Ca^{2+}$ influx and produce specific cytosolic $Ca^{2+}$ signatures that control many physiological processes when activated by cyclic nucleotides of cAMP and cGMP (Leng et al., 1999; Balagué et al., 2003; Jha et al., 2016; Dietrich et al., 2020). By regulating $Ca^{2+}$ and ROS, some isoforms, such as *AtCNGC2*, *AtCNGC4*, and *AtCNGC6*, are implicated in pathogen defense, thermotolerance, and guard cell signaling (Jha et al., 2016; Jarratt-Barnham et al., 2021; Wang et al., 2013). Additionally, *CNGCs* contribute to the transfer of $Na^{+}$ and $K^{+}$, then preserving ionic equilibrium in the face of heavy-metal stress, drought, and salinity (Ali et al., 2007; Jha et al., 2016; Jarratt-Barnham et al., 2021). Plant CNGCs were characterized as non-selective cation channels (Ward et al., 2009). Several CNGCs show inward $K^{+}$ and $Na^{+}$ currents when expressed in heterologous systems or mutant plants (Christopher et al., 2007; Mori et al., 2018). It has also been reported that external $Ca^{2+}$ can limit the $K^{+}$ conductance (Leng et al., 2002). Nevertheless, there has been very little evidence to date regarding the electrophysiological characterizations of plant CNGCs (Leng et al., 2002; Mori et al., 2018; Zhang et al., 2019; Wang et al., 2025). Several plant CNGCs have been shown to localize predominantly at the plasma membrane (PM). In Arabidopsis, AtCNGC3, AtCNGC10, AtCNGC11, and AtCNGC12 were identified as PM channels (Gobert et al., 2006; Christopher et al., 2007; Baxter et al., 2008), with AtCNGC10 also trafficking via the endoplasmic reticulum and Golgi. GFP-tagged AtCNGC18, AtCNGC7, and AtCNGC8 were also localized at the PM in pollen tubes (Frietsch et al., 2007; Tunc-Ozdemir et al., 2013). Similarly, AtCNGC5 and AtCNGC6 were detected at the PM in guard cells (Wang et al., 2013). In rice, 13 of 16 OsCNGCs were predicted and experimentally confirmed to localize at the PM (Nawaz et al., 2014). Consistent with previous reports that most plant

CNGCs localize to the plasma membrane, our transient expression assays confirmed that OsCNGC2 is also a PM-localized channel (Figure 4.7). Our protoplast-based localization assay further substantiates this, as both N- and C-terminal GFP fusions of OsCNGC2 showed clear co-localization with FM4-64, whereas free GFP remained cytosolic (Figure 4.7).

In the present study, the electrophysiological analysis of OsCNGC2 in *X. laevis* oocytes revealed that this channel exhibits selective activation and cation permeability regulated by cyclic nucleotides and ion composition. When oocytes were exposed to the external solutions containing single-ion (96 mM NaCl or 96 mM KCl), *OsCNGC2* cRNA-injected cells showed ionic currents and conductance values similar to water-injected controls (Figure 4.1), indicating that neither $Na^+$ nor $K^+$ alone can activate the channel. In contrast, in mixed-ion conditions (48 mM NaCl + 48 mM KCl), OsCNGC2 oocytes exhibited pronounced inward currents and significantly higher conductance (Figure 4.2) in the presence of a membrane-permeable cAMP analog (8Br-cAMP) in the external solution. These results indicate that OsCNGC2 requires the co-presence of $Na^+$ and $K^+$ for activation. A similar ion-dependent activation pattern has been reported for HvCNGC2-3, that is, significant inward currents appeared only when both $Na^+$ and $K^+$ were present together in the bathing solution, but not with either ion individually (Mori et al., 2018). Anion permeability was assessed by replacing NaCl with gluconate or choline (Figure 4.3). Substitution of $Cl^-$ with gluconate did not alter current amplitude or reversal potential, indicating that $Cl^-$ does not contribute to channel conductance. In contrast, a marked negative shift in reversal potential (−39.66 mV) in choline chloride solution confirmed $Na^+$ permeability but not $Cl^-$ through OsCNGC2 (Figure 4.3). Analysis under varying $Na^+/K^+$ ratios showed similar inward currents with only minor reversal potential changes, indicating that OsCNGC2 is a largely non-selective $Na^+/K^+$ channel (Figure 4.4). Additionally, OsCNGC2 mediated $Ca^{2+}$ transport, as higher extracellular $Ca^{2+}$ significantly increased inward currents and conductance. A negative shift in reversal potential upon reducing $Ca^{2+}$ concentration further confirmed $Ca^{2+}$ permeability (Figure 4.5). Similarly, several Arabidopsis CNGCs have been shown to mediate $Ca^{2+}$ influx across the plasma membrane. For example, CNGC12 expressed in *Xenopus* oocytes generated strong inward currents in $Ca^{2+}$-containing solutions, with current amplitude increasing proportionally to external $Ca^{2+}$ concentration (Zhang et al., 2019). Moreover, Arabidopsis CNGC1 and CNGC5 have been shown to mediate $Ca^{2+}$-dependent inward currents when expressed in

HEK293T cells, with current amplitude increasing markedly as external $Ca^{2+}$ concentration rose from 1 to 10 mM, indicating strong $Ca^{2+}$ dependence (Wang et al., 2025). In contrast, increasing $Ca^{2+}$ from 1.8 mM to 18 mM reduced OsCNGC2-mediated inward $K^+$ and $Na^+$ currents and substantially decreased conductance (Figure 4.6A, C), suggesting that $Ca^{2+}$ blocks the $K^+$- and $Na^+$ permeation. Recent cryo-EM structures of AtCNCG1 and AtCNCG5 (Wang et al., 2025) provide an insightful framework for interpreting the ion transport function of OsCNCG2. Wang et al. (2025) identified a conserved Gln in the selectivity filter as the key determinant of $Ca^{2+}$ selectivity and an Arg occupying the CNBHD pocket as the structural basis for cNMP-independent gating. However, sequence inspection revealed that both residues are conserved in OsCNGC2 (Gln350 and Arg556), which may support our electrophysiological results indicating that OsCNGC2 is permeable to $Ca^{2+}$ (Figures 4.5, 4.9).

Additional residues surrounding the filter or extracellular domain of OcCNGS2 may modulate ion coordination differently from AtCNGC1/5. The activation of OsCNCG2 by cAMP, despite the conservation of the CNBHD-occupying Arg, further suggests that rice CNGCs may have a modified regulatory configuration that allows subtype-specific cyclic nucleotide responsiveness. Moreover, the $Ca^{2+}$-dependent inhibition and negative shift in reversal potential were observed (Figure 4.6), aligning with the presence of a conserved $Ca^{2+}$-coordinating Gln, as elevated $Ca^{2+}$ likely binds within the pore and competes directly with $Na^+$ for permeation. Together, these structural considerations indicate that OsCNGC2 retains the canonical $Ca^{2+}$-binding architecture of plant CNGCs while functionally diverging to support rice-specific ion transport. Further molecular insights and experiments are needed to reveal the molecular mechanism in cation-selectivity and cNMP-dependency of OsCNGC2. In-silico evidence shows that *AtCNGC2* is strongly induced in Arabidopsis shoots under salt stress, with a marked increase after 6 hr of 150 mM NaCl and sustained elevated levels at 12 hr, while its root expression remains consistently low (Oranab et al., 2021), and further studies confirmed maximal shoot-specific induction after 6 hr and 12 hr, with negligible root expression (Oranab et al., 2023). Similarly, in the halophyte Suaeda japonica, *CNGC2* is strongly upregulated—over threefold—in both leaves and roots under 600 mM NaCl (Shinta et al., 2025). By contrast, *OsCNGC2* exhibits generally low to moderate expression across rice tissues and is not among the highly tissue-specific *OsCNGC* genes (Wang et al., 2023; Chang et al., 2024).


**Figure 4.9.** Amino acid sequence alignment of AtCNGC1, AtCNGC5, and OsCNCG2. GENETYX ver. 16 was used for comparisons.

Under salt stress, *OsCNGC2* showed lower expression than *OsCNGC3*, *OsCNGC10* (Wang et al., 2023). In the present study, *OsCNGC2* expression remained stable in roots and leaves during 100 mM NaCl treatment. In contrast, the stem displays a transient but significant decline at 6 hr followed by a nonsignificant partial recovery (Figure 4.8), indicating that its salt-induced regulation is predominantly stem-specific. This pattern suggests a possible role for *OsCNGC2* in modulating long-distance ion signaling rather than direct ion uptake in roots or stress perception in leaves. Early stem-

specific downregulation may limit excessive cation influx during the initial ionic shock. In contrast, stable root and leaf expression implies that *OsCNGC2* activity in these tissues may rely more on post-transcriptional or activation-dependent mechanisms. Overall, our findings demonstrated that OsCNGC2 is a plasma membrane–localized non-selective cation channel uniquely activated by the co-presence of $Na^+$ and $K^+$. The stem-specific transcriptional response under salt stress highlights a specialized role in maintaining ionic balance and mediating long-distance signaling. These insights provide the first electrophysiological characterization of a rice CNGC channel and lay a foundation for further exploration of *OsCNGC2* function in stress adaptation and crop improvement.

**References**


Ali R, Ma W, Lemtiri-Chlieh F, Tsaltas D, Leng Q, Von Bodman S, Berkowitz GA. Death don't have no mercy and neither does calcium: *Arabidopsis* CYCLIC NUCLEOTIDE GATED CHANNEL2 and innate immunity. The Plant Cell. **2007**;19(3):1081-1095. https://doi.org/10.1105/tpc.106.045096

Arazi T, Sunkar R, Kaplan B, Fromm H. A tobacco plasma membrane calmodulin-binding transporter confers $Ni^{2+}$ tolerance and $Pb^{2+}$ hypersensitivity in transgenic plants. The Plant Journal. **1999**;20(2):171-182. https://doi.org/10.1046/j.1365-313x.1999.00588.x

Balagué C, Lin B, Alcon C, Flottes G, Malmström S, Köhler C, Neuhaus G, Pelletier G, Gaymard F, Roby D. HLM1, an essential signaling component in the hypersensitive response, is a member of the cyclic nucleotide–gated channel ion channel family. The Plant Cell. **2003**;15(2):365-379. https://doi.org/10.1105/tpc.006999

Baxter J, Moeder W, Urquhart W, Shahinas D, Chin K, Christendat D, Kang HG, Angelova M, Kato N, Yoshioka K. Identification of a functionally essential amino acid for Arabidopsis cyclic nucleotide gated ion channels using the chimeric *AtCNGC11/12* gene. The Plant Journal. **2008**;56(3):457-469. https://doi.org/10.1111/j.1365-313X.2008.03619.x

Borsics T, Webb D, Andeme-Ondzighi C, Staehelin LA, Christopher DA. The cyclic nucleotide-gated calmodulin-binding channel AtCNGC10 localizes to the plasma membrane and influences numerous growth responses and starch

accumulation in *Arabidopsis thaliana*. Planta. **2007**;225(3):563-573. https://doi.org/10.1007/s00425-006-0372-3

Bridges D, Fraser ME, Moorhead GB. Cyclic nucleotide binding proteins in the *Arabidopsis thaliana* and *Oryza sativa* genomes. BMC Bioinformatics. **2005**;6(1):6. https://doi.org/10.1186/1471-2105-6-6

Chang J, Zhang R, Fu Z, Wang Y, Lei J, Cheng J, Ren C, Xu K, Gu C, Song Y, Zeng R. OsCNGC7 modulates calcium dynamics and accelerates leaf senescence in rice. Plant Physiology and Biochemistry. **2024**;216:109193. https://doi.org/10.1016/j.plaphy.2024.109193

Chin K, DeFalco TA, Moeder W, Yoshioka K. The Arabidopsis cyclic nucleotide-gated ion channels AtCNGC2 and AtCNGC4 work in the same signaling pathway to regulate pathogen defense and floral transition. Plant Physiology. **2013**;163(2):611-624. https://doi.org/10.1104/pp.113.225680

Chiu WL, Niwa Y, Zeng W, Hirano T, Kobayashi H, Sheen J. Engineered GFP as a vital reporter in plants. Current Biology. **1996**;6(3):325-330. https://doi.org/10.1016/S0960-9822(02)00483-9

Christopher DA, Borsics T, Yuen CY, Ullmer W, Andème-Ondzighi C, Andres MA, Kang BH, Staehelin LA. The cyclic nucleotide gated cation channel AtCNGC10 traffics from the ER via Golgi vesicles to the plasma membrane of Arabidopsis root and leaf cells. BMC Plant Biology. **2007** ;7(1):48. https://doi.org/10.1186/1471-2229-7-48

Clough SJ, Fengler KA, Yu IC, Lippok B, Smith Jr RK, Bent AF. The *Arabidopsis dnd1* "defense, no death" gene encodes a mutated cyclic nucleotide-gated ion channel. Proceedings of the National Academy of Sciences. **2000**;97(16):9323-9328. https://doi.org/10.1073/pnas.150005697

Dietrich P, Moeder W, Yoshioka K. Plant cyclic nucleotide-gated channels: new insights on their functions and regulation. Plant Physiology. **2020**;184(1):27-38. https://doi.org/10.1104/pp.20.00425

Duszyn M, Świeżawska B, Szmidt-Jaworska A, Jaworski K. Cyclic nucleotide gated channels (CNGCs) in plant signalling—Current knowledge and perspectives. Journal of Plant Physiology. **2019**;241:153035. https://doi.org/10.1016/j.jplph.2019.153035

Fesenko EE, Kolesnikov SS, Lyubarsky AL. Induction by cyclic GMP of cationic conductance in plasma membrane of retinal rod outer segment. Nature. **1985**;313(6000):310-313. https://doi.org/10.1038/313310a0

Maathuis FJ, Sanders D. Sodium uptake in Arabidopsis roots is regulated by cyclic nucleotides. Plant Physiology. **2001**;127(4):1617-1625. https://doi.org/10.1104/pp.010502

Frietsch S, Wang YF, Sladek C, Poulsen LR, Romanowsky SM, Schroeder JI, Harper JF. A cyclic nucleotide-gated channel is essential for polarized tip growth of pollen. Proceedings of the National Academy of Sciences. **2007**;104(36):14531-14536. https://doi.org/10.1073/pnas.0701781104

Gobert A, Park G, Amtmann A, Sanders D, Maathuis FJ. *Arabidopsis thaliana* cyclic nucleotide gated channel 3 forms a non-selective ion transporter involved in germination and cation transport. Journal of Experimental Botany. **2006**;57(4):791-800. https://doi.org/10.1093/jxb/erj064

Hua BG, Mercier RW, Zielinski RE, Berkowitz GA. Functional interaction of calmodulin with a plant cyclic nucleotide gated cation channel. Plant Physiology and Biochemistry. **2003**;41(11-12):945-954. https://doi.org/10.1016/j.plaphy.2003.07.006

Imran S, Horie T, Katsuhara M. Expression and ion transport activity of rice OsHKT1;1 variants. Plants. **2020**;9(1):16. https://doi.org/10.3390/plants9010016

Isner JC, Maathuis FJ. cGMP signalling in plants: from enigma to main stream. Functional Plant Biology. **2018**;45(2):93-101. https://doi.org/10.1071/fp16337

Jarratt-Barnham E, Wang L, Ning Y, Davies JM. The complex story of plant cyclic nucleotide-gated channels. International Journal of Molecular Sciences. **2021**;22(2):874. https://doi.org/10.3390/ijms22020874

Jha SK, Sharma M, Pandey GK. Role of cyclic nucleotide gated channels in stress management in plants. Current Genomics. **2016**;17(4):315-329. https://doi.org/10.2174/1389202917666160331202125

Kaplan B, Sherman T, Fromm H. Cyclic nucleotide-gated channels in plants. FEBS Letters. **2007**;581(12):2237-2246. https://doi.org/10.1016/j.febslet.2007.02.017

Katsuhara M, Akiyama Y, Koshio K, Shibasaka M, Kasamo K. Functional analysis of water channels in barley roots. Plant and Cell Physiology. **2002**;43(8):885-893. https://doi.org/10.1093/pcp/pcf102

Leng Q, Mercier RW, Yao W, Berkowitz GA. Cloning and first functional characterization of a plant cyclic nucleotide-gated cation channel. Plant Physiology. **1999**;121(3):753-761. https://doi.org/10.1104/pp.121.3.753

Leng Q, Mercier RW, Hua BG, Fromm H, Berkowitz GA. Electrophysiological analysis of cloned cyclic nucleotide-gated ion channels. Plant Physiology. **2002**;128(2):400-410. https://doi.org/10.1104/pp.010832

Ma W, Ali R, Berkowitz GA. Characterization of plant phenotypes associated with loss-of-function of AtCNGC1, a plant cyclic nucleotide gated cation channel. Plant Physiology and Biochemistry. **2006**;44(7-9):494-505. https://doi.org/10.1016/j.plaphy.2006.08.007

Mahdieh M, Mostajeran A, Horie T, Katsuhara M. Drought stress alters water relations and expression of PIP-type aquaporin genes in *Nicotiana tabacum* plants. Plant and Cell Physiology. **2008**;49(5):801-813. https://doi.org/10.1093/pcp/pcn054

Mäser P, Thomine S, Schroeder JI, Ward JM, Hirschi K, Sze H, Talke IN, Amtmann A, Maathuis FJ, Sanders D, Harper JF. Phylogenetic relationships within cation transporter families of Arabidopsis. Plant physiology. **2001**;126(4):1646-67. https://doi.org/10.1104/pp.126.4.1646

Mori IC, Nobukiyo Y, Nakahara Y, Shibasaka M, Furuichi T, Katsuhara M. A cyclic nucleotide-gated channel, HvCNGC2-3, is activated by the co-presence of $Na^+$ and K+ and permeable to $Na^+$ and $K^+$ non-selectively. Plants. **2018**;7(3):61. https://doi.org/10.3390/plants7030061

Nakamura T, Gold GH. A cyclic nucleotide-gated conductance in olfactory receptor cilia. Nature. **1987**;325(6103):442-444. https://doi.org/10.1038/325442a0

Nawaz Z, Kakar KU, Saand MA, Shu QY. Cyclic nucleotide-gated ion channel gene family in rice, identification, characterization and experimental analysis of expression response to plant hormones, biotic and abiotic stresses. BMC Genomics. **2014**;15(1):853. https://doi.org/10.1186/1471-2164-15-853

Oranab S, Ghaffar A, Ahmad A, Pasha MF, Munir B, Arif S, Ishaq S, Mahfooz SH, Kousar R, Zakia S, Ahmad HM. Genome-wide analysis of cyclic nucleotide-gated ion channels (CNGCS) of *Arabidopsis thaliana* under abiotic stresses. SABRAO Journal of Breeding and Genetics. **2023**;55(1): 38-49. http://doi.org/10.54910/sabrao2023.55.1.4

Oranab S, Ghaffar A, Kiran S, Yameen M, Munir B, Zulfiqar S, Abbas S, Batool F, Farooq MU, Ahmad B, Ilyas H. Molecular characterization and expression of

cyclic nucleotide gated ion channels 19 and 20 in *Arabidopsis thaliana* for their potential role in salt stress. Saudi Journal of Biological Sciences. **2021**;28(10):5800-5807. https://doi.org/10.1016/j.sjbs.2021.06.027

Podda MV, Grassi C. New perspectives in cyclic nucleotide-mediated functions in the CNS: the emerging role of cyclic nucleotide-gated (CNG) channels. Pflügers Archiv - European Journal of Physiology. 2014;466:1241-1257. https://doi.org/10.1007/s00424-013-1373-2

Sasaki T, Tsuchiya Y, Ariyoshi M, Nakano R, Ushijima K, Kubo Y, Mori IC, Higashiizumi E, Galis I, Yamamoto Y. Two members of the aluminum-activated malate transporter family, *SlALMT4* and *SlALMT5*, are expressed during fruit development, and the overexpression of *SlALMT5* alters organic acid contents in seeds in tomato (*Solanum lycopersicum*). Plant and Cell Physiology. **2016**;57(11):2367-2379. https://doi.org/10.1093/pcp/pcw157

Sherman T, Fromm H. Physiological Roles of Cyclic Nucleotide Gated Channels in Plants. In: Mancuso S, Baluka F. (eds) Signaling in Plants. Signaling and Communication in Plants. Springer, Berlin, Heidelberg. **2009**;pp 91-106. https://doi.org/10.1007/978-3-540-89228-1_5

Shinta, Bentoy KM, Fauzia AN, Nampei M, Linh NM, Ueda A. Physiological and transcriptomic insights into mechanisms of salt tolerance in the leaves and roots of the halophyte *Suaeda japonica* makino under high salinity stress. Journal of Plant Growth Regulation. **2025**:1-9. https://doi.org/10.1007/s00344-025-11864-8

Tunc-Ozdemir M, Rato C, Brown E, Rogers S, Mooneyham A, Frietsch S, Myers CT, Poulsen LR, Malho R, Harper JF. Cyclic nucleotide gated channels 7 and 8 are essential for male reproductive fertility. PLoS One. **2013**;8(2):e55277. https://doi.org/10.1371/journal.pone.0055277

Ungerer N, Mücke N, Broecker J, Keller S, Frings S, Möhrlen F. Distinct binding properties distinguish LQ-type calmodulin-binding domains in cyclic nucleotide-gated channels. Biochemistry. **2011**;50(15):3221-3228. https://doi.org/10.1021/bi200115m

Urquhart W, Chin K, Ung H, Moeder W, Yoshioka K. The cyclic nucleotide-gated channels AtCNGC11 and 12 are involved in multiple $Ca^{2+}$-dependent physiological responses and act in a synergistic manner. Journal of

Experimental Botany. **2011**;62(10):3671-3682. https://doi.org/10.1093/jxb/err074

Wang J, Du BY, Zhang X, Qu X, Yang Y, Yang Z, Wang YF, Zhang P. Cryo-EM structures of *Arabidopsis* CNGC1 and CNGC5 reveal molecular mechanisms underlying gating and calcium selectivity. Nature Plants. **2025**;11:632-642. https://doi.org/10.1038/s41477-025-01923-z

Wang X, Wu F, Zhang J, Bao Y, Wang N, Dou G, Meng D, Wang X, Li J, Shi Y. Identification of the CNGC gene family in rice and mining of alleles for application in rice improvement. Plants. **2023**;12(24):4089. https://doi.org/10.3390/plants12244089

Wang YF, Munemasa S, Nishimura N, Ren HM, Robert N, Han M, Puzõrjova I, Kollist H, Lee S, Mori I, Schroeder JI. Identification of cyclic GMP-activated nonselective $Ca^{2+}$-permeable cation channels and associated CNGC5 and CNGC6 genes in Arabidopsis guard cells. Plant Physiology. **2013**;163(2):578-590. https://doi.org/10.1104/pp.113.225045

Ward JM, Mäser P, Schroeder JI. Plant ion channels: gene families, physiology, and functional genomics analyses. Annual review of physiology. **2009**;71(1):59-82. https://doi.org/10.1146/annurev.physiol.010908.163204

Wu FH, Shen SC, Lee LY, Lee SH, Chan MT, Lin CS. Tape-*Arabidopsis* Sandwich-a simpler *Arabidopsis* protoplast isolation method. Plant Methods. **2009**;5(1):16. https://doi.org/10.1186/1746-4811-5-16

Yoo SD, Cho YH, Sheen J. *Arabidopsis* mesophyll protoplasts: a versatile cell system for transient gene expression analysis. Nature Protocols. **2007**;2(7):1565-1572. https://doi.org/10.1038/nprot.2007.199

Zhang Z, Hou C, Tian W, Li L, Zhu H. Electrophysiological studies revealed CaM1-mediated regulation of the *Arabidopsis* calcium channel CNGC12. Frontiers in Plant Science. **2019**;10:1090. https://doi.org/10.3389/fpls.2019.01090

# CHAPTER 5

# General Discussion

Cereals' ability to withstand salinity is a complicated characteristic that results from the coordinated action of several ion transport systems functioning at various spatial and regulatory levels (Roy et al., 2014). Rather than being governed by a single dominant transporter, effective tolerance depends on how selective transporters, regulatory variants, and non-selective channels collectively control $Na^+$, $K^+$, and $Cl^-$ fluxes. In this dissertation, I investigated this integrated network through comparative and functional analyses of the HKT1;1 transporter in rice and barley (Chapters 2 and 3) and a non-selective cyclic nucleotide-gated channel, OsCNGC2, in rice (Chapter 4). Together, these studies provide a unified view of how cereals partition ionic functions among distinct transport components to achieve salinity tolerance.

A central outcome of this work is the clarification that salinity tolerance in rice involves functional diversification and regulatory plasticity. In contrast, barley relies more strongly on conserved and robust $Na^+$ exclusion mechanisms. Moreover, the results demonstrate that selective $Na^+$ transporters, alternative splice variants with altered ion selectivity, and non-selective channels involved in $Na^+$ and $K^+$ transport play complementary rather than redundant roles during salt stress.

## Clarified Roles of HKT Transporters in Salinity Tolerance

HKT1-type transporters are crucial for plant salinity tolerance due to their role in controlling long-distance $Na^+$ movement and maintaining a healthy $Na^+/K^+$ balance in above-ground tissues (Munns and Tester, 2008; Horie et al., 2009; Hauser and Horie, 2010). Chapters 2 and 3 confirm this conserved function in cereals and expand current understanding by showing that functional diversification and species-specific regulation significantly influence *HKT1;1* activity. Full-length OsHKT1;1 (OsHKT1;1-FL) shows strong $Na^+$ selectivity, aligning with earlier electrophysiological and genetic studies highlighting its role in $Na^+$ retrieval from the xylem and limiting $Na^+$ transport to shoots (Ren et al., 2005; Jabnoune et al., 2009; Wang et al., 2015). Expression analyses indicate that *OsHKT1;1-FL* is mainly active in roots, supporting its role in long-distance $Na^+$ exclusion. These results reinforce the idea that *OsHKT1;1-FL* serves as a core, conserved $Na^+$ exclusion system in rice,

similar to the HKT1;1 mechanism in *Arabidopsis* and other cereals (Sunarpi et al., 2005; Møller et al., 2009; Horie et al., 2009). Conversely, this study reveals that alternative splicing of *OsHKT1;1* produces a distinct variant, *OsHKT1;1-V2*, which localizes to the plasma membrane and exhibits $Cl^-$-dependent transport activity rather than $Na^+$ selectivity. This marks a significant conceptual shift because HKT1 transporters have been traditionally viewed as $Na^+$-selective or $Na^+/K^+$ co-transporters due to their conserved pore structure (Mäser et al., 2002; Platten et al., 2006; Horie et al., 2009). The discovery of OsHKT1;1-V2 shows that post-transcriptional regulation can expand a single HKT gene's functions beyond $Na^+$ transport, linking HKT1 transporters to $Cl^-$ homeostasis. Expression data reveal that *OsHKT1;1-V2* is expressed at much lower levels than *OsHKT1;1-FL* and shows regulation dependent on cultivar and stress conditions, with differing expression patterns between salt-tolerant and salt-sensitive rice varieties. This suggests that *OsHKT1;1-V2* does not replace the main $Na^+$ exclusion role of *OsHKT1;1-FL* but may have a conditional or modulatory function, possibly involving $Cl^-$ transport or redistribution during salt stress. This is especially relevant given the growing evidence that $Cl^-$ toxicity, alongside $Na^+$ toxicity, significantly hampers rice growth under salinity conditions (Munns and Tester, 2008; Dao and Hirai, 2018). The presence of both $Na^+$-selective and $Cl^-$-permeable OsHKT1;1 supports a model where rice manages $Na^+$ and $Cl^-$ through different protein forms derived from the same gene via alternative splicing. Chapter 3's comparative analysis highlights notable differences between rice and barley in *HKT1;1* regulation. Barley's HvHKT1;1 variants maintain strong $Na^+$ selectivity and do not exhibit the functional diversification seen in OsHKT1;1. Their relatively stable expression across tissues and conditions aligns with barley's inherent higher salt tolerance and reliance on robust, constant $Na^+$ exclusion mechanisms (Han et al., 2018). These interspecies differences suggest that rice and barley have evolved different strategies to cope with salinity stress. Rice, being more salt-sensitive, seems to depend on regulatory flexibility, including alternative splicing, to adjust ion transport during stress. In contrast, barley mainly relies on the consistent function and efficiency of $Na^+$-selective HKT transporters, with less dependence on post-transcriptional diversification. Despite these insights, some critical questions remain. The physiological role of *OsHKT1;1-V2* in rice is still uncertain. While heterologous systems confirm $Cl^-$-dependent transport activity, it's unknown whether *OsHKT1;1-V2* facilitates $Cl^-$ uptake, long-distance transport, intracellular redistribution, or ion signaling in rice under salinity stress.

Future studies using transgenic overexpression, knockout, or genome editing are necessary to clarify its contribution to whole-plant ion homeostasis and salt tolerance. Additionally, the molecular mechanisms controlling *OsHKT1;1* splicing are not well understood. Although salinity stress is known to trigger widespread alternative splicing in rice (Ganie and Reddy, 2021), the specific splicing factors, cis-elements, and signaling pathways regulating *OsHKT1;1* splice-site choice have yet to be identified. Lastly, while *HvHKT1;1*'s function appears conserved, it remains to be seen whether barley fine-tunes HKT activity through transcriptional regulation, protein modifications, or interactions with other ion transport systems.

**Emerging Role of Non-Selective Channels in Ionic Homeostasis**

Beyond selective $Na^+$ transporters, non-selective ion channels are increasingly seen as vital for ionic balance under salinity stress. Among these, cyclic nucleotide-gated channels (CNGCs) operate at the crossroads of ion transport and stress signaling (Kaplan et al., 2007; Jha et al., 2016; Duszyn et al., 2019). Chapter 4 identified OsCNGC2 as a non-selective channel permeable to $Na^+$ and $K^+$, activated specifically by the presence of both ions. This suggests *OsCNGC2* reacts to $Na^+/K^+$ balance changes rather than being constantly open, functioning as a sensor–integrator during salt stress. Electrophysiology showed OsCNGC2 conducts $Na^+$ and $K^+$ with little selectivity and no visible $Cl^-$ permeability. These features differentiate it from HKT transporters, which are selective and key for directional $Na^+$ transport and long-distance ion distribution (Munns and Tester, 2008; Horie et al., 2009). Therefore, *OsCNGC2* likely isn't the main factor in $Na^+$ exclusion or xylem $Na^+$ retrieval. Instead, it may work locally at the plasma membrane to adjust cation fluxes and membrane potential based on $Na^+$ and $K^+$ levels. Its $Ca^{2+}$ permeability hints at a signaling role linked to monovalent cation fluxes, rather than a primary role in $Ca^{2+}$ transport. This limited $Ca^{2+}$ permeability aligns with the idea that many plant CNGCs modulate signals instead of enabling bulk $Ca^{2+}$ entry (Kaplan et al., 2007; Duszyn et al., 2019), connecting ionic status to downstream responses (Zhu, 2002; Shabala and Cuin, 2008). Functionally, OsCNGC2 likely works alongside HKT systems. While HKT1;1 governs $Na^+$ exclusion and long-distance transport (Ren et al., 2005; Wang et al., 2015; Kobayashi et al., 2017), *OsCNGC2* could offer flexibility by allowing quick cellular responses under mixed $Na^+/K^+$ conditions. These findings support a model where salinity tolerance involves coordinated action between selective transporters and regulated non-selective channels

(Assaha et al., 2017; Malakar and Chattopadhyay, 2021). However, the specific role of *OsCNGC2* in rice salinity tolerance needs further in planta studies that consider tissue-specific expression, regulation, and interactions with broader ion homeostasis networks like the SOS pathway (Zhu, 2002; Horie et al., 2009).

**References**


Assaha DV, Ueda A, Saneoka H, Al-Yahyai R, Yaish MW. The role of $Na^+$ and $K^+$ transporters in salt stress adaptation in glycophytes. Frontiers in Physiology. **2017**;8:509. https://doi.org/10.3389/fphys.2017.00509

Dao HD, Hirai Y. $Cl^-$ More Detrimental Than $Na^+$ in Rice Under Long-Term Saline Conditions. Journal of Agricultural Science. **2018**;10(10):66. https://doi.org/10.5539/jas.v10n10p66

Duszyn M, Świeżawska B, Szmidt-Jaworska A, Jaworski K. Cyclic nucleotide gated channels (CNGCs) in plant signalling—Current knowledge and perspectives. Journal of Plant Physiology. **2019**;241:153035. https://doi.org/10.1016/j.jplph.2019.153035

Ganie SA, Reddy AS. Stress-induced changes in alternative splicing landscape in rice: functional significance of splice isoforms in stress tolerance. Biology. **2021**;10(4):309. https://doi.org/10.3390/biology10040309

Han Y, Yin S, Huang L, Wu X, Zeng J, Liu X, Qiu L, Munns R, Chen ZH, Zhang G. A sodium transporter HvHKT1;1 confers salt tolerance in barley via regulating tissue and cell ion homeostasis. Plant and Cell Physiology. **2018**;59(10):1976-1689. https://doi.org/10.1093/pcp/pcy116

Hauser F, Horie T. A conserved primary salt tolerance mechanism mediated by HKT transporters: a mechanism for sodium exclusion and maintenance of high $K^+/Na^+$ ratio in leaves during salinity stress. Plant, Cell & Environment. **2010**;33(4):552-565. https://doi.org/10.1111/j.1365-3040.2009.02056.x

Horie T, Hauser F, Schroeder JI. HKT transporter-mediated salinity resistance mechanisms in Arabidopsis and monocot crop plants. Trends in Plant Science. **2009**;14(12):660-668. https://doi.org/10.1016/j.tplants.2009.08.009

Jabnoune M, Espeout S, Mieulet D, Fizames C, Verdeil JL, Conéjéro G, Rodríguez-Navarro A, Sentenac H, Guiderdoni E, Abdelly C, Véry AA. Diversity in expression patterns and functional properties in the rice HKT transporter family.

Plant Physiology. **2009**;150(4):1955-1971. https://doi.org/10.1104/pp.109.138008

Jha SK, Sharma M, Pandey GK. Role of cyclic nucleotide gated channels in stress management in plants. Current Genomics. **2016**;17(4):315-329. https://doi.org/10.2174/1389202917666160331202125

Kaplan B, Sherman T, Fromm H. Cyclic nucleotide-gated channels in plants. FEBS Letters. **2007**;581(12):2237-2246. https://doi.org/10.1016/j.febslet.2007.02.017

Kobayashi NI, Yamaji N, Yamamoto H, Okubo K, Ueno H, Costa A, Tanoi K, Matsumura H, Fujii-Kashino M, Horiuchi T, Nayef MA. OsHKT1;5 mediates $Na^+$ exclusion in the vasculature to protect leaf blades and reproductive tissues from salt toxicity in rice. The Plant Journal. **2017**;91(4):657-670. https://doi.org/10.1111/tpj.13595

Malakar P, Chattopadhyay D. Adaptation of plants to salt stress: the role of the ion transporters. Journal of Plant Biochemistry and Biotechnology. **2021**;30(4):668-683. https://doi.org/10.1007/s13562-021-00741-6

Mäser P, Eckelman B, Vaidyanathan R, Horie T, Fairbairn DJ, Kubo M, Yamagami M, Yamaguchi K, Nishimura M, Uozumi N, Robertson W. Altered shoot/root $Na^+$ distribution and bifurcating salt sensitivity in Arabidopsis by genetic disruption of the $Na^+$ transporter *AtHKT1*. FEBS Letters. **2002**;531(2):157-1561. https://doi.org/10.1016/S0014-5793(02)03488-9

Møller IS, Gilliham M, Jha D, Mayo GM, Roy SJ, Coates JC, Haseloff J, Tester M. Shoot $Na^+$ exclusion and increased salinity tolerance engineered by cell type–specific alteration of $Na^+$ transport in *Arabidopsis*. The Plant Cell. **2009**;21(7):2163-78. https://doi.org/10.1105/tpc.108.064568

Munns R, Tester M. Mechanisms of salinity tolerance. Annual Review of Plant Biology. **2008**;59(1):651-681. https://doi.org/10.1146/annurev.arplant.59.032607.092911

Platten JD, Cotsaftis O, Berthomieu P, Bohnert H, Davenport RJ, Fairbairn DJ, Horie T, Leigh RA, Lin HX, Luan S, Mäser P. Nomenclature for HKT transporters, key determinants of plant salinity tolerance. Trends in Plant Science. **2006**;11(8):372-374. https://doi.org/10.1016/j.tplants.2006.06.001

Ren ZH, Gao JP, Li LG, Cai XL, Huang W, Chao DY, Zhu MZ, Wang ZY, Luan S, Lin HX. A rice quantitative trait locus for salt tolerance encodes a sodium

transporter. Nature Genetics. **2005**;37(10):1141-1146. https://doi.org/10.1038/ng1643

Roy SJ, Negrão S, Tester M. Salt resistant crop plants. Current opinion in Biotechnology. 2014 Apr 1;26:115-24. https://doi.org/10.1016/j.copbio.2013.12.004

Shabala S, Cuin TA. Potassium transport and plant salt tolerance. Physiologia Plantarum. **2008**;133(4):651-69. https://doi.org/10.1111/j.1399-3054.2007.01008.x

Sunarpi X, Horie T, Motoda J, Kubo M, Yang H, Yoda K, Horie R, Chan WY, Leung HY, Hattori K, Konomi M. Enhanced salt tolerance mediated by AtHKT1 transporter-induced $Na^+$ unloading from xylem vessels to xylem parenchyma cells. The Plant Journal. **2005**;44(6):928-938. https://doi.org/10.1111/j.1365-313X.2005.02595.x

Wang R, Jing W, Xiao L, Jin Y, Shen L, Zhang W. The rice high-affinity potassium transporter1;1 is involved in salt tolerance and regulated by an MYB-type transcription factor. Plant Physiology. **2015**;168(3):1076-1090. https://doi.org/10.1104/pp.15.00298

Zhu JK. Salt and drought stress signal transduction in plants. Annual Review of Plant Biology. **2002**;53(1):247-273. https://doi.org/10.1146/annurev.arplant.53.091401.143329

# SUMMARY

This thesis presents a molecular and electrophysiological investigation of ion transporters and channels in cereal crops—primarily rice and barley—to elucidate their transport properties, regulatory diversity, and potential roles in plant responses to salinity stress. Chapter 1 emphasizes the global significance of salinity stress and summarizes existing information on the molecular and physiological roles of ion transporters and channels in plant salt tolerance, focusing on HKTs and CNGCs in cereal crops. It establishes the conceptual outline and research objectives that guide the studies described in successive chapters. After the general introduction in Chapter 1, Chapter 2 starts with the conceptual and electrophysiological examination of the OsHKT1;1 in rice, moving to Chapter 3, discovery and characterization of HvHKT1;1 splice variants in barley, and concluding with Chapter 4, analysis of a non-selective, cyclic nucleotide-gated cation channel of OsCNGC2. Molecular biology, electrophysiology, and stress-responsive signaling were integrated into a broader understanding of plant salt tolerance mechanisms.

Chapter 2 investigates the molecular and physiological complexity of the rice transporter *OsHKT1;1*, a key gene in salinity tolerance. Historically, HKT1 transporters have been associated with $Na^+$ selective transport and $Na^+$ exclusion from shoots, particularly in salt-tolerant cultivars like Pokkali. However, earlier observations hinted at OsHKT1;1 variants with unusual transport properties. This chapter focuses on OsHKT1;1-V2, a 172-aa isoform generated by alternative splicing. Even though it lacks typical HKT structure, OsHKT1;1-V2 localizes to the plasma membrane like the full-length (FL) protein, ruling out localization differences as the cause of functional divergence. Electrophysiological assays in *X. laevis* oocytes show that OsHKT1;1-FL shows as expected for the HKT1 subfamily, mediating strong $Na^+$-selective inward currents. In contrast, OsHKT1;1-V2 generates large, bidirectional currents that are strongly dependent on external $Cl^-$ concentrations. Reversal potential shifts, substrate-dependence assays, and in-oocyte $Cl^-$ accumulation all confirm that OsHKT1;1-V2 primarily conducts $Cl^-$ rather than $Na^+$—a surprising deviation within the HKT family. Both Pokkali and Nipponbare express this variant, although at different levels, suggesting that the balance between OsHKT1;1-FL and OsHKT1;1-V2 may affect cultivar-specific salt responses. The discovery of a $Cl^-$-permeable HKT highlights alternative splicing as a mechanism that allows rice to expand HKT functionality

beyond $Na^+$ transport, enabling coordinated regulation of both cation and anion fluxes during salinity stress.

Chapter 3 extends this idea to barley, examining whether comparable splicing-derived diversity exists in another major cereal. Barley is known to possess a $Na^+$-selective HKT1 transporter central to its salinity tolerance, but whether HvHKT1;1 undergoes alternative splicing has not been tested. Using RT-PCR and sequencing, the study identifies four isoforms in Haruna-Nijo: the full-length *HvHKT1;1-FL* and three splice variants (-*V1*, -*V2*, -*V3*) that differ in length, predicted topology, and domain composition. *HvHKT1;1-FL* is the dominant isoform, particularly in leaves, highlighting its foundational role in $Na^+$ homeostasis. Among the variants, -*V3* shows the highest expression, especially in leaves, while -*V1* and -*V2* occur at lower levels. Salt-stress expression analysis reveals a coordinated but isoform-specific response. All variants, including *HvHKT1;1-FL*, show rapid induction—generally peaking at 2 hr—suggesting that barley rapidly activates multiple transporter forms during early salinity exposure. Electrophysiological characterization demonstrates that the HvHKT1;1-FL protein maintains strong $Na^+$ selectivity with high transport capacity, whereas all three variants conduct much weaker $Na^+$ currents. Reduced *V*max, increased *K*m, and poor conductance of other monovalent cations ($K^+$, $Rb^+$, $Li^+$, $Cs^+$) indicate that the variants act as functionally attenuated versions of the OsHKT1;1-FL transporter. This spectrum of transport strengths suggests a conserved monocot strategy: alternative splicing generates isoforms with differing conductance profiles, enabling plants to fine-tune ion movement across tissues and developmental stages. Notably, electrophysiological analyses provided no evidence for $Cl^-$-permeable HvHKT1;1 splice variants, as all barley isoforms retained $Na^+$ selectivity with reduced conductance rather than altered ion preference. This contrasts sharply with rice OsHKT1;1, in which alternative splicing generates a variant (OsHKT1;1-V2) that functions primarily as a $Cl^-$ transporter, indicating that transcript diversification can lead to fundamentally different ion selectivities in a species-dependent manner. These findings broaden understanding of HKT-mediated ion regulation in barley and highlight that, unlike rice, transcript diversification in HvHKT1;1 modulates $Na^+$ transport capacity without conferring alternative anion permeability.

Chapter 4 shifts focus from HKTs to cyclic nucleotide-gated channels and presents the first detailed electrophysiological characterization of OsCNGC2 in rice. Although CNGCs have been implicated in $Ca^{2+}$- and $K^+$-related signaling in

*Arabidopsis*, their electrophysiological properties in monocots have been largely unexamined. *OsCNGC2* is broadly expressed and presumed to participate in stress and developmental signaling, yet its ion conductance remains unknown. Surprisingly, *OsCNGC2* does not behave like a typical non-selective CNGC. In $Na^+$-only or $K^+$-only solutions, with or without cyclic nucleotide activation, the channel exhibits negligible currents. Strong activation occurs only when $Na^+$ and $K^+$ coexist and when 8Br-cAMP is added. This reveals a highly specific dual-gating requirement—cyclic nucleotide binding plus a mixed $Na^+/K^+$ environment—for channel opening. Such ion-dependent gating is common to HvCNGC2-3 but uncommon among other plant CNGCs. OsCNGC2 may be activated only under physiologically balanced ion conditions, potentially preventing uncontrolled $Na^+$ influx during severe stress. Electrophysiological data indicated that the activated channel is a non-selective $Na^+$ and $K^+$ channel, while $Cl^-$ conductance is absent. Plasma membrane localization and inducible expression of the transcript by moderate salinity further support its role as a regulated $Na^+$ transporter. This discovery highlights a new layer of conditional ion-channel activation in monocots, in which both intracellular messenger levels and external ionic composition may tightly control $Na^+$ influx.

Together, the three chapters reveal how cereal crops integrate transporter diversity, ion selectivity, and signal-dependent channel gating to maintain ionic homeostasis under salinity stress. Alternative splicing in *OsHKT1;1* and *HvHKT1;1* generates a functional range of isoforms, while *OsCNGC2* introduces a cyclic nucleotide–dependent regulatory element to $Na^+$ transport. Collectively, these findings provide a unified framework for understanding how plants coordinate multiple transport systems to achieve effective salinity tolerance and offer valuable conceptual foundations for engineering stress-resilient crops.

# ACKNOWLEDGEMENTS

All praise and thanks are due to Almighty Allah, the ultimate source of knowledge and wisdom, who granted me the strength and opportunity to pursue and complete this study. This dissertation would not have been possible without the guidance, support, and generosity of many individuals and institutions.

It is my great pleasure to express my deepest gratitude and profound appreciation to my esteemed supervisor, Professor Dr. Maki Katsuhara, for his patience, professional instruction, insightful advice throughout my experiments and thesis preparation, and tremendous support in my daily life. I am truly grateful for the opportunity to study in his laboratory. I also extend my sincere thanks to my co-supervisors, Associate Professor Dr. Takayuki Sasaki and Dr. Izumi Mori, for their useful suggestions and insightful comments on my research and thesis.

I respectfully thank Professor Dr. Tomoaki Horie (Shinshu University) for providing experimental materials and for his valuable intellectual guidance. I am also grateful to Mr. Yoshiyuki Tsuchiya for his essential technical assistance during the experimentation period. My heartfelt thanks go to all laboratory members for their continuous help, encouragement, and warm support throughout my stay in Japan.

I gratefully acknowledge the financial support from OU-SPRING, Okayama University, which made my doctoral studies in Japan possible. I also thank the Graduate School of Environmental, Life, Natural Science, and Technology, Okayama University, for providing an excellent academic environment. I am thankful to the Department of Agronomy, Faculty of Agriculture, Khulna Agricultural University, for their encouragement.

Last but not least, I wish to express my deepest sense of gratitude and immense indebtedness to my beloved family for their everlasting love, unlimited sacrifice, patience, and cooperation. Especially, I thank my wife, Sharmin Akter, for her warmest support and constant encouragement, which helped me overcome difficulties and pursue my goals.

2026, March

Shahin Imran